Contrasting TiO_2 compositions in Early Cenozoic mafic sills of the Faroe Islands: an example of basalt formation from distinct melting regimes

How to cite:

***"Hansen et al. (2019). Contrasting TiO_2 compositions in Early Cenozoic mafic sills of the Faroe Islands: an example of basalt formation from distinct melting regimes".* Derived from a Doctoral thesis, Durham University, UK, awaiting publication in a reputable peer-reviewed international journal.**

DOI: http://(URL to be given by OSF)

This manuscript is awaiting publication in a reputable peer-revieved international journal (As of July 15, 2019)

Contrasting TiO_2 compositions in Early Cenozoic mafic sills of the Faroe Islands: an example of basalt formation from distinct melting regimes

Jógvan Hansen[a, *], Jon P. Davidson[a, †], Dougal. A. Jerram[b, c, d], Christopher. J. Ottley[a], Mike Widdowson[e]

[a]Dept. of Earth Sciences, Durham University, South Road, Durham DH1 3LE, Durham, UK

[b]CEED, Oslo University, Sem Sælands vei 24, Blindern, 0371 Oslo,

[c] DougalEARTH Ltd., Solihull, UK

[d]Visiting Fellow, Earth, Environmental and Biological Sciences, Queensland University of Technology, Brisbane, Queensland, Australia

[e]Geology, School of Environmental Science, University of Hull, HU6 7RX, Hull, UK

[†]J. P. Davidson sadly passed away in September 2016.

*Present address: Rygsgøta 8, FO 370 Midvag, Faroe Islands (Denmark)

Correspondence: Jógvan Hansen (jogvanha@post.olivant.fo; jogvan.hansen@dunelm.org.uk)

Abstract. The Paleocene lava succession of the Faroe Islands Basalt Group (FIBG), which is a part of the North Atlantic Igneous Province (NAIP), is intruded by numerous basaltic sills. These can be grouped into three main categories according to their geochemical characteristics: A low-TiO_2 sill category (TiO_2 = 0.7-0.9), a relatively high-TiO_2 sill category (TiO_2 = 1.95-2.6) and an intermediate-TiO_2 sill that displays major element compositions laying between the other two categories. Mantle normalised plots for the high-TiO_2 and low-TiO_2 sills display relatively uniform flat LREE trends, with $(Ce/Sm)_N$ ratios ranging from 1.11 to 1.27. Mantle normalised HREE trends representing the low-TiO_2 sills show relatively low $(Sm/Yb)_N$ ratios ranging from 1.09 to 1.26, as compared to ratios of 1.59 to 2.38 for the high-TiO_2 sills. The intermediate-TiO_2 Morskranes Sill is LREE depleted with an average $(Ce/Sm)_N$ ratio of ~0.6, but displays a flat HREE trend with an average $(Sm/Yb)_N$ ratio of ~1.

Mantle normalised trace elements of the low-TiO_2 sill samples define positive Eu and Sr anomalies, whereas trace elements representing high-TiO_2 sill samples display negative anomalies, thus probably indicating the involvement of plagioclase at some stage(s) during magma genesis. Different Nb and Ta anomalies (positive versus negative) in many high-TiO_2 versus low-TiO_2 sill samples indicate that their respective mantle sources were affected by metasomatism prior to partial melting. Two main isotope discriminators can be detected

amongst the actual sill samples: The intermediate-TiO_2 sill displays noticeably lower $^{87}Sr/^{86}Sr$, $^{206}Pb/^{204}Pb$ and $^{208}Pb/^{204}Pb$ ratios relative to both the high-TiO_2 and the low-TiO_2 sill samples. Pb isotope compositions displayed by local contaminated basaltic lavas imply that some of these assimilated distinct crustal material from E Greenland or basement from NW Britain, while others probably assimilated only distinct E Greenland type of crustal material. However, a third distinct crustal source of E Greenland or Rockall-type basement may be required in order to explain the range in compositions of some lead isotopes of the intermediate-TiO_2 Morskranes Sill, unless these were caused by hitherto undetected isotopic heterogeneities in the mantle.

Geochemical modelling indicates that primary melts, which subsequently evolved to Faroese high-TiO_2 sills, could have formed by a range of ~4 to 7.5 % batch melting of moderately fertile lherzolitic sourches, while a range of 16 to 21 % batch melting of likewise fertile sources seems to be required in order to produce Faroese low-TiO_2 sills. The moderately fertile source inferred for Faroese low-TiO_2 sill samples in particular are at odds with the depleted sources envisaged for their low-TiO_2 basaltic host-rocks. Primary melts that gave rise to the intermediate-TiO_2 sill samples could have formed by a range of 6 to 7 % batch melting of a depleted mantle source, probably with a composition comparable to sources that gave rise to local low-TiO_2 and intermediate-TiO_2 host-rocks.

The modelling points to garnet-free residues during mantle melting in order to produce the primary melts that subsequently evolved to most of the Faroese sills. These are envisaged to have formed by batch melting of mantle materials comparable in composition to materials reported for the sub-continental lithospheric mantle (SCLM) at depths of ≤ 85 km. Their relative enrichments in LREE (and LILE in general), as well as their varying Nb and Ta anomalies, may well point to sources affected by metasomatism. These could have been caused by earlier Cenozoic local basaltic magmatism or by earlier events linked to the complex geologic history of the N Atlantic area.

Keywords: Flood basalts; NAIP; Faroe Islands; North Atlantic; basaltic sill; basaltic rocks; partial melting, fractional crystallisation, mineral accumulation, geochemistry; isotope geology

1. Introduction

A number of hypotheses on the petrogenetic evolution of large basaltic igneous provinces (LIPs) such as flood basalts like the North Atlantic Igneous Province (NAIP) have been proposed (e.g. Svensen et al., submitted; Meyer et al., 2007 and references therein). In order to characterise and distinguish between various units/suites within LIPs in general and flood basalts in particular, TiO_2 contents are commonly described (Waagstein, 1988; Gibson et al., 1995; Peate and Hawkesworth, 1996; Jerram et al., 1999; Holm et al., 2001; Søager and Holm, 2011; Millett et al., 2017). Formation of low-TiO_2 basalts have at times been attributed to relatively large-degree melting of enriched material from the continental lithospheric mantle or else developed in response to melting of other mantle sources contaminated with subducted crust/sediments and/or associated expulsion of fluids (Walker et al., 1990; Xiao et al., 2004; Ivanov et al., 2008). Alternatively, they could also result from relatively large-degree melting (~20 %) of depleted mantle sources (e.g. Holm et al., 2001, Søager and Holm, 2011). By contrast, high-TiO_2 basaltic magmas probably form by relatively low-degree mantle melting from sources that may reside at relatively deeper mantle levels (Prytulak and Elliot, 2007; Niu et al., 2011; Millet et al., 2017), or else the sources may originate from mantle plumes, perhaps owing some of their geochemical characteristics to recycled oceanic crust (Xiao et al., 2004; 2007; Søager and Holm, 2011).

Within the NAIP, TiO_2 compositions have been widely used to distinguish their mainly basaltic compositions. Early Cenozoic high-TiO_2 basaltic rocks from W Greenland are thought to have developed by periodical replenishment-tapping-fractionation (RTF) processes from local low-TiO_2 basaltic melts, with plagioclase and clinopyroxene as the main fractionating assemblages and relatively high (16 to 20 %) degrees of partial melting of a moderately depleted mantle are also invoked (Larsen and Pedersen, 2009). Early Cenozoic basaltic rocks from E Greenland, which gave rise to high-TiO_2 basalts, resulted from ~4 to ~8 % mantle melting (e.g Tegner et al., 1998; Momme et al., 2006) compared to the 19 to 20 % mantle melting needed to generate primary magmas that produced the low-TiO_2 basalts in parts of this region (e.g. Momme et al., 2006). Compositional differences between their respective mantle sources likely also affected the ultimate geochemistry of low-TiO_2 versus high-TiO_2 basaltic rocks of this region (Momme et al., 2006; Waight and Baker, 2012). Heterogeneous mantle sources have been inferred for basaltic rocks from E Greenland (Hanghøj et al., 2003; Peate and Stecher, 2003); W Greenland (Larsen and Pedersen, 2009); Iceland (Kitagawa et al., 2008), NW Britain (Ellam and Stuart, 2000) and the Faroe Islands (Gariépy et al., 1983; Holm et al., 2001; Søager and Holm, 2011; Millet et al., 2017). In addition to geochemical variations of magma sources, variations in lithospheric thicknesses

could in theory explain some of the spatial variations of TiO_2 magma types within the lava sequences of the Faroes (e.g. Millett et al., 2017). Assimilation of crustal material during evolution of igneous products of the NAIP have been inferred to have contributed to the petrogenesis of basaltic rocks from E Greenland (Fram and Lesher, 1997; Hanghøj et al., 2003; Waight and Baker, 2012), W Greenland (Larsen and Pedersen, 2009), NW Britain (Font et al., 2008) and the Faroe Islands (Hald and Waagstein, 1983; Holm et al., 2001).

The lava successions of the Faroe Islands have been intruded by a number of sills. These provide insight to some of the later stages of magma generation. Although these sills have previously been characterised in terms of their geometries and stratigraphic relationships within the lava sequences (Hansen et al., 2011), limited information exists regarding their petrogenesis, and in particular the likely sources of melting and how they may or may not relate to the lava sequences that they intersect. Understanding the later stages of magma generation during the evolution of the NAIP is desirable to better understand the wider temporal and spatial evolution of the province as a whole (e.g. Jerram and Widdowson 2005; Meyer et al., 2007; Hansen et al. 2009).

Accordingly, we focus on the compositions of primary magmas that ultimately evolved to form the sills of the Faroe Islands. The sill samples are categorised according to major element compositions (especially TiO_2), trace elements (including REE) and isotopic compositions (Pb, Sr and Nd). The sills are then grouped into three main units defined primarily by their TiO_2 compositions. Their evolution is examined by partial melting modelling in order to help characterise their formation and mantle sources in terms of the degrees of melting and source rock compositions. The petrogenetic interpretations presented for the Faroese sills in this study are considered in the context of late-stage magmatic processes during the formation of the NAIP, and in particular we look at the effects of partial melting at relatively shallow mantle levels during the waning stages of basaltic magmatism in this LIP.

2. Geological frameworks

The Faroe Islands Basalt Group (FIBG) was emplaced at the NW European margin as a central part of the contemporaneous NAIP magmatism (Upton, 1988; Waagstein, 1988; Saunders et al., 1997; Passey and Jolley, 2009). Geophysical studies indicate that the basaltic rocks of the Faroese block lie on ~30 km thick stretched ancient continental crust (Bott et al., 1974; Richardson et al., 1998; Raum et al., 2005; Sammarco et al., 2017), with total

stratigraphic thickness of exposed and drilled lavas of this region of ~6.6 km (Rasmussen and Noe-Nygaard, 1969; Rasmussen and Noe-Nygaard, 1970; Waagstein, 1988; Passey and Bell, 2007; Passey and Jolley, 2009) (Fig. 1).

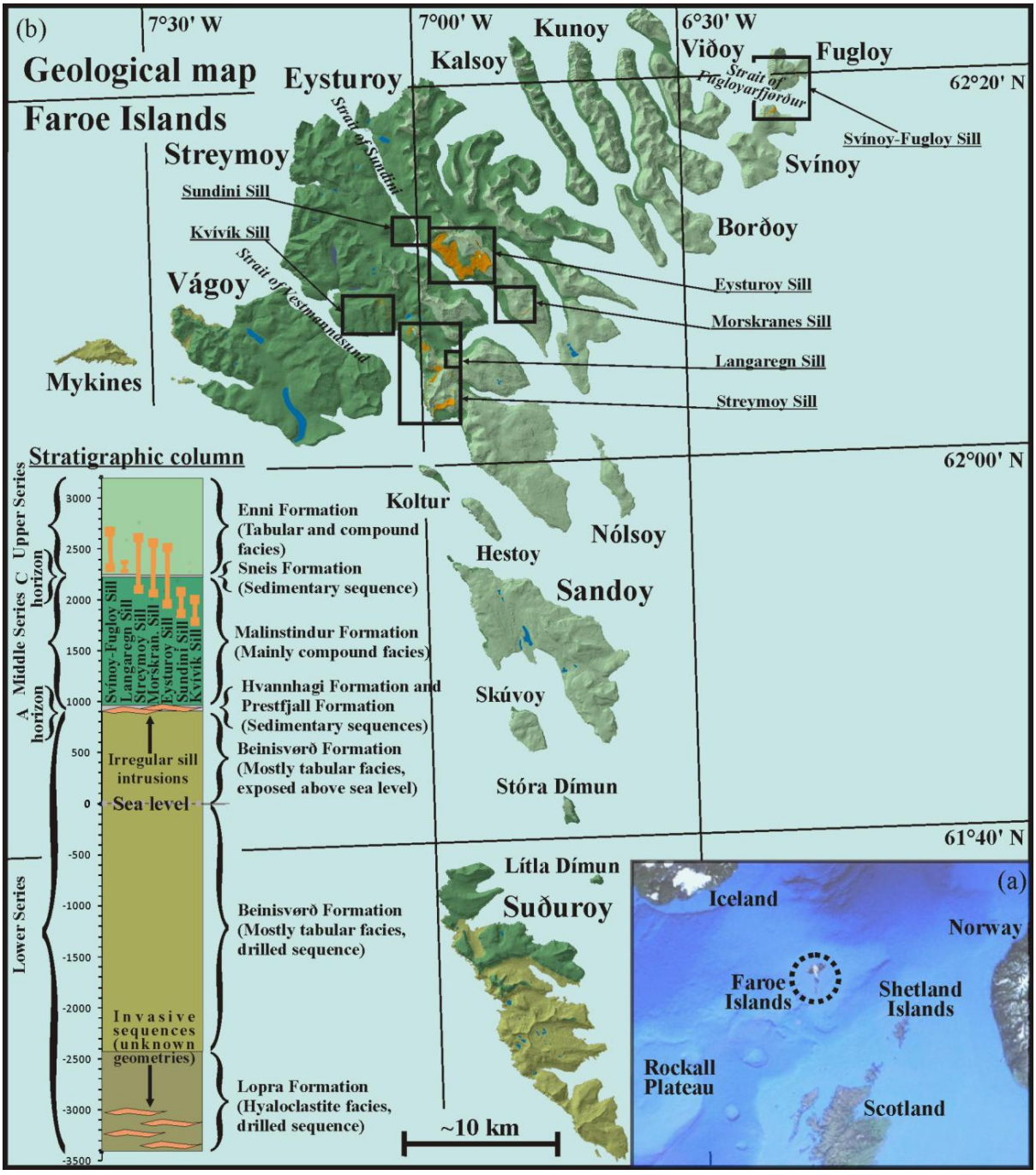

Fig. 1. North Atlantic maps. a) Relative location of the Faroe Islands. b) The geological map shows the main basaltic formations of the Faroe Islands and sites of sill exposures. The stratigraphic column indicates the vertical extents of the actual sills and of local geological formations. Initial nomenclature from Noe-Nygaard and Rasmussen (1968); Rasmussen and Noe-Nygaard (1970) and Waagstein (1988) is indicated to the left of the stratigraphic column, while the revised nomenclature from Passey and Bell (2007) is shown to the right. (Modified from Hansen, 2011 and Hansen et al., 2011).

by these basalts is estimated at ~120000 km^2 (Passey and Jolley, 2009). The Faroe lava succession was previously grouped into Upper, Middle and Lower Series basalts (Rasmussen and Noe-Nygaard, 1970; Waagstein, 1988), but a revised nomenclature with seven formations was recently proposed (Passey and Jolley, 2009). From the bottom to top of the lava succession these are: the ~1075 m thick Lopra Formation; the ~3250 m thick Beinisvørð Formation; the ~9 m thick Prestfjall Formation; the 40-50 m thick Hvannhagi Formation; the 1250-1350 m thick Malinstindur Formation; the ~30 m thick Sneis Formation and finally the ~900 m thick Enni Formation (Passey and Bell, 2007; Passey and Jolley, 2009 and refs. therein) (Stratigraphic column Fig. 1). Individual lava flows within the Beinisvørð, Malinstindur and Enni formations are often separated by thin volcaniclastic lithologies or weathering surfaces measuring a few centimetres, a few tens of centimetres and occasionally a few metres in thickness (Rasmussen and Noe-Nygaard, 1970; Passey and Bell, 2007; Passey and Jolley, 2009). Basalts of the Beinisvørð Formation are generally aphyric whereas those of the Malinstindur and Enni formations include both olivine and plagioclase phyric rocks in addition to aphyric basalts (Rasmussen and Noe-Nygaard, 1969; Waagstein, 1988; Passey and Jolley, 2009). Dating by the $^{40}Ar/^{39}Ar$ method has yielded ages of ~61 Ma for a lava sequence within the Beinisvørð Formation (Waagstein et al., 2002) and ~55 Ma for another lava sequence belonging to the Enni Formation (Storey et al., 2007). An additional study on age(s) of Faroese lavas based on local palynoflora stated that the entire lava succession was deposited in the time span from 57.5 to 60.56 Ma (Ellis et al., 2002).

Dykes are ubiquitous throughout the exposed parts of the lava succession while 'saucer-shaped' sills are confined to the uppermost parts of the Malinstindur Formation, the Sneis Formation and the lowermost parts of the Enni Formation (Rasmussen and Noe-Nygaard, 1970; Passey and Bell, 2007; Passey and Jolley, 2009; Hansen, 2011; Hansen et al., 2011) (Fig. 1). High-TiO_2 lavas (TiO_2 >1.5 wt %) make up most of the volume in the lowermost ~5.5 km of the Faroese lava succession, while low-TiO_2 lavas (TiO_2 <1.5 wt %) become increasingly common in the remaining upper parts (Rasmussen and Noe-Nygaard, 1969; Hald and Waagstein, 1984; Waagstein, 1988; Passey and Jolley, 2009; Søager and Holm, 2009, 2011; Millett et al., 2017). High-TiO_2 dykes and lavas of the Malinstindur and Enni formations are exposed throughout the archipelago, while low-TiO_2 dykes and lavas of these formations are most common in the northern parts of the islands (Hald and Waagstein, 1991; Søager and Holm, 2011). Low-TiO_2 sills are exposed in the central parts of the Faroe Islands whereas high-TiO_2 sills are exposed in the N and NE parts of the archipelago (Hald and Waagstein, 1991; Holm et al., 2001). A few lava flows of the Malinstindur Formation display

anomalously high SiO_2 contents of ~54.0 wt % (Hald and Waagstein, 1983). In the Beinisvørð Formation, clear stratigraphic trends of MgO and TiO2 contents are recorded and associated with large scale magma pulses (Jolley et al., 2012). However, in the Malinstindur and Enni Formations, the chemical stratigraphy is more erratic between individual lava flows irrespective of stratigraphic levels (e.g. Hald and Waagstein, 1984; Søager and Holm, 2009, 2011), and this has recently been demonstrated to relate to multiple inter-digitating lava flow packages fed from distinct magma batches (Millett et al., 2017)..

3. Previous petrogenetic models on Faroese magmatism

Primary magmas that gave rise to high-TiO_2 basaltic dykes and lavas of the Faroe Islands are thought to have formed in response to 2.5 to 3.5 % mantle melting compared to ~20 % melting during production of primary magmas that yielded local low-TiO_2 rocks (Holm et al., 2001). Relatively primitive samples of Faroese dykes and lavas fall on olivine control lines in plots of e.g. MgO versus TiO_2 (Holm et al., 2001). Internal geochemical variations amongst relatively evolved basaltic rocks represented by local low-TiO_2 dykes have previously been interpreted in terms of low-pressure fractional crystallisation of olivine, plagioclase and clinopyroxene previously (Hald and Waagstein, 1991), while spread in major element composition within evolved high-TiO_2 lavas of the Beinisvørð Formation have been attributed to high-pressure fractional crystallisation of plagioclase, clinopyroxene and garnet earlier (Bernstein, 1994). A scenario that also involved melting of a North Atlantic end-member mantle component (NAEM) was envisaged for Faroese basaltic lavas in a more recent study (Søager and Holm, 2011). These authors further argued in favour of distinct sources for the low and high-Ti Faroese lavas. Most recently, Millet et al. (2017) identified four mantle sources to high-TiO_2 lavas of the Enni and Malinstindur formations and an additional source to low-TiO_2 lavas of the same formations.

Compositional variations in high-TiO_2 versus low-TiO_2 mantle sources have also been inferred for E Greenland (Waight and Baker, 2012; Peate and Stecher, 2003) and Iceland (e.g. Thirlwall et al. 2004). Other authors argue in favour of a depleted asthenospheric source to local LREE-depleted (low-TiO_2) basalts and a sub-continental lithospheric mantle or a deep mantle plume source to local LREE-enriched (high-TiO_2) basalts (Gariépy et al., 1983). Coherent up-section variations in MgO, TiO_2, Y and Zr compositions within rocks of the Beinisvørð Formation led Hald and Waagstein (1984) to infer magma supplies from at least two independent volcanic systems. Combined geochemical and isotopic characteristics of

local contaminated basaltic lavas (~54 wt % SiO_2) have previously been explained in terms of contamination with Lewisian-type amphibolite facies gneisses (Gariépy et al., 1983; Holm et al., 2001). While Gariépy et al. (1983) attributed non-linear isotopic trends of "common" tholeiitic Faroese lava/dyke samples to mild crustal contamination; Holm et al. (2001) ascribed such insignificant variations to slight isotopic heterogeneities originating within their mantle sources. Larsen et al. (1999) and Søager and Holm (2009) argued in favour of a trans-Atlantic chemostratigraphic correlation between units of the Nansen Fjord area in the central parts of E Greenland and sections of the Faroese lava pile. However, a more recent study suggests that albeit the dominant progression of high-TiO_2 basaltic rocks in these regions appears broadly equivalent, these characteristics cannot be directly used for correlation, since Faroese high-TiO_2 lava flows can be chronostratigraphically constrained only on local (~10's km) scale (Millet et al., 2017). Their study also indicated that low-TiO_2 lava flows in these two regions could have been fed across a broader area of still relatively thick lithosphere associated with a strike-slip zone between the FIBG and Blosseville Kyst region of East Greenland.

The new data sets introduced in this paper present additional constraints on the nature of mantle sources and petrogenetic processes involved during the final known phases of magmatism in the Faroese region that ultimately resulted in the emplacement of sills within the volcanic successions. Our study provides both propositions regarding igneous processes acting during waning stages of NAIP formation and more general implications for LIP formation.

4. Petrography, geochemistry and isotope geology of the Faroese sills

4.1. Petrography

Samples were collected from 7 Faroes sills, as well as from a number of selected local dykes and irregular intrusions in order to further constrain the petrogenesis of the magmas: Previous work of Hansen (2011) and Hansen et al. (2011) outline locations of sills and collected samples. Petrographically, the Faroese sills comprise ca. 40 to 55 % plagioclase, 40 to 45 % clinopyroxene, 5 to 10 % olivine and 3 to 10 % Fe/Ti oxides. More specifically, the Streymoy and Kvívík sills are feldspar-phyric; the Langaregn Sill is feldspar- and olivine-phyric; the Eysturoy and Sundini sills display intergranular texture, but clinopyroxene oikocrysts are also common within these; the Svínoy-Fugloy and Morskranes sills both

display ophitic to sub-ophitic textures. Late clinopyroxene crystallisation is suggested by the ophitic/subophitic texture in the Svínoy-Fugloy and Morskranes sills in particular, but also to some degree in the Eysturoy Sill. Early olivine crystallisation is suggested by the occurrences of partly altered large olivine phenocrysts in the Streymoy and Kvívík sills and by the presence of olivine microphenocrysts occurring as inclusions within larger plagioclase grains of the Langaregn Sill. The occurrences of plagioclase grains in feeder dykes, which display increasing degrees of resorption with increasing distances from contacts with their host-rocks, seem to suggest that Ca-rich plagioclases were dominating early crystallisation phases, which subsequently reacted with surrounding melts to produce fine grained Na-rich plagioclases and clinopyroxenes. Earlier studies on basalts of the Faroe Islands have indicated olivine compositions of Fo_{86-88} in low-TiO_2 basalts and Fo_{72-73} in high-TiO_2 basalts whereas An_{64-70} has been measured for plagioclases representing both these rock types (Holm et al., 2001). See Supplement 1 below for further details on petrography.

4.2. Analytical methods

Following careful selection, 56 rock samples representing 7 Faroese sills and a number of local dykes and irregular intrusions selected for analysis, then crushed and milled according to standard methods in preparation for analysis. Major elements and selected trace elements representing 44 sill samples (Table 1) and 12 dyke and irregular intrusion samples (Table C in Supplement 3 below) were determined on rock powder fused to glass discs and pressed powder tablets respectively using an ARL 8420+ dual goniometer wavelength dispersive XRF spectrometer at the Department of Earth Sciences, Open University, Milton Keynes, UK. Major elements representing 3 additional samples from the Sundini and Morskranes sills were analysed at the Geological Survey of Norway (NGU), using a PANalytical Axios 4 kW. For further details see Supplement 2 below.

Trace elements and REEs representing 14 sill samples (Table 2) and 8 dyke and irregular intrusion samples (Supplement 3 below) were determined on powdered rock samples were carried out on an Elan 6000 Perkin Elmer-Sciex inductively coupled plasma mass spectrometer (ICP-MS) at the Arthur Holmes Trace Element Laboratory, Department of Earth Sciences, Durham University, UK (for preparation and analytical methods see supplement 3 below). In addition, trace elements for a further three sill samples (Table 2) were determined using a modified version of the dissolution procedure described in Turner et al. (1999) and Ottley et al. (2003). These analyses were carried out at GEUS, Denmark, by

inductively coupled plasma mass spectrometry (ICP-MS) using a Perkin-Elmer Elan 6100 DRC quadrupole ICP-MS instrument. For further details see Supplement 2 below.

Sr and Nd isotope ratios for 8 selected sill samples and Pb isotope ratios of 7 selected sill samples (Table 3) were determined according to the preparation methods described in Dowall et al. (2003) and Charlier et al. (2006) respectively. Sr and Nd fractions were taken up in 1ml of 3 % HNO_3 separately and introduced into a mass spectrometer using an ESI PFA50 nebuliser and a dual cyclonic–Scott Double Pass spraychamber. Pb samples were taken up in 1ml of 3 % HNO_3 and spiked with Tl prior to introduction into a mass spectrometer using an ESI PFA50 nebuliser and a dual cyclonic–Scott Double Pass spraychamber. All isotopes were analysed on a ThermoElectron Neptune Multi-collector Plasma Mass Spectrometer (MC-ICP-MS) at the Arthur Holmes Isotope Geology Laboratory, Durham University, UK.

Whole-rock MC-ICP-MS lead isotope analyses were carried out on 6 additional sill samples on a VG Sector 54-IT TIMS at the Geological Institute, University of Copenhagen, Denmark (Table 3). Dissolution of the powdered samples was achieved in two successive, but identical steps, which consisted of a strong 8 N HBr attack that has been shown to effectively dissolve accessory phosphates (Frei et al., 1997; Schaller et al., 1997), followed by a concentrated HF-14 N HNO_3 mixture, and finally by strong 9 N HCl. Chemical separation of Pb from whole rocks was performed over conventional glass stem and subsequently miniature glass-stem anion exchange columns containing, respectively 1 ml and 200 µl 100–200 mesh Bio-Rad AG 1×8 resin. Lead was analyzed in a static multi-collection-mode where fractionation was controlled by repeated analysis of the NBS 981 standard using values of Todt et al. (1993). For further details see Supplement 2 below.

4.3. Geochemistry

4.3.1. Major elements

The 47 Faroese sill samples analysed for major elements (Table 1; Fig. 2) display SiO_2 contents ranging from 47.5 to 50.5 wt %, while their combined Na_2O and K_2O contents range from 1.9 to 2.9 wt %, thus indicating subalkaline or tholeiitic composition basalts (e.g. Rickwood, 1989). The MgO contents for all Faroese sills combined range from ~6.15 to ~8.2 wt %. Here, the range in MgO for the Morskranes Sill is ~7 to ~8.2 wt %, which is a much wider MgO spread than are displayed by any of the other local individual sills. The sills define three main categories according to their TiO_2 contents. Here, samples of the Kvívík and Streymoy sills display low TiO_2 contents ranging from 0.7 to 0.9 wt %, while samples of

the Eysturoy, Langaregn, Sundini and the Svínoy-Fugloy sills exhibit high TiO_2 contents spanning from 1.95 to 2.6 wt % (Fig. 2). Morskranes Sill samples display intermediate TiO_2 contents of ~1.20 wt %. The Kvívík and Streymoy sills display relatively high Al_2O_3 and CaO, while the Eysturoy, Langaregn, Sundini and Svínoy-Fugloy sills exhibit relatively high Na_2O and Fe_2O_3. Major elements such as Al_2O_3, Fe_2O_3 and CaO of the intermediate-TiO_2 Morskranes Sill plot in between those of the low-TiO_2 and the high-TiO_2 sill categories (Table 1; Fig. 2). Generally, the compositional range of major elements representing the investigated intrusions generally correlate well with published major element data on Faroese lava/dyke samples and with lava/dyke data obtained in this work (Supplement 3 below); however, the Streymoy and Kvívík sills in particular display higher SiO_2, Al_2O_3 and CaO contents and lower TiO_2 and Fe_2O_3 contents when compared to host-rock lava/dyke samples with comparable MgO contents (insets in Fig. 2). More specifically, the published host-rock data show that most local basaltic lavas/dykes display SiO_2 contents ranging from ~47 to ~49.5 wt %, their MgO generally range from ~7 to ~9 wt % (their entire MgO range span from ~4.5 to ~23 wt %), while their TiO_2 contents range from ~0.6 to ~4.0 wt % (e.g. Hald and Waagstein, 1984, 1991; Waagstein, 1988; Holm et al., 2001; Søager and Holm, 2009, 2011).

Table 1

Whole rock XRF data on major and selected trace elements representing basaltic sills of the Faroe Islands (Analysed by John Watson, OU, UK, and Ana Banica, NGU, NO)

	Streymoy Sill															
Sample	09-JSS-02	07-JSS-21	07-JSS-23	08-JSS-24	07-JSS-26	07-JSS-28	07-JSS-29	08-JSS-29	07-JSS-38	07-JSS-39	07-JSS-40	07-JSS-42	07-JSS-43	07-JSS-44	07-JSS-45	07-JSS-52
Wt. %	Sill	Sill	Sill	Sill	Sill	Sill	Sill	Sill	Sill	Sill	Sill	Sill	Sill	Sill	Sill	Sill
SiO_2	49.05	49.58	49.55	50.00	49.64	49.19	49.23	49.55	47.80	49.70	49.42	49.37	49.67	50.29	50.44	50.29
TiO_2	0.76	0.76	0.75	0.80	0.79	0.76	0.78	0.78	1.13	0.78	0.73	0.76	0.76	0.77	0.82	0.82
Al_2O_3	17.04	16.90	17.75	16.90	16.61	17.00	17.15	16.51	14.76	16.68	17.55	16.71	17.41	17.45	17.03	16.95
Fe_2O_3	9.91	10.13	9.68	10.25	10.35	9.99	10.06	10.34	12.05	10.27	9.65	10.27	9.93	10.01	10.34	10.42
MnO	0.16	0.16	0.16	0.16	0.17	0.16	0.16	0.17	0.19	0.17	0.16	0.16	0.16	0.16	0.17	0.17
MgO	6.74	6.92	6.56	7.03	6.93	6.73	6.76	6.92	8.46	6.94	6.74	6.86	6.83	6.83	6.92	6.86
CaO	12.98	13.07	13.40	13.18	13.01	13.08	13.07	13.11	12.96	13.09	13.31	13.22	13.40	13.25	13.13	13.22
Na_2O	1.88	1.96	1.87	1.95	1.96	1.92	1.93	1.92	1.89	1.93	1.91	1.91	1.91	1.93	1.95	2.00
K_2O	0.20	0.21	0.21	0.21	0.22	0.21	0.22	0.21	0.06	0.19	0.20	0.19	0.20	0.20	0.22	0.20
P_2O_5	0.08	0.08	0.08	0.08	0.08	0.08	0.08	0.08	0.09	0.08	0.07	0.07	0.08	0.08	0.08	0.09
[a]LOI	0.14	0.33	0.45	0.11	0.19	0.28	0.27	0.19	0.43	0.11	0.18	0.23	0.32	0.26	0.46	0.14
Total	98.92	100.11	100.46	100.67	99.95	99.40	99.71	99.77	99.81	99.95	99.91	99.73	100.67	101.24	101.58	101.17
ppm																
Sr	197	199	205	195	199	196	196	190	113	197	203	180	198	193	189	198
Y	16	18	16	18	18	17	18	18	27	18	16	18	17	17	18	19
Zr	50	50	49	49	52	49	51	51	58	52	46	46	47	48	50	53
Nb	3.4	2.7	2.8	2.8	3.1	3.4	3.1	2.8	2.2	3.1	2.8	2.9	3	2.4	2.8	2.9
Ba	64	66	63	67	75	66	66	64	25	69	65	54	63	57	59	72
Sc	36	37	35	43	39	34	40	38	46	39	36	37	36	38	37	38
V	242	228	229	251	247	228	250	252	298	254	228	248	218	247	244	244
Cr	181	176	166	200	184	170	182	179	359	176	183	174	175	181	178	168
Ni	80	78	73	86	81	78	76	77	132	79	74	79	85	86	81	74
Cu	118	110	114	114	122	113	113	106	137	118	107	127	114	114	122	115
Zn	56	56	53	60	60	54	58	58	74	60	55	60	52	59	59	59
Y/TiO_2	21.67	24.03	21.73	22.41	22.81	22.65	23.31	23.74	23.89	22.59	22.25	23.31	22.72	21.39	21.46	22.57
Zr/Y	3.06	2.7	3.01	2.72	2.91	2.87	2.8	2.76	-------	2.94	2.82	2.57	2.73	2.89	2.82	2.83
Nb/Y	0.21	0.15	0.17	0.16	0.17	0.2	0.17	0.15	-------	0.18	0.17	0.16	0.17	0.15	0.16	0.16

Table 1 (continued)

	Streymoy Sill						Kvívík Sill			Langaregn Sill		Sundini Sill				[b]Ey. S.
Sample	07-JSS-55	07-JSS-57	07-JSS-58	07-JSS-09	09-JSS-09	09-JSS-10	08-JKS-05	08-JKS-18	07-JSS-49	07-JSS-50	07-JSS-51	08-JES-01	09-JH-01	09-JH-05	16-JSuS-02	08-JES-03
Wt. %	Sill	Sill	Sill	F.Dyke	F.Dyke	F.Dyke	Sill	Sill	Sill	Sill	Sill	Sill	Sill	Dyke	[c]Sill	Sill
SiO_2	50.27	49.56	49.67	49.39	50.00	49.98	49.15	49.04	49.51	48.86	48.84	49.44	49.43	49.11	49.20	50.28
TiO_2	0.75	0.80	0.71	0.79	0.81	0.79	0.79	0.76	0.76	2.58	2.51	2.12	2.19	2.84	2.20	2.07
Al_2O_3	17.72	16.90	17.82	16.50	17.02	17.11	16.74	16.85	17.16	13.80	13.81	13.43	13.40	13.83	13.10	13.54
Fe_2O_3	9.68	10.37	9.53	10.57	10.41	10.36	10.47	10.20	10.11	14.97	14.79	15.16	14.92	14.05	15.30	14.60
MnO	0.16	0.17	0.15	0.17	0.17	0.17	0.17	0.17	0.17	0.21	0.22	0.21	0.22	0.19	0.22	0.21
MgO	7.21	6.70	6.79	6.63	6.75	6.65	6.60	6.68	6.81	6.47	6.35	6.32	6.16	6.84	6.11	6.47
CaO	13.35	12.86	13.50	13.31	13.38	13.27	13.07	13.46	13.42	10.80	10.76	11.01	10.85	10.41	10.60	11.15
Na_2O	1.96	2.00	1.91	1.91	1.88	1.86	1.91	1.82	1.89	2.36	2.36	2.34	2.38	2.30	2.43	2.36
K_2O	0.22	0.23	0.20	0.14	0.09	0.18	0.20	0.10	0.18	0.20	0.25	0.31	0.30	0.36	0.31	0.33
P_2O_5	0.08	0.09	0.08	0.07	0.08	0.08	0.08	0.07	0.07	0.24	0.24	0.21	0.23	0.26	0.23	0.21
[a]LOI	0.39	0.17	0.20	0.36	0.28	0.17	0.27	0.50	0.24	0.01	-0.23	-0.12	-0.29	-0.19	0.31	0.07
Total	101.78	99.86	100.57	99.84	100.88	100.62	99.46	99.64	100.31	100.51	99.90	100.45	99.79	99.99	100.00	101.29
ppm																
Sr	195	202	200	176	181	181	185	180	178	255	253	170	176	-----	-----	169
Y	17	19	16	19	18	18	18	18	18	34	34	38	38	-----	-----	37
Zr	47	52	46	48	51	50	50	46	47	166	164	139	145	-----	-----	132
Nb	2.7	3	2.3	2.6	3.5	4	3.6	2.8	2.7	13	13	11	11	-----	-----	9.5
Ba	65	74	64	55	34	55	55	43	60	73	66	89	91	-----	-----	90
Sc	34	36	33	43	39	37	39	39	37	41	39	48	41	-----	-----	47
V	217	236	214	252	250	254	260	252	238	378	392	419	433	-----	-----	422
Cr	189	159	178	171	162	166	154	170	162	148	140	59	52	-----	-----	65
Ni	81	75	74	80	83	80	79	79	77	94	94	68	63	-----	-----	64
Cu	106	117	99	131	133	128	129	127	121	192	216	253	264	-----	-----	228
Zn	53	57	52	65	64	61	60	62	56	104	106	97	100	-----	-----	94
Y/TiO_2	22.82	23.57	23.02	23.82	22.61	22.19	23.15	23.94	24.05	13.00	13.53	17.69	17.20	-----	-----	17.71
Zr/Y	2.71	2.77	2.81	2.54	2.77	2.82	2.71	2.55	2.59	4.93	4.82	2.69	3.86	-----	-----	3.6
Nb/Y	0.16	0.16	0.14	0.14	0.19	0.23	0.2	0.15	0.15	0.38	0.37	0.29	0.29	-----	-----	0.26

Table 1 (continued)

	Eysturoy Sill								Morskranes Sill					Svínoy-Fugloy Sill		
Sample	08-JES-04	08-JES-07	08-JES-08	08-JES-10	08-JES-11	08-JES-19	08-JES-20	09-JES-08	08-JMS-14	08-JMS-16	08-JMS-17	16-JMS-18	16-JMS-19	08-JFS-21	08-JSVS-22	08-JSVS-23
Wt. %	Sill	Sill	Sill	Sill	Sill	Sill	Sill	F.Dyke	Sill	Sill	Sill	[c]Sill	[c]Sill	Sill	Sill	Sill
SiO_2	49.67	49.27	49.69	49.23	49.59	49.33	49.28	49.13	48.73	48.87	47.65	48.30	47.90	48.37	48.49	48.58
TiO_2	2.11	1.97	2.09	2.06	2.01	2.13	2.06	2.16	1.20	1.20	1.21	1.20	1.16	2.09	2.10	2.10
Al_2O_3	13.47	13.26	13.22	13.41	13.39	13.31	13.34	13.54	15.19	14.48	13.83	14.60	14.30	13.89	13.54	13.86
Fe_2O_3	14.99	14.62	14.94	13.48	14.94	14.69	15.13	14.89	14.85	12.33	12.66	12.50	12.50	12.83	14.37	14.22
MnO	0.22	0.21	0.22	0.22	0.22	0.22	0.22	0.22	0.21	0.20	0.21	0.21	0.19	0.21	0.21	0.20
MgO	6.25	6.23	6.18	6.26	6.55	6.22	6.46	6.26	7.06	8.09	8.22	7.25	7.81	7.00	7.07	6.95
CaO	10.91	10.87	10.83	10.75	11.19	11.07	11.16	11.10	13.26	12.86	11.86	12.60	12.50	11.74	11.66	11.77
Na_2O	2.45	2.37	2.39	2.32	2.33	2.34	2.32	2.32	1.95	1.86	1.68	2.02	1.92	2.26	2.18	2.26
K_2O	0.34	0.36	0.32	0.57	0.30	0.26	0.31	0.23	0.04	0.03	0.79	0.07	0.04	0.17	0.15	0.18
P_2O_5	0.22	0.22	0.22	0.21	0.20	0.22	0.21	0.22	0.10	0.10	0.10	0.09	0.09	0.19	0.19	0.19
[a]LOI	0.06	0.07	-0.10	0.07	0.09	-0.09	-0.15	-0.17	0.64	0.61	2.01	1.03	0.86	-0.22	0.00	-0.22
Total	100.67	99.44	100.01	100.65	100.04	100.56	100.15	100.10	99.85	100.70	100.95	99.80	99.20	100.39	100.08	99.80
ppm																
Sr	174	167	170	168	171	174	170	175	88	86	94	-----	-----	215	213	214
Y	37	37	38	36	35	36	36	37	29	27	29	-----	-----	29	28	29
Zr	138	139	141	135	125	141	134	142	63	61	62	-----	-----	124	117	126
Nb	11	10	10	8.9	9.2	10	10	11	2.7	1.9	2	-----	-----	9.7	9.7	10
Ba	88	88	96	101	95	84	90	79	19	18	25	-----	-----	56	64	63
Sc	43	44	43	44	44	45	45	45	49	44	45	-----	-----	39	39	38
V	426	419	426	427	413	432	418	425	350	326	349	-----	-----	352	359	371
Cr	59	63	60	66	66	62	72	58	361	344	352	-----	-----	215	237	228
Ni	58	64	61	61	60	64	63	66	119	109	112	-----	-----	100	118	101
Cu	236	243	236	221	208	257	219	250	173	157	132	-----	-----	194	203	210
Zn	93	98	101	95	91	101	95	95	83	77	77	-----	-----	89	92	93
Y/TiO_2	17.46	18.89	18.04	17.61	17.28	17.08	17.25	17.11	23.70	22.73	23.67	-----	-----	14.00	13.28	13.93
Zr/Y	3.76	3.72	3.73	3.71	3.61	3.87	3.75	3.83	2.22	2.25	2.17	-----	-----	4.23	4.2	4.32
Nb/Y	0.29	0.27	0.26	0.25	0.27	0.28	0.29	0.29	0.09	0.07	0.07	-----	-----	0.33	0.35	0.36

Major elements are in weight percent and trace elements are in parts per million. Total iron is given as Fe_2O_3. Sample 07-JSS-38 represents a weathered basaltic rock specimen. The abbreviation F. Dyke refers to feeder dyke. [a]LOI indicates loss on ignition. [b]Ey.S. refers to the Eysturoy Sill. [c]Sill refer to samples analysed at NGU, Norway.

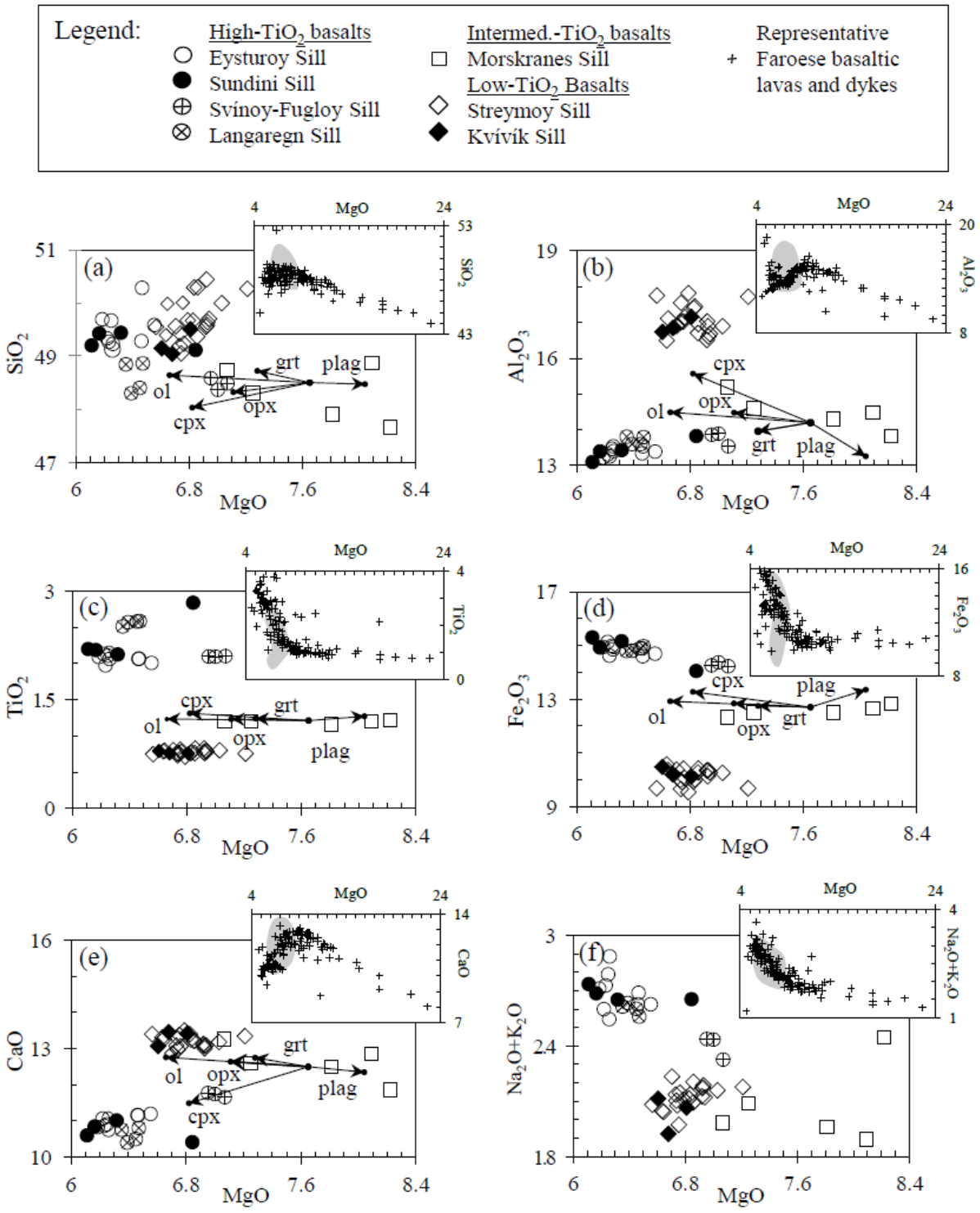

Fig. 2. The diagrams show bivariate plots of major element data from Table 1. The Faroese sills define three main categories (high-TiO_2, intermediate-TiO_2 and low-TiO_2), albeit somewhat scattered for the intermediate TiO_2 and high-TiO_2 specimen. The vectors in sub-figures a) to e) represent calculated crystallisation trends with ol = 2 wt %, opx = 2 wt %, cpx = 10 wt %, plag = 5 wt % and grt = 3 wt % fractional crystallisation. Vector calculations are based on major element compositions from the compilation of Deer et al. (1992). Insets show major element compositions representing local lavas and dykes (black crosses) and range in compositions of Faroese sills (semi-transparent grey fields). Data on Faroese lavas and dykes are from Hald and Waagstein (1984, 1991); Holm et al. (2001); Søager and Holm (2009, 2011) and from this study (see Supplement 3 below

for host-rock data from this study). plag = plagioclase; other abbreviations are from Kretz (1983). Datasets on calculated crystallisation trends are shown in: Hansen et al. (2019).

4.3.2. Selected trace elements

Mantle-normalised trace element data from 17 representative sill samples (Table 2; Fig. 3) define three main tendencies. The low-TiO_2 and high-TiO_2 sills generally display separate well-defined, relatively flat sub-parallel trends with the latter being comparatively more enriched in most elements; by contrast, the intermediate TiO_2 content sill generally exhibits a gradual depletion towards the most incompatible elements (Fig. 3a). All sills display negative P anomalies and some samples of the intermediate TiO_2 sill are characterised by distinctive positive and moderately negative Rb and K anomalies. The low-TiO_2 sill samples display relatively uniform positive Ba, Rb, Th, K and Sr anomalies, whereas most of the high-TiO_2 sill samples exhibit negative anomalies for these same elements (Fig. 3). It is clear however, that some relative differences in these elements exist internally within the high-TiO_2 sills, where the Eysturoy and Sundini sills display slightly larger Sr and slightly smaller Ba, Rb, Th and K anomalies respectively compared to those of the Svínoy-Fugloy and Langaregn sills (Fig. 3d; Fig. 3e). Perhaps less conspicuous features are (i) the weak positive and moderately positive Nb and Ta anomalies exhibited in the Eysturoy and Sundini sills, and in the Svínoy-Fugloy and Langaregn sills respectively, and (ii) moderately negative Nb and Ta anomalies in the Streymoy and Kvívík sills (Fig. 3a; Fig. 3b; Fig. 3d; Fig. 3e). Local high-TiO_2 and intermediate-TiO_2 host-rock samples (analysed in this study and shown in Supplement 3 below) display mantle-normalised trace element trends that are broadly similar to those of most sills with similar TiO_2 contents, but local low-TiO_2 host-rocks (analysed in this study too) exhibit trends that are considerably more depleted in incompatible elements relative to those of comparable low-TiO_2 sills (insets in Fig. 3a; Fig.3b).

Table 2

Whole rock ICP-MS data on trace elements representing basaltic sills of the Faroe Islands (Analyses guided by C. J. Ottley, DU, UK, and analyses by O. Nielsen, GEUS, DK)

	[a]Str. S.				[b]Kv. S.	[c]Lr. S.	[d]Su. S.	[e]Ey. S.				[f]Mn. S.				[g]Sv.-Fu. S.	
Ppm	**07**-JSS-26	**07**-JSS-40	**07**-JSS-52	**07**-JSS-09	**07**-JSS-49	**07**-JSS-50	**08**-JES-01	**08**-JES-08	**08**-JES-10	**08**-JES-11	**08**-JES-19	**08**-JMS-14	**08**-JMS-16	**08**-JMS-17	**16**-JMS-18	**08**-JFS-21	**08**-JSVS-22
Rb	3.81	3.45	1.98	1.42	3.00	3.40	6.71	7.03	10.34	7.14	4.83	0.367	0.321	24.04	1.07	3.50	3.19
Sr	208	215	204	186	185	260	176	176	174	174	180	87.0	85.5	97.9	87.4	220	217
Y	18.8	17.1	18.7	19.4	18.2	34.9	38.9	39.8	38.9	36.6	39.1	27.9	27.4	29.9	27.3	31.2	29.1
Zr	50.8	46.3	50.9	47.4	45.2	173	144	147	142	135	147	57.5	56.9	61.7	58.0	132	123
Nb	2.87	2.61	2.81	2.65	2.47	13.98	11.89	11.81	11.57	10.85	11.73	1.47	1.42	1.54	1.46	11.05	10.47
Ba	59.3	53.8	62.8	47.7	44.9	64.9	77.4	84.4	87.0	76.4	74.0	10.0	7.73	15.8	13.4	47.1	49.4
La	4.24	3.62	4.24	3.50	3.28	11.37	10.37	10.87	10.48	9.38	10.61	1.84	1.72	2.65	1.79	8.76	8.47
Ce	10.28	8.74	10.20	8.55	8.04	29.7	25.7	26.8	26.2	23.2	26.1	5.37	5.20	6.54	5.35	22.4	21.6
Pr	1.60	1.36	1.57	1.34	1.28	4.80	3.99	4.13	4.01	3.60	4.05	0.964	0.961	1.11	1.00	3.59	3.43
Nd	7.40	6.39	7.39	6.48	6.09	22.76	18.80	19.47	18.83	17.34	19.03	5.59	5.71	6.67	5.94	17.22	16.53
Sm	2.04	1.78	2.03	1.86	1.79	6.00	4.98	5.22	5.03	4.63	5.07	2.33	2.39	2.57	2.45	4.61	4.50
Eu	0.757	0.663	0.744	0.719	0.674	1.973	1.642	1.702	1.667	1.545	1.668	0.935	0.941	1.004	0.920	1.532	1.507
Gd	2.57	2.25	2.65	2.57	2.41	7.03	6.14	6.38	6.17	5.63	6.17	3.53	3.47	4.39	3.48	5.45	5.30
Tb	0.457	0.403	0.484	0.464	0.440	1.10	1.02	1.07	1.03	0.945	1.055	0.649	0.664	0.787	0.665	0.900	0.876
Dy	2.84	2.46	2.95	2.93	2.77	6.11	6.15	6.31	6.24	5.70	6.16	4.57	4.59	4.83	4.52	5.15	4.88
Ho	0.634	0.540	0.647	0.654	0.604	1.20	1.28	1.33	1.30	1.18	1.30	0.989	0.993	1.06	0.986	1.04	0.988
Er	1.79	1.54	1.86	1.82	1.80	3.08	3.53	3.68	3.57	3.24	3.51	2.87	2.87	2.95	2.80	2.74	2.64
Yb	1.79	1.56	1.87	1.92	1.75	2.70	3.37	3.45	3.39	3.13	3.39	2.62	2.66	2.90	2.77	2.49	2.36
Lu	0.294	0.254	0.307	0.315	0.294	0.422	0.557	0.554	0.547	0.499	0.550	0.427	0.417	0.475	0.401	0.395	0.380
Hf	1.34	1.17	1.40	1.25	1.21	4.37	3.56	3.67	3.53	3.30	3.63	1.65	1.65	1.81	1.72	3.31	3.07
Ta	0.177	0.150	0.180	0.160	0.158	0.869	0.696	0.707	0.699	0.625	0.697	0.085	0.088	0.105	0.105	0.667	0.636
Pb	0.770	0.730	0.844	0.731	0.681	1.09	1.20	1.23	1.23	1.26	1.22	0.443	0.332	0.336	0.364	0.845	0.900
Th	0.525	0.439	0.526	0.421	0.374	0.854	0.961	0.993	0.949	0.854	0.944	0.153	0.152	0.171	0.163	0.692	0.661
U	0.140	0.127	0.138	0.112	0.111	0.262	0.287	0.287	0.285	0.252	0.284	0.050	0.044	0.050	0.041	0.216	0.208
Nb/Ta	16.21	17.37	15.63	16.53	15.61	16.09	17.09	16.70	16.55	17.36	16.84	17.33	16.08	14.70	16.47	16.57	16.47
[h](Ce/Sm)$_N$	1.25	1.19	1.20	1.12	1.11	1.21	1.27	1.25	1.26	1.25	1.27	0.56	0.53	0.61	1.13	1.19	1.16
[h](Sm/Yb)$_N$	1.24	1.26	1.19	1.09	1.10	2.38	1.59	1.61	1.61	1.60	1.61	0.97	0.98	1.00	2.06	1.97	2.02
[h](Zr/Nd)$_N$	0.82	0.86	0.82	0.87	0.88	0.91	0.91	0.90	0.90	0.93	0.92	1.22	1.19	1.10	1.16	0.92	0.89
[h](Nb/Ce)$_N$	0.71	0.76	0.70	0.79	0.78	1.20	1.18	1.12	1.12	1.19	1.14	0.70	0.70	0.60	0.69	1.26	1.23
[h]Eu/Eu*	1.05	1.05	1.01	1.05	1.05	0.97	0.97	0.95	0.93	0.99	0.96	0.99	1.00	0.95	0.96	0.99	0.97
[h]Sr/Sr*	1.73	2.09	1.71	1.82	1.92	0.73	0.58	0.56	0.57	0.63	0.59	1.14	1.12	1.07	1.11	0.82	0.84

Trace elements in parts per million. [a]Str.S. = Streymoy Sill; [b]Kv.S. = Kvívík Sill; [c]Lr.S. = Langaregn Sill; [d]Su.S. = Sundini Sill; [e]Ey.S. = Eysturoy Sill; [f]Mn.S. = Morskranes Sill; [g]Sv.-Fu.S. = Svínoy-Fugloy Sill; [h]Normalised to primitive mantle (McDonough and Sun, 1995). Eu/Eu* = $(Eu)_N$ / $((Sm + Gd)_N / 2)$ and Sr/Sr* = $(Sr)_N$ / $((Ce + Nd)_N / 2)$. Samples 08-JMS-14, 08-JMS-16 and 16-JMS-18 were analysed at GEUS, DK. The rest were analysed at DU, UK.

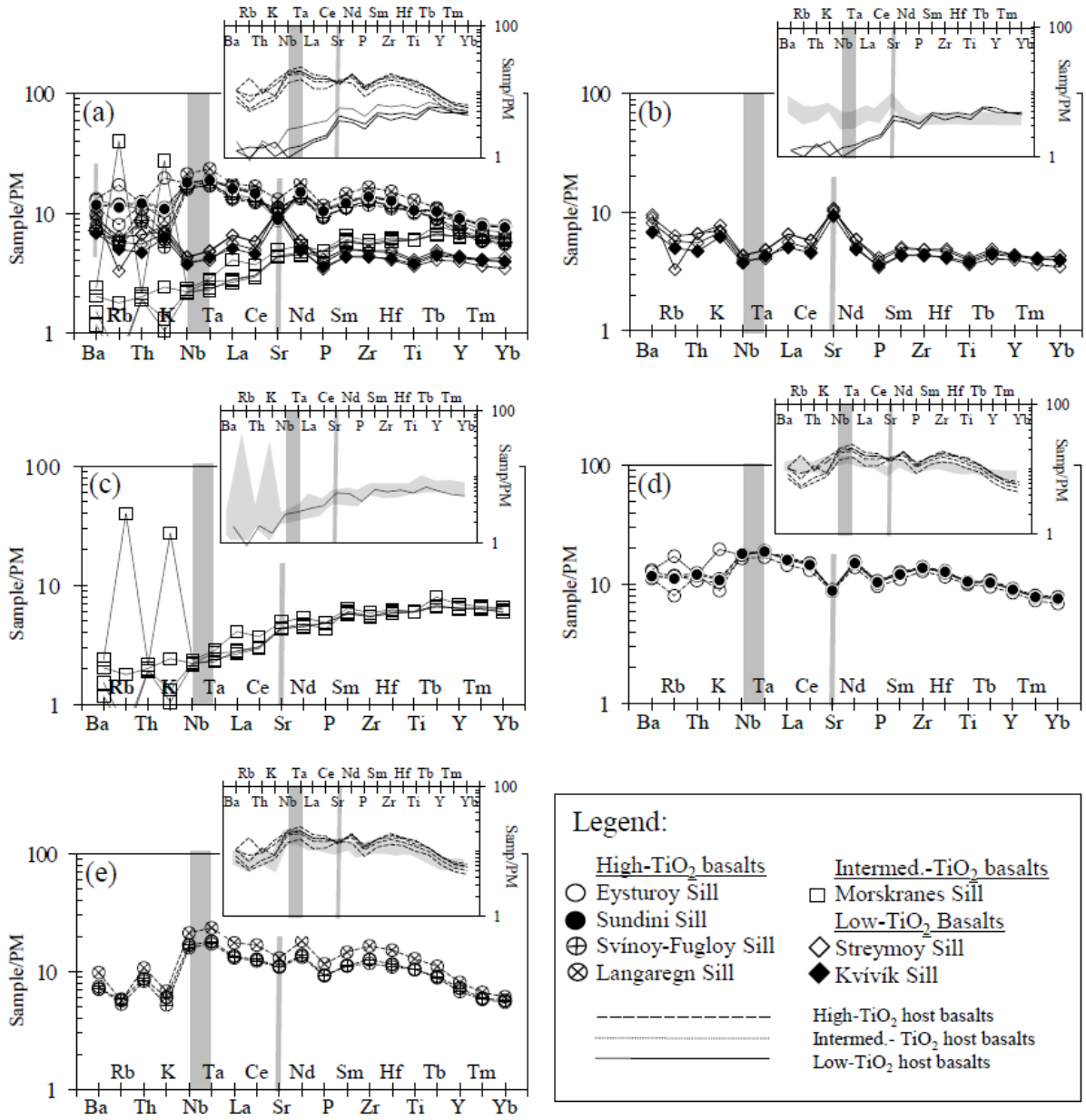

Fig. 3. The diagrams show mantle normalised trace element data from Table 2. a) All sills combined define three main trends. b) Low-TiO_2 sill samples display strong positive Sr and moderately negative Nb and Ta anomalies. d) The intermediate-TiO_2 samples are generally depleted with respect to incompatible elements, but some samples display noticeable enrichment or depletion in Rb and K in particular. d) Most samples from the high-TiO_2 Eysturoy and Sundini sills display negative Sr, Ba,Rb, Th and K anomalies and weak positive Nb and Ta anomalies. e) Samples representing the high-TiO_2 Svínoy-Fugloy and Langaregn sills display moderately negative Sr and positive Nb and Ta anomalies, while their Ba,Rb, Th and K contents are depleted to various degrees. All sills display negative P anomalies. Trace elements of selected local host-rocks, as shown in Supplement 3 below, are plotted in insets attached to the main plots, in where their TiO_2 contents are identical to those of their attached main sill plots. Semi-transparent grey fields in all insets represent multi-element ranges from the main diagrams. Normalising mantle values are from McDonough and Sun (1995).

4.3.3. REE

Mantle-normalised REE data representing 17 sill samples (Table 2; Fig. 4) define three main tendencies. The low-TiO_2 and high-TiO_2 sills (excluding the Langaregn Sill) display moderately negatively sloping LREE trends with $(Ce/Sm)_N$ ratios ranging from 1.11 to 1.27. The low-TiO_2 sills also display relatively flat negative HREE slopes with $(Sm/Yb)_N$ ratios ranging from 1.09 to 1.26. The samples representing the high-TiO_2 sills are characterised by steeper negative HREE slopes that can be further categorised into three sub-trends, where $(Sm/Yb)_N$ ratios for the Eysturoy and Sundini sills range from 1.59 to 1.61 and from 1.97 to 2.02 for the Svínoy-Fugloy Sill compared to 2.38 for the Langaregn Sill. The Morskranes Sill is LREE depleted with an average $(Ce/Sm)_N$ ratio of ~0.6, but displays a flat HREE trend with an average $(Sm/Yb)_N$ ratio of ~1. Local low-TiO_2 basaltic host-rock samples (analysed in this study) display relatively steep positive LREE and MREE slopes in contrast to the gentle negative slopes for these same elements representing comparable low-TiO_2 sill samples. Local high-TiO_2 host-rocks (analysed in this study and shown in Supplement 3 below) display positive LREE slopes, which is slightly at odds with the relatively flat negative slopes for these same elements that represent comparable high-TiO_2 sill samples, when the Langaregn Sill is excluded (insets in Fig. 4b; Fig. 4e). The REE trends of the low-TiO_2 local host-rock samples analysed in this study are virtually identical to those of local MgO-rich (including picritic) low TiO_2 host-rock samples reported in earlier studies as outlined below, but are much more depleted in their LREE and MREE compared to the low-TiO_2 samples (Fig.4c). Intermediate-TiO_2 sill samples are almost identical to those of comparable local host-rocks (Fig. 4d).

With respect to published REE data on local host-rocks, low-TiO_2 dykes (0.75-1.75 wt % TiO_2) generally display flat or MORB-like depleted trends with $(La/Sm)_N$ = 0.4-1.2 and $(Sm/Yb)_N$ = 0.5-1.15; intermediate-TiO_2 dykes (1.45-2.45 wt % TiO_2) display $(La/Sm)_N$ = 1.0 – 1.6 and $(Sm/Yb)_N$ = 1.35-2.35 while high-TiO_2 dykes (2.6-3.8 wt % TiO_2) display $(La/Sm)_N$ = 1.25-1.75 and $(Sm/Yb)_N$ = 1.95-2.65 (Holm et al., 2001). Lava flows of the Beinisvørð Formation (exposed above sea level) and the Malinstindur Formation are LREE enriched ($(La/Yb)_N$ = 1.4-3.3) with a relatively wide range in overall REE concentrations, whereas some parts of the Enni Formation display depleted MORB-like LREE trends with $(La/Yb)_N$ = 0.45-0.62 (Gariépy et al., 1983).

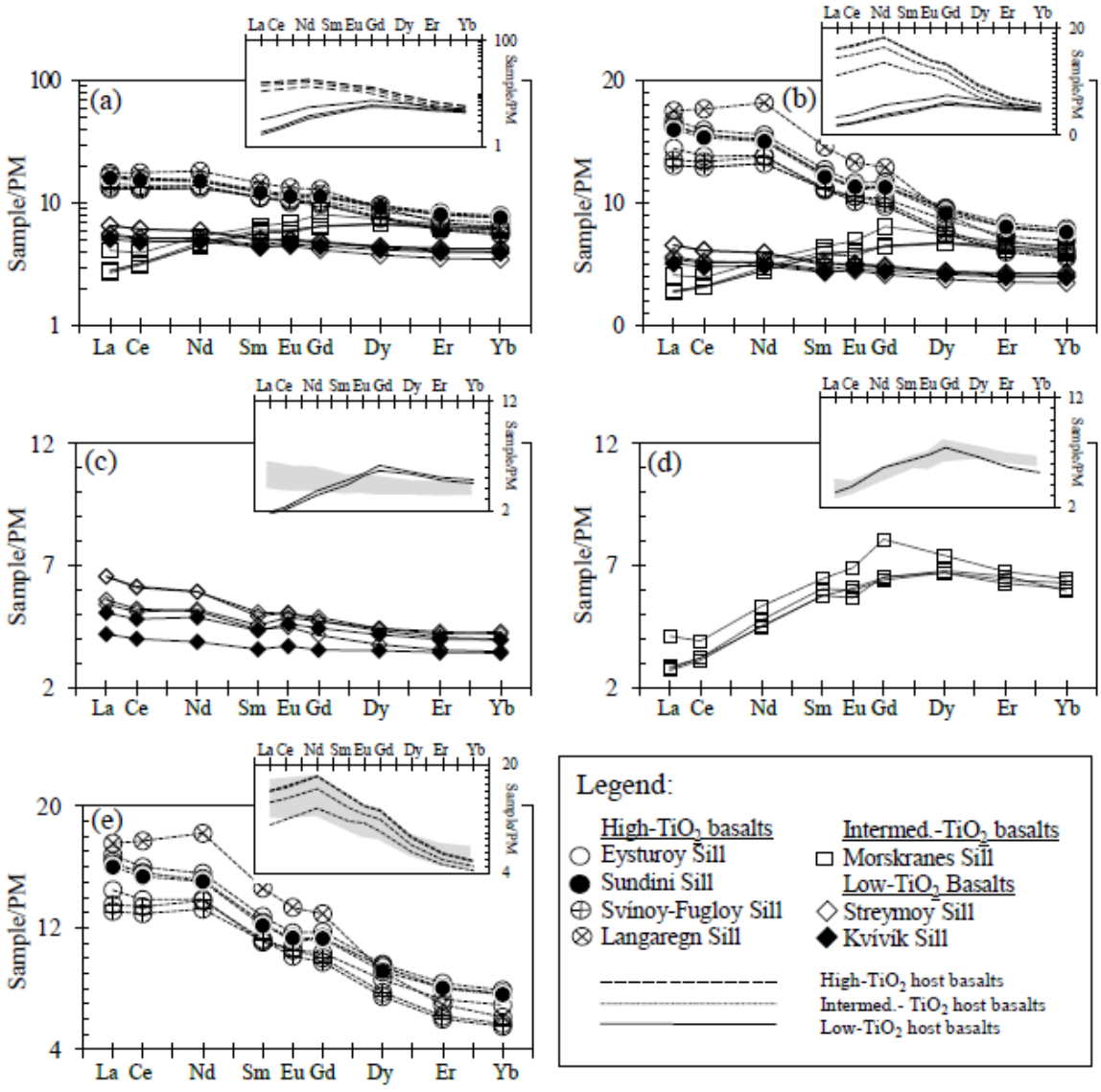

Fig. 4. The diagrams show mantle normalised REE data from Table 2. a) In these logarithmic plots, the REE data of Faroese sills define the same three main categories as those detected in Fig. 2 and Fig. 3. b) Low-TiO_2 and intermediate TiO_2 Faroese sills plotted with linear scale on y axis. Samples of the low-TiO_2 sills display very gentle negative slopes/trends while intermediate TiO_2 samples display depletion with respect to their LREE and MREE. c) Most high-TiO_2 Faroese sills display relatively gentle negative trends/slopes (linear scale on y axis). Insets represent the same local host rocks from Supplement 3 below, as those shown in Fig. 3. Semi-transparent grey fields in all insets of Fig. 4, represent sill samples from the main diagrams, i.e. they possess TiO_2 compositions identical to those of the host-rocks. Normalising mantle values are from McDonough and Sun (1995).

4.4. Isotopes

4.4.1. Sr and Nd isotopes

On the assumption that all sills were emplaced broadly contemporaneously and are slightly younger than the ~55 Ma determined for the uppermost parts of the host lava pile, the

eight samples from seven sills analysed for Sr and Nd isotopes were age corrected to 54 Ma (Table 3; Fig. 5). The $^{87}Sr/^{86}Sr(t)$ ratios of the sills range from 0.7028 to 0.7033, while their $^{143}Nd/^{144}Nd(t)$ ratios range from 0.512910 to 0.512976 (Nd(t) range from 6.7 to 7.9). When these isotope data are displayed graphically, they define a negative slope, but they plot in two separate main clusters with two samples of the intermediate-TiO_2 Morskranes Sill displaying a $^{87}Sr/^{86}Sr(t)$ range from 0.7028 to 0.7029 and a $^{143}Nd/^{144}Nd(t)$ range from 0.512966 to 0.512976 compared to ranges of 0.7032 to 0.7033 and 0.51291 to 0.51296 respectively for the six samples representing low-TiO_2 and high-TiO_2 sills (Fig. 5a). The sill Sr and Nd isotope ranges plot entirely within ranges for similar isotopes reported for samples representing other basaltic rocks of the Faroe Islands, and partly within those Sr and Nd isotopic ranges reported for Icelandic samples (inset in Fig. 5a).

4.4.2. Lead isotopes

Lead isotopes were determined on 13 samples representing 7 Faroese sills (Table 3; Fig. 5). Total measured $^{206}Pb/^{204}Pb$ ratios range from ~17.89 to ~18.48, the measured total $^{207}Pb/^{204}Pb$ ratios range from ~15.39 to ~15.48 while total measured $^{208}Pb/^{204}Pb$ ratios span from ~37.85 to ~38.31. Similar to the Sr and Nd isotopes representing Faroese sills, lead isotope ratios of samples representing Faroese sills define two main fields, where the intermediate-TiO_2 Morskranes Sill defines one field and all the remaining Faroese sills define another field. The Morskranes Sill displays Pb isotope ratio ranges of $^{206}Pb/^{204}Pb$ = 17.89-17.98; $^{207}Pb/^{204}Pb$ = 15.39-15.45 and $^{208}Pb/^{204}Pb$ = 37.85-38.02 compared to ranges of $^{206}Pb/^{204}Pb$ = 18.23-18.48; $^{207}Pb/^{204}Pb$ = 15.43-15.48 and $^{208}Pb/^{204}Pb$ = 38.17-38.31 for the remaining sills, i.e. the Morskranes Sill displays larger spread in $^{207}Pb/^{204}Pb$ and $^{208}Pb/^{204}Pb$ ratios than all the remaining sills combined (Fig. 5b-d). Both of these two sill categories define perfectly linear (but different) trends in $^{206}Pb/^{204}Pb$ versus $^{208}Pb/^{204}Pb$ plots (Fig. 5c), while some (three) samples of the Morskranes Sill in particular as well as samples representing the Eysturoy and Sundini sills are shifted towards higher $^{207}Pb/^{204}Pb$ ratios in $^{206}Pb/^{204}Pb$ versus $^{207}Pb/^{204}Pb$ and $^{207}Pb/^{204}Pb$ versus $^{208}Pb/^{204}Pb$ ratio plots (Fig. 5b; Fig. 5d). The values of lead isotope ratios of all Faroese sills combined generally plot within fields delineating similar isotope ratios representing other basaltic rocks of the Faroe Islands, E Greenland and Iceland (insets in Fig. 5b-d). An overview on measured versus age corrected (at 54 Ma) lead isotopes from samples representing Faroese sills is presented in Supplement 4 below.

Table 3

Whole rock MC-ICP-MS isotope data representing basaltic sills of the Faroe Islands (Analysed by Geoff Nowell, DU, UK, and Robert Frey, CU, DK)

Samples	$^{206/204}$Pb	$^{207/204}$Pb	$^{208/204}$Pb	$^{208/206}$Pb	Pb	Rb	Sr	$^{87/86}$Sr	^{87}Rb/^{86}Sr	$^{87/86}$Sr (t)	Sm	Nd	$^{143/144}$Nd (0)	^{147}Sm/^{144}Nd	$^{143/144}$Nd (t)	εNd (t)
08-JSVS-22	[a]18.3736	[b]15.4482	[c]38.2266	[d]2.0804	0.85	3.19	217	[e]0.703306	[f]0.060346	0.703260	4.52	16.5	[g]0.512987	[h]0.211594	0.512912	6.7
07-JSS-49	[i]18.4802	[j]15.4765	[k]38.3115	[l]2.0731	0.68	3.00	185	[e]0.703255	[f]0.066592	0.703204	1.79	6.09	[g]0.513032	[h]0.223383	0.512953	7.5
07-JSS-50	[a]18.2326	[b]15.4246	[c]38.1692	[d]2.0935	1.08	3.40	259	[e]0.703266	[f]0.053838	0.703225	5.93	22.80	[g]0.512999	[h]0.201413	0.512928	7.0
07-JSS-52	[a]18.4444	[b]15.4756	[c]38.2700	[d]2.0749	0.85	1.98	203	[e]0.703313	[f]0.039892	0.703282	2.06	7.39	[g]0.513023	[h]0.215840	0.512947	7.4
08-JES-01	[a]18.2442	[b]15.4493	[c]38.1727	[d]2.0922	1.19	6.71	176	[e]0.703308	[f]0.156658	0.703188	4.93	18.80	[g]0.512986	[h]0.202623	0.512914	6.8
08-JES-10	[a]18.2501	[b]15.4493	[c]38.1765	[d]2.0919	1.28	10.30	174	[e]0.703380	[f]0.244165	0.703193	5.02	18.80	[g]0.512983	[h]0.206201	0.512910	6.7
08-JMS-14	[a]17.9131	[b]15.4536	[c]37.8876	[d]2.1150	0.44	0.37	87	[e]0.702895	[f]0.129173	0.702796	2.33	5.59	[g]0.513086	[h]0.312780	0.512976	7.9
16-JMS-14	[i]17.8932	[j]15.4525	[k]37.8611	[l]2.1160	0.44	-----	-----	----------	----------	----------	-----	-----	----------	----------	----------	-----
08-JMS-16	[i]17.9314	[j]15.3916	[k]37.9184	[l]2.1146	0.33	-----	-----	----------	----------	----------	-----	-----	----------	----------	----------	-----
08-JMS-17	[a]17.9505	[b]15.4086	[c]37.9737	[d]2.1153	0.32	24.00	98	[e]0.703693	[f]1.008897	0.702919	2.62	6.67	[g]0.513073	[h]0.303742	0.512966	7.8
16-JMS-18	[i]17.9825	[j]15.4315	[k]38.0194	[l]2.1143	0.36	-----	-----	----------	----------	----------	-----	-----	----------	----------	----------	-----
16-JMS-19	[i]17.9490	[j]15.3901	[k]37.9272	----------	-----	-----	-----	----------	----------	----------	-----	-----	----------	----------	----------	-----
16-JMS-20	[i]17.8862	[j]15.3878	[k]37.8542	----------	-----	-----	-----	----------	----------	----------	-----	-----	----------	----------	----------	-----

(t) refer to Sr and Nd isotopic ratios corrected back to 54 Ma; [a]2SE range from 0.0013 to 0.0053; [b]2SE range from 0.0015 to 0.0051; [c]2SE range from 0.0049 to 0.0190; [d]2SE range from 0.0001 to 0.0005; [e]2SE range from 0.000013 to 0.000023; [f]calculated ratios; [g]2SE range from 0.000006 to 0.000014; [h]calculated ratios; [i]2SE range from 0.0215 to 0.0314; [j]2SE range from 0.02 to 0.0277; [k]2SE range from 0.0515 to 0.0702; [l]2SE range from 0.0008 to 0.0013. Decay constants: $^{87}Rb \rightarrow {}^{87}Sr = 1.42\times10^{-11}$ yr^{-1} (Steiger and Jäger, 1977) and $^{147}Sm \rightarrow {}^{143}Nd = 6.54\times10^{-12}$ yr^{-1} (Lugmair and Marti, 1978). The bulk of the analyses were carried out at Durham University, UK, while lead isotopes for samples 07-JSS-49, 16-JMS-14, 08-JMS-16, 16-JMS-18, 16-JMS-19 and 16-JMS-20 were analysed at Copenhagen University, DK.

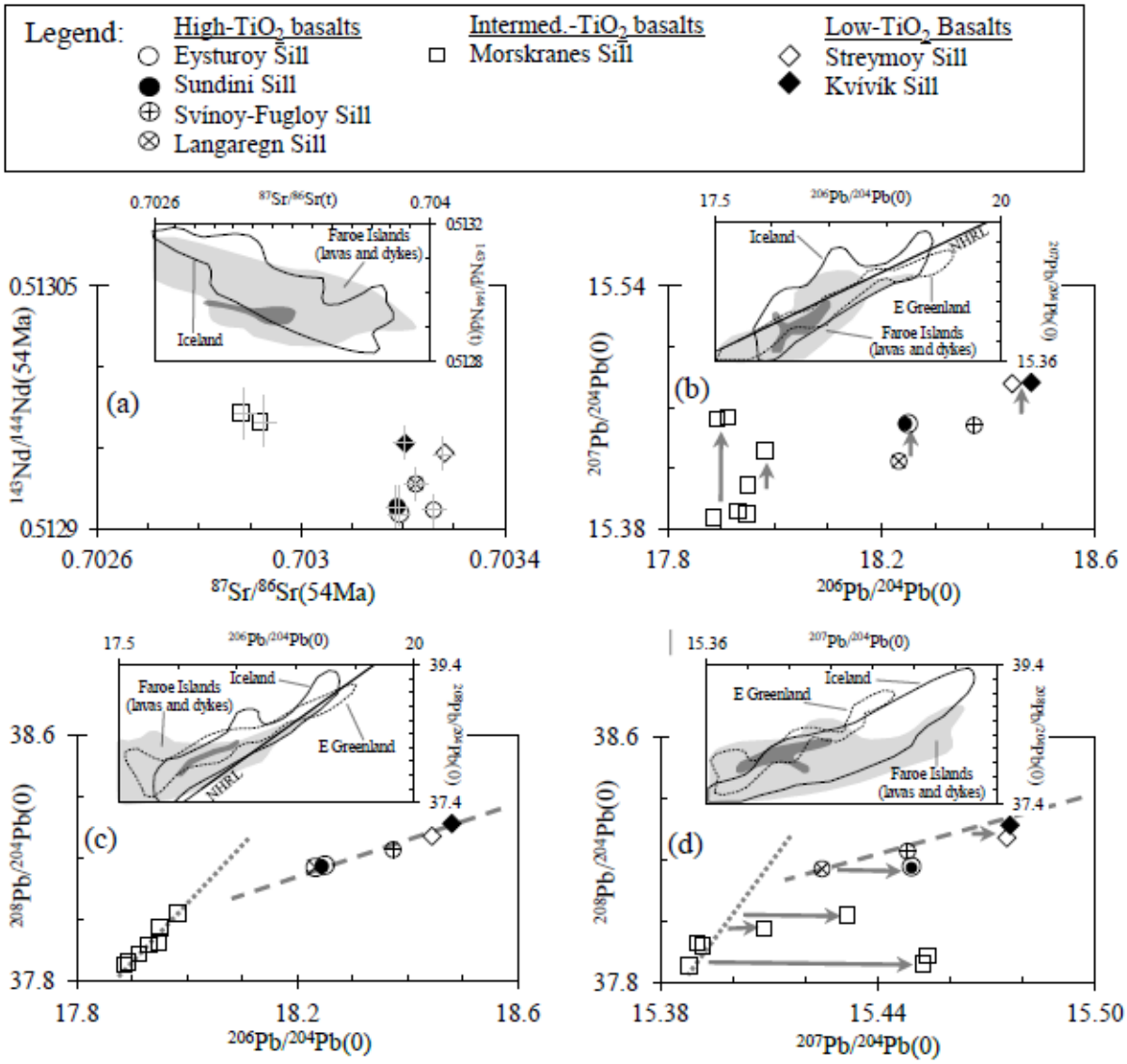

Fig. 5. The diagrams show isotope data from Table 3. a) Age-corrected (to 54 Ma) $^{87}Sr/^{86}Sr$ versus $^{143}Nd/^{144}Nd$ ratios, representing the actual sill samples, define two main clusters with high-TiO_2 and low-TiO_2 sill samples combined in one and intermediate-TiO_2 sill samples in another. 2SE analytical errors are indicated by vertical and horizontal semi-transparent bars. b), c) and d) It is noticeable that, while Faroese sill samples define two perfectly linear trends in $^{206}Pb/^{204}Pb$ versus $^{208}Pb/^{204}Pb$ ratio plots for the same groups/clusters as shown in diagram a), some samples of the Morskranes Sill and a few samples of the Eysturoy and Sundini sills display relative enrichments in $^{207}Pb/^{204}Pb$ ratios (see main text). The insets show isotopic compositions of Faroese sills (darker shaded fields) contrasted against those of other Faroese basaltic rocks (from Holm et al., 2001; Søager and Holm, 2009, 2011), against those of Icelandic basaltic rocks (from Mertz and Haase, 1997; Stracke et al., 2003; Thirlwall et al., 2004; Kokfeldt et al., 2006) and against those of basaltic rocks from Central East Greenland (from Søager and Holm, 2011). (t) and (0) at diagram axes refer to age corrected and measured isotope ratios respectively.

5. Discussion

5.1. Element mobility

The reliability of geochemical data as petrogenetic indicators must be evaluated carefully, as igneous rocks exposed at the Earth's surface commonly experience post-magmatic mineral break-down and associated mobilisation of major and trace elements, in addition to recrystallisation (e.g. Rollinson, 1998). Major elements like Si, Mg and K and large ion lithophile elements (LILE) may be mobilised by low-grade metamorphism or weathering (Wood et al., 1976; Higgins et al., 1985; Babechuk et al., 2014), while high field strength elements (HFSE) such as Th, Nb, Ta, Zr, Y and Ti commonly remain relatively unaffected during low or moderate grades of metamorphism (Wood et al., 1976; Babechuk et al., 2014).

Some of the investigated Faroese sill samples display evidences of element mobilisation at the microscopic (single grain) scale, including minute olivine grains being partially or entirely altered to phyllosilicates (see details on petrography in Supplement 1 below). Greenish coatings occurring in <0.5 mm wide joints represent low-temperature hydrous minerals, and suggest element mobilisation at the whole-rock scale within some parts of these intrusions. For instance, comparison between the slightly jointed sill sample 07-JSS-38 and another fresh/intact sill sample 09-JSS-02 (Table 1), collected less than 100 metres apart within the Streymoy Sill, illustrates these effects of element mobilisation and geochemical modification. Sample 07-JSS-38 is relatively depleted in Si, Al, K, Sr and Ba and relatively enriched in Mg, Fe, Ti and Y. A relative enrichment in Ti and Y thus may indicate the relative immobility of Ti and Y in the more weathering-resistant phases such as Fe-Ti oxides and/or clinopyroxene. Accordingly, for the purposes of petrogenetic investigation, only samples without signs of element mobilisation have been utilised in this work.

5.2. Crustal contamination

5.2.1. Geochemical constraints on crustal contamination

The incorporation of crustal materials into magmas en-route to the upper crust is commonly attributed to bulk assimilation with concomitant fractional crystallisation or to net assimilation of the most fusible crustal materials (e.g. Thompson et al., 1983; Kerr et al., 1995; Font et al., 2008).

Since no geochemical data are available for the continental basement underneath the Faroese lava succession, samples representing Proterozoic/Archaean continental basements from NW Britain, the Rockall Plateau and E Greenland were utilised to evaluate potential crustal contamination of precursor melts to Faroese basaltic rocks. In theory, less than 4-5 % bulk assimilation of material similar to average basement composition for E Greenland, NW Britain and the Rockall Plateau would be required in order to shift $(Zr/Nd)_N$ and $(Nb/Ce)_N$ ratios from those of typical N-MORB and E-MORB to those representing intermediate-TiO_2 and high-TiO_2 Faroese sills respectively (Fig. 6). Substantially less assimilated basement material would be required to account for the internal variations in these elements displayed by the Faroese low-TiO_2 and high-TiO_2 sills. Around 5 % crustal assimilation by Faroese sills appears quite unrealistic based on bulk geochemistry and would become apparent from additional isotopic evidences. The pronounced positive Rb and K anomalies displayed by one sample of the Morskranes Sill (Fig. 3a; Fig. 3c) seem to indicate selective enrichment in these elements. In theory, K-rich material could originate from residual mantle melts, or else from small-scale melting of suitable sources; but such melts also tend to be SiO_2 and Na_2O enriched (e.g. Spulber and Rutherford, 1983). Given the relative depletion of these two major elements within this sample (Table 2) such scenario is unlikely. Hence, potential enrichment candidates may include net assimilation of crustal materials or perhaps LILE-rich metasomatic fluids leached from other adjacent basalts (i.e. secondary processes like the infilling of vesicles), which would also be in accordance with negative Rb and K anomalies displayed by many Faroese sill samples of all TiO_2 compositions (Fig. 4).

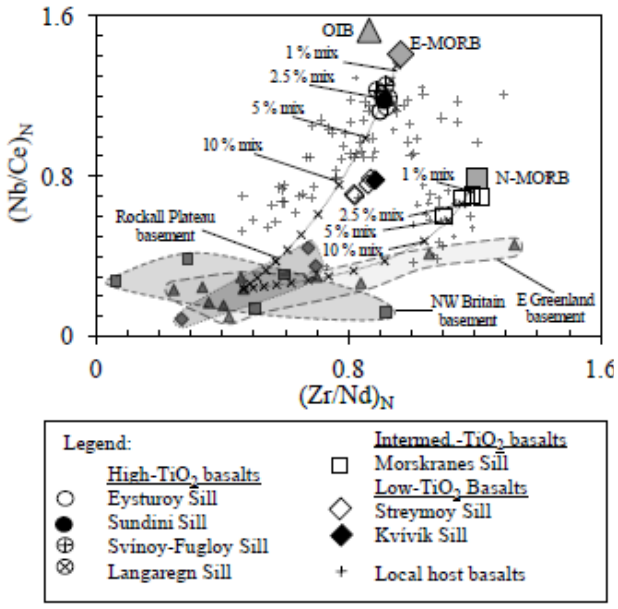

Fig. 6. Intermediate-TiO_2 and high-TiO_2 sill samples plot close to representative N-MORB and E-MORB specimens respectively in this $(Zr/Nd)_N$ versus $(Nb/Ce)_N$ diagram. Around 1 to 2.5 % contributions to the N-MORB with materials comparable to average N Atlandic basement could in theory account for most of the range in trace element ratios of the intermediate-TiO_2 sill shown in this diagram, while around 2 to 3 % addition to the E-MORB with the same materials could in theory account for the range in the trace element ratios displayed by the high-TiO_2 sills. OIB, E-MORB and N-MORB data are from Sun and McDonough (1989); basement data on E Greenland from Kays et al. (1989), Kalsbeek (1995) and Thrane (2002); on NW Britain basement data from Weaver and Tarney (1980), Thompson et al. (1986), Kerr et al. (1995) and Meyer et al. (2009); on Rockall Plateau data from Morton and Taylor (1991). Data on Faroese host-rocks are from Hald and Waagstein (1984); Holm et al. (2001); Søager and Holm (2009, 2011) and from this study (Supplement 3 below). Normalising mantle values are from McDonough and Sun (1995). Datasets on calculated mixing trends are shown in: Hansen et al. (2019).

5.2.2. Isotopic constraints on potential crustal contamination

The Pb isotopic compositions of presumed uncontaminated Faroese basaltic rocks compared with those of local contaminated basaltic lavas, of the Enni Formation, indicate involvement of two contamination sources characterised by different $^{208}Pb/^{204}Pb$ ratios in particular, but also with various $^{207}Pb/^{204}Pb$ ratios (Fig. 7b-d). While the low $^{208}Pb/^{204}Pb$ contaminated samples could owe their Pb isotopic characteristics to assimilation of materials comparable to those reported for felsic and intermediate granulites or amphibolitic gneisses from E Greenland and NW Britain, the contaminated basalts with higher $^{208}Pb/^{204}Pb$ ratios most likely assimilated felsic or intermediate materials with Pb isotopic compositions corresponding to those of basement samples reported for E Greenland (Fig. 7b-d). If precursor melts to the contaminated Faroese basalts (silicic basalts) originally possessed Sr and Nd isotopic compositions similar to those of the present-day MgO-rich Faroese dykes (e.g. sample Sv-12 of Holm et al., 2001), then between 10 and 20 % assimilation of materials similar to representative Proterozoic/Archean continental basement samples from E Greenland or NW Britain would be required in order to modify them to the isotopic range currently measured for these contaminated basalts (Fig. 7a).

Gariépy et al. (1983) and Holm et al. (2001) attributed the enriched isotopic signatures of these contaminated Faroese basalts to contamination with continental basement material possessing isotopic characteristics comparable to Lewisian amphibolites. Alternatively, Søager and Holm (2011) suggested that the isotopic compositions of these contaminated Faroese basalts pointed to the probable existence of two distinct contamination sources beneath the archipelago, which possessed isotopic characteristics similar to basement material recorded for E Greenland earlier. Our results above, suggesting 10 to 20 %

assimilation of crustal material for the entire isotopic range displayed by these basalts, are in good accordance with the 12-13 % assimilation of crustal material calculated for one of these contaminated basalt samples by Søager and Holm (2011).

At present, it is un-clear whether the noticeable variations in $^{207}Pb/^{204}Pb$ ratios between some samples of the small Morskranes Sill, as well as those within the Eysturoy and Sundini sills (Fig. 5b, Fig. 5d), reflect characteristics inherited from their mantle source(s), or if contamination with crustal materials is the most likely source. Indeed, noticeable differences in Pb isotopic compositions between melt inclusions and crystals versus their host phenocrysts and matrix respectively (thought to reflect isotopic heterogeneities at short length scales in their mantle sources) have been measured at a number of sites worldwide (Saal et al., 1998; Bryce and DePaolo, 2004). However, it is noticeable that samples of the Morskranes Sill with decreasing $^{207}Pb/^{204}Pb$ ratios also display increasing MgO contents (e.g. samples: 08-JMS-14 $\rightarrow$ 16-JMS-18 $\rightarrow$ 08-JMS-16 display increasing MgO contents and decreasing $^{207}Pb/^{204}Pb$ ratios in direction of arrows), i.e. Table 1; Table 3.

If assimilation indeed modified the Pb isotopic composition of the Morskranes Sill in particular and (to a lesser degree) that of the Eysturoy and Sundini sills, minor involvement of crustal materials with Pb isotopic compositions comparable to those of basement samples of the Rockall Plateau and of E Greenland could be an explanation (inset in Fig. 7b). In this context, it is worth noting that isotopic compositions of Rockall granites led Faure (2001) to conclude that there existed a genetic relationship between Rockall granites and alkali-rich intrusives of E Greenland. The inset in Fig. 7d does not conclusively point to any particular of the three potential contamination sources, discussed in this sub-Sect.

If variations in Sr and Nd isotopic ratios of Faroese sill samples reflect assimilation of crustal material into their precursor melts, then less than 0.5 % contamination with basement materials comparable to those of E Greenland and NW Britain would be required in order to shift the Nd isotopic compositions from those of the Faroese LREE depleted MgO-rich lava/dyke samples to those of LREE depleted samples of the Morskranes Sill (inset in Fig. 7a). In theory, the Sr and Nd isotopic variations within high-TiO_2 and low-TiO_2 sills of this study, as well as Sr and Nd isotopic differences between high-TiO_2 and low-TiO_2 sills versus intermediate-TiO_2 sill samples, could have been generated by $\leq$ 0.25 % assimilation of materials comparable to those of Proterozoic/Archean continental basement material from E Greenland, Rockall Plateau or NW Britain (e.g. Fig. 7a including inset).

To summarise, the isotopic compositions of the contaminated silicic basalts of the Faroe Islands together with some samples of the Morskranes Sill in particular (if differences in their isotopic signatures are not source related) suggest that at least three distinct crustal contamination sources could have affected their precursor melts during ascent through the local palaeo crust (Fig. 5; Fig. 7).

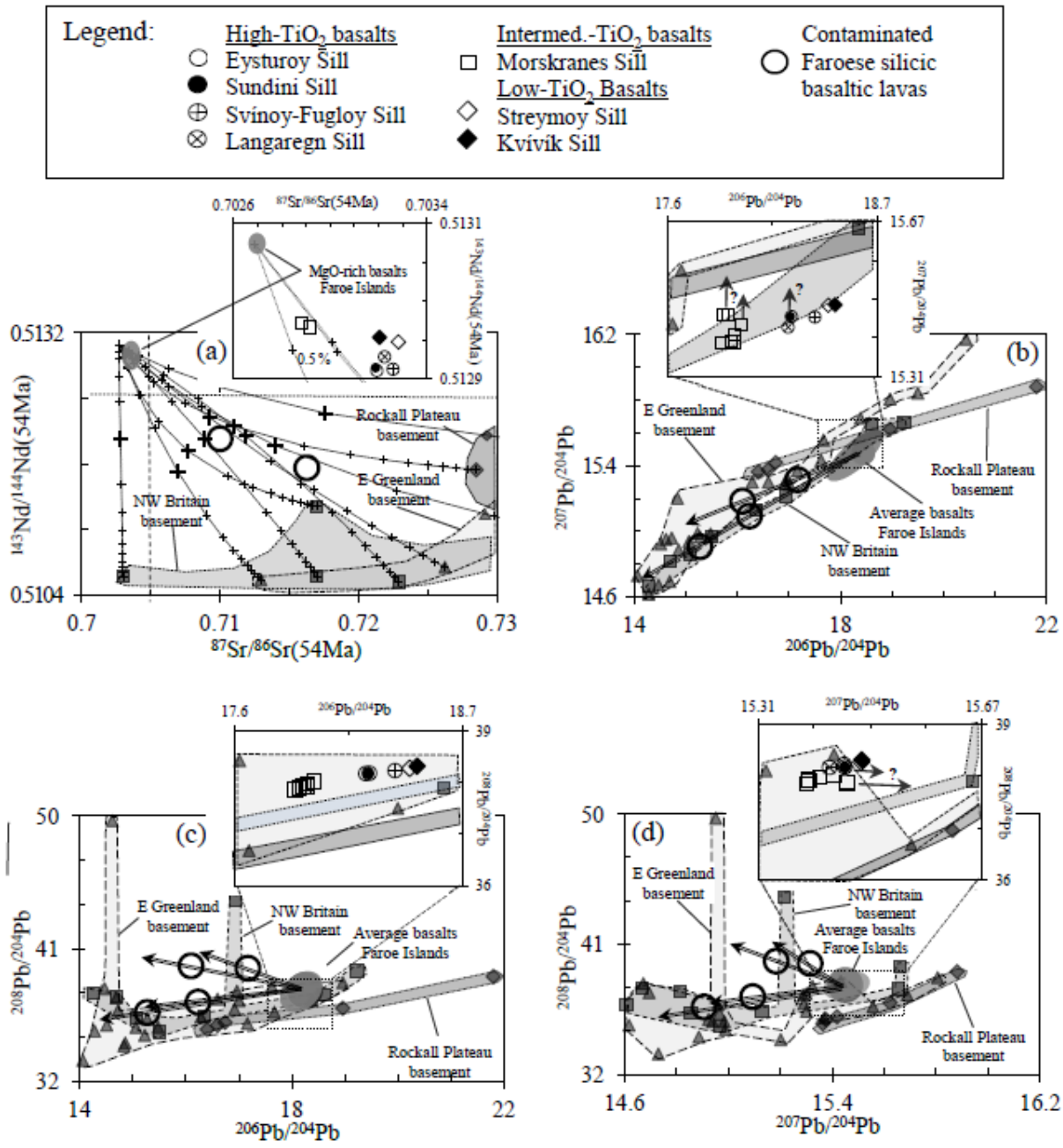

Fig. 7. Sr, Nd and Pb isotopes, representing average Faroese basaltic rock samples, contaminated Faroese silicic basaltic samples as well as sill samples from this study (darkest shaded fields), are contrasted against Proterozoic/Archaean N Atlantic basement samples. a) Age corrected (at 54 Ma) Sr and Nd isotopic ratios. Between 10 and 20 % contributions from N Atlantic basement materials (NW Britain or E Greenland) to

average Faroese basalts (dark shaded field) can explain the Sr and Nd isotopic compositions of local contaminated silicic basalts. Each of the large crosses on mixing curves indicates 10 % contamination. Contributions with roughly 0.5 % of average E Greenland and/or NW Britain basement sources to relatively primitive Faroese basalts could in theory explain some of the Sr and Nd isotopic variations of Faroese sill samples (inset). b), c) and d) Measured Pb isotopic ratios. Two distinct contamination sources are required in order to explain the configuration of contaminated silicic basalts versus average Faroese basalts namely, one purely E Greenland-like basement source and one E Greenland-like and/or NW Britain-like basement source. Arrows point towards Pb isotope compositions of their probable contamination sources. Contamination with materials similar to those of the Rockall Plateau and those of E Greenland could explain variations of Pb isotope ratios of some samples of the Morskranes Sill, if these heterogeneities were not inherited from their mantle source (insets). Basement data for E Greenland are from Kays et al. (1989), Blichert-Toft et al. (1992) and Taylor et al. (1992); NW Britain basement data are from Dickin (1981), Thompson et al. (1986), Kerr et al. (1995), Geldmacher et al. (1998), Troll et al. (2004) and Meyer et al. (2009); Rockall Plateau basement data are from Morton and Taylor (1991). Datasets on calculated mixing trends in a) are shown in: Hansen et al. (2019).

5.2.3. Implications from mixing calculations

Calculations (not shown) show that basaltic rocks with initial Pb concentrations of ~0.5 ppm and initial average $^{208}Pb/^{204}Pb$ ratios of ~38 that experience ~0.5 % assimilation of basement material with Pb concentrations of ~15 ppm and $^{208}Pb/^{204}Pb$ ratios being ~5 higher and lower respectively than those of the target basalts (i.e. $^{208}Pb/^{204}Pb$ ratios of ~43 and ~33 respectively) will experience an increase and decrease of ~0.65 in their $^{208}Pb/^{204}Pb$ ratios to ~38.65 and ~37.35 respectively. Accordingly, contributions with fractions of a percent of high or low $^{208}Pb/^{204}Pb$ basement materials comparable to some of those reported for E Greenland (e.g. samples KS 60 and 229642 of Kays et al., 1989 and Taylor et al., 1992 respectively) to melts comparable to Faroese dykes or lavas (i.e. Holm et al., 2001; Søager and Holm, 2011) could account for the poor correlation between their $^{208}Pb/^{204}Pb$ ratio plots. The same would apply for basaltic rock samples from Iceland and E Greenland (e.g. insets in Fig. 5c; Fig. 5d). A relatively recent study based on geochemistry and isotopes suggested that low-TiO_2 tholeiitic Faroese lavas with the highest probabilities of contamination would require less than 1 % contributions with crustal components if they assimilated local continental material (Søager and Holm, 2011). Similar arguments on potential contamination in low-TiO_2 basalts of E Greenland were made by Waight and Baker (2012). Collectively, the results of this sub-Sect. suggest that parts of the Morskranes Sill could have been affected by crustal contamination, while it is somewhat more uncertain if the high-TiO_2 and low-TiO_2 sills were affected as well. Small-scale crustal contamination of these two latter sill categories would probably have resulted in slightly elevated La and Ce values, but assimilation of ≤ 1 %

crustal components would hardly be detectable in normalised REE diagrams (e.g. Hansen, 2011) and cannot account for the observed differences between LREE in sills versus their host-rocks with similar TiO_2 compositions (e.g. Fig. 4).

5.3. Fractional crystallisation and accumulation

5.3.1. Constraints on Faroese tholeiite formation from fractional crystallisation

MgO-rich primary basaltic melts typically evolve to less magnesian varieties by fractional crystallisation of olivine (Yaxley, 2000). Further melt modifications may occur in response to e.g. plagioclase, clinopyroxene or garnet fractionation (Hald and Waagstein, 1991; Bernstein, 1994). Basaltic magmas can also evolve in response to complex RTF processes (e.g. Sect. 1; O'Hara and Mathews, 1981; Larsen and Pedersen, 2009).

Around 15 wt % olivine fractionation combined with minor amounts of fractionated magnetite and ilmenite from MgO-rich melts, which are geochemically similar to selected Faroese picrites (MgO-rich [picrite] sample Ey-129 from Holm et al., 2001), will generate tholeiitic melts with SiO_2, MgO and K_2O values comparable to those of samples from the Morskranes Sill. Values for the other calculated major elements resemble those of low-TiO_2 and high-TiO_2 Faroese sills (Table 1; Table 4). Additional fractionation of clinopyroxene with typical SiO_2 values of 51 to 54 wt % (e.g. Deer et al., 1992; Falloon et al., 1999; Dasgupta et al., 2007) from the same MgO-rich magmas would result in silica depletion, thus requiring compensation by further Fe – Ti oxide fractionation, which in turn would result in unrealistically low Fe_2O_3 and TiO_2 values in the calculated melts. In addition, the average Sc concentrations in samples representing the Faroese sills are broadly similar to the average concentrations of this element in local picrites and local MgO-rich olivine basaltic dykes. Hence, it is not likely that clinopyroxene was a dominating fractionating phase during early stages of magmatic evolution of melts that gave rise to most Faroese sills, if the geochemical compositions of their primary melts resembled those of local picrites. Moreover, the similarities in Sc concentrations between sills and local picrites also argue against any noticeable fractionation of garnet, provided that the picrites and primary melts that developed to the Faroese sills displayed matching compositions.

5.3.2. Trace element constraints on fractional crystallisation and assimilation

While the pronounced positive Sr anomalies displayed by samples of the low-TiO_2 Streymoy – Kvívík sills and the likewise conspicuous negative Sr anomalies of the high-TiO_2

Eysturoy - Sundini sills (Fig. 3) clearly indicate the involvement of plagioclase at some point during melt evolution, there remains a slight uncertainty regarding the reliability of the weak Eu anomalies of samples from these same sills (Fig. 4) given the small sizes of these compared to analytical error. Olivine fractionation and accumulation from/to modelled primitive basaltic melts (partition coefficients and the equation used are shown in Supplement 5 below) do not result in noticeable changes of their Sr/Sr* and Eu/Eu* ratios (definitions outlined in caption to Table 2), but around 15 wt % fractionated olivine in combination with minor amounts of fractionated magnetite and ilmenite would increase their Nb, Ta, Er and Y concentrations slightly. Similar calculations involving clinopyroxene fractionation from similar melts would not affect their Eu/Eu* ratios and would only result in very minor changes in their Sr/Sr* ratios. Addition of ~25 wt % plagioclase from external sources to magmas, generated by ~20 % mantle melting (modelled), could explain much of the span in Sr/Sr* and Eu/Eu* ratios displayed by the low-TiO_2 Streymoy and Kvívík sills, while around 20 wt % plagioclase fractionation from magmas, generated by 10 to 12 % mantle melting (modelled), could explain much of the range in the Sr/Sr* and Eu/Eu* ratios displayed by the Eysturoy and Sundini sills (Table 2; Fig. 8). Plagioclase fractionation in the range 10 to ~20 wt % from magmas formed by ~10 % mantle melting are required in order to recreate the Sr/Sr* and Eu/Eu* ratios of the Svínoy-Fugloy and Langaregn sills (Fig. 8). The differences in calculated plagioclase accumulation and fractionation required to recreate Sr/Sr* versus Eu/Eu* ratios representing the Faroese sills, as shown in Fig. 8, could in theory stem from either analytical error during analyses of Faroese sill samples, or the actual Sr/Sr* and Eu/Eu*ratios of these elements in their respective mantle sources differed from those used in the modelling. Around 20 wt % plagioclase accumulation and fractionation to/from liquids with geochemical compositions broadly similar to those of Faroese low-TiO_2 and high-TiO_2 sill samples would decrease/increase their overall REE concentrations respectively by amounts corresponding to around 2 % larger/lesser degrees of partial melting of their respective mantle sources, while ~10 to ~15 wt % olivine fractionation would increase their overall REE concentrations by amounts corresponding to around 1 % lesser degree of partial mantle melting (calculations not shown).

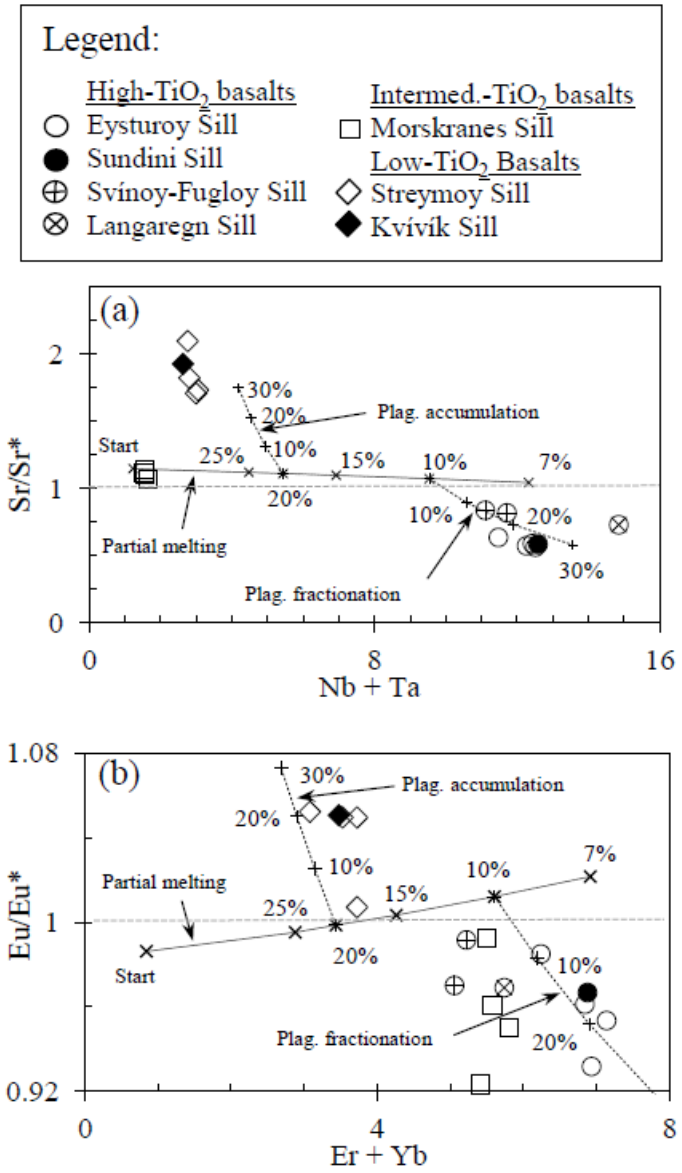

Fig. 8. Trace element constraints on plagioclase fractionation and accumulation. a) Partial melting calculations, utilising a selected initial mantle composition, are shown at 7, 10, 15, 20 and 25 % melting intervals. Plagioclase accumulation and fractionation, shown at 10, 20 and 30 wt % intervals, are modelled from ~20 % and ~10 % calculated partial melts respectively. Initial selected fertile mantle composition: (Nb + Ta) = (1.2 + 0.025) and Sr/Sr* = 1.145, where Sr = 35, Ce = 2.6 and Nd = 1.9 (i.e. Lesnov et al., 2009). Residual minerals during partial melting calculations were ~82 % ol + 16 % opx in addition to ~2 % of mainly cpx and spl. b) Same as in a), but with (Er + Yb) = (0.42 + 0.42) and Eu/Eu* = 0.9862, where Eu = 0.182, Sm = 0.52 and Gd = 0.65 (i.e. Lesnov et al., 2009). Residual minerals were the same as in a). See Table 2 for definition of Sr/Sr* and Eu/Eu*. Mineral abbreviations are from Kretz (1983). Numbers along dotted lines indicate melting percentages and numbers along dashed lines indicate plagioclase fractionation/accumulation percentages. Datasets on calculated partial mantle melting, calculated fractionation and calculated accumulation of plagioclase are shown in: Hansen et al. (2019).

5.3.3. Constraints on fractionation/accumulation from mass-balance calculations

Mass-balance calculations, involving all major elements apart from MnO and P_2O_5, suggest that fractionation and accumulation of plagioclase from/to basaltic melts with compositions comparable to Faroese low-TiO_2 and high-TiO_2 sills chiefly affect their Al_2O_3, Fe_2O_3 and MgO compositions and to some degree their CaO and TiO_2 compositions, while the other major elements remain relatively unaffected (Table 4). If low-TiO_2 sills of this study evolved by ~25 wt % plagioclase accumulation, their precursor melts would possess significantly lower Al_2O_3 and higher Fe_2O_3 contents relative to values measured for these sills, while evolvement of their high-TiO_2 counterparts by ~20 wt % plagioclase fractionation would produce parental melts being significantly enriched with respect to their Al_2O_3 and depleted with respect to their Fe_2O_3 contents relative to values measured for these particular sills (Table 4). Consequently, in contrast with measured relative abundances of Al_2O_3 and Fe_2O_3 in Faroese high-TiO_2 sills versus low-TiO_2 sills, which define positive and negative slopes respectively when connected and plotted against MgO, the relative abundances of these major elements in their calculated parental melts would define negative and positive partial melting slopes respectively when connected and plotted against MgO (Fig. 9a; Fig. 9b). The scenario is different for the TiO_2 and CaO contents of the same samples, when exposed to the same accumulation/fractionation calculations as discussed above. Both these major elements in the calculated parental melts maintain their original graphical trends (i.e. negative and positive slopes respectively) when connected and plotted against MgO, but the gradients for their calculated parents are gentler than those of the measured samples (Fig. 9c; Fig. 9d; Table 4). Configurations of Al_2O_3, Fe_2O_3, TiO_2 and CaO versus MgO in calculated parents to low-TiO_2 and high-TiO_2 sills resemble results from previous experimental studies on partial mantle melting to produce low-TiO_2 and high-TiO_2 basaltic rocks (Hirose and Kushiro, 1993; Hirose and Kawamoto, 1995; Kogiso et al., 1998) and would also support inferences in the discussion on trace elements above. Insets in Fig. 9 illustrate similarities between calculated high-TiO_2 versus low-TiO_2 melts of this study and experimental basaltic melts, produced at roughly 5 to 20 % melting and extrapolated to lower MgO contents in response to 12-15 wt % olivine fractionation. The differences in slopes and concentrations of experimental versus calculated melts are due to low pressures (1 GPa) and the hydrated nature of the experimental mantle materials. The discussion above strongly suggests that noticeable accumulation and fractionation of plagioclase in mid crustal staging chambers affected the melts, which eventually evolved to low-TiO_2 and high-TiO_2 Faroese sills.

Table 4

Mass-balance calculations on olivine and plagioclase fractionation, in addition to plagioclase accumulation

Major elements	[a]olivine	[a]magnetite	[a]ilmenite	[b]MgO-rich magma	[c]calc. melts	[a]plag	[d]high-TiO_2 sill	[e]calc. parent 1	[f]low-TiO_2 sill	[g]calc. parent 2
SiO_2	41.85	0.27	0.10	45.89	48.50	49.60	50.28	50.04	50.29	50.59
Al_2O_3	0.00	0.21	1.53	12.94	15.76	32.14	13.54	17.26	16.95	13.15
Fe_2O_3	2.05	99.63	68.80	10.82	9.10	0.27	14.60	11.73	10.42	12.96
MgO	56.17	0.00	1.76	15.11	8.40	0.20	6.47	5.22	6.86	8.52
CaO	0.00	0.00	0.00	10.90	13.29	15.38	11.15	12.00	13.22	12.68
Na_2O	0.00	0.00	0.00	1.53	1.87	2.57	2.36	2.40	2.00	1.86
K_2O	0.00	0.00	0.00	0.05	0.06	0.17	0.33	0.30	0.20	0.21
TiO_2	0.07	0.00	27.40	0.96	0.81	0.00	2.07	1.65	0.82	1.03

[a]Mineral compositions are from Deer et al. (1992). [b]Similar to Faroese MgO-rich (picrite) sample Ey-129 (Holm et al., 2001). [c]Geochemical composition calculated by fractionation of 14.6 wt% olivine, 2.4 wt% magnetite and 1.0 wt% ilmenite from the MgO-rich magma. [d]High-TiO_2 Faroese sample 08-JES-03 from Table 1; [e]Geochemical composition of parent 1 from backtrack/reiteration calculations on the high-TiO_2 sill sample on the assumption that parent 1 represents its precursor melt prior to ~20 wt% plagioclase fractionation; [f]Low-TiO_2 Faroese sample 07-JSS-52 from Table 1; [g]Geochemical composition of parent 2 from backtrack/reiteration calculations on the low-TiO_2 sill sample on the assumption that parent 2 represents its precursor melt prior to ~25 wt% plagioclase accumulation.

A scenario where plagioclase, originating from different sites of storage and differentiation during magma ascent, accumulated in magmas, which subsequently evolved to the Faroese low-TiO_2 sills, would be in accordance with earlier studies on basaltic magmas of the NAIP (e.g. Font et al., 2008). More specifically, Lange et al. (2013) suggested that three criteria must be fulfilled in order for melts containing accumulated plagioclase to reach the upper crust: 1) the initial plagioclase-free melt must pass through conduits in which plagioclase cumulates are present; 2) the ascent velocity of the magma within the conduit must be greater than the settling velocity of the entrained phenocrysts and 3) the magma must not travel through a conduit system containing an axial magma chamber, which would halt the upward ascent of the magma and allow denser plagioclase crystals to segregate.

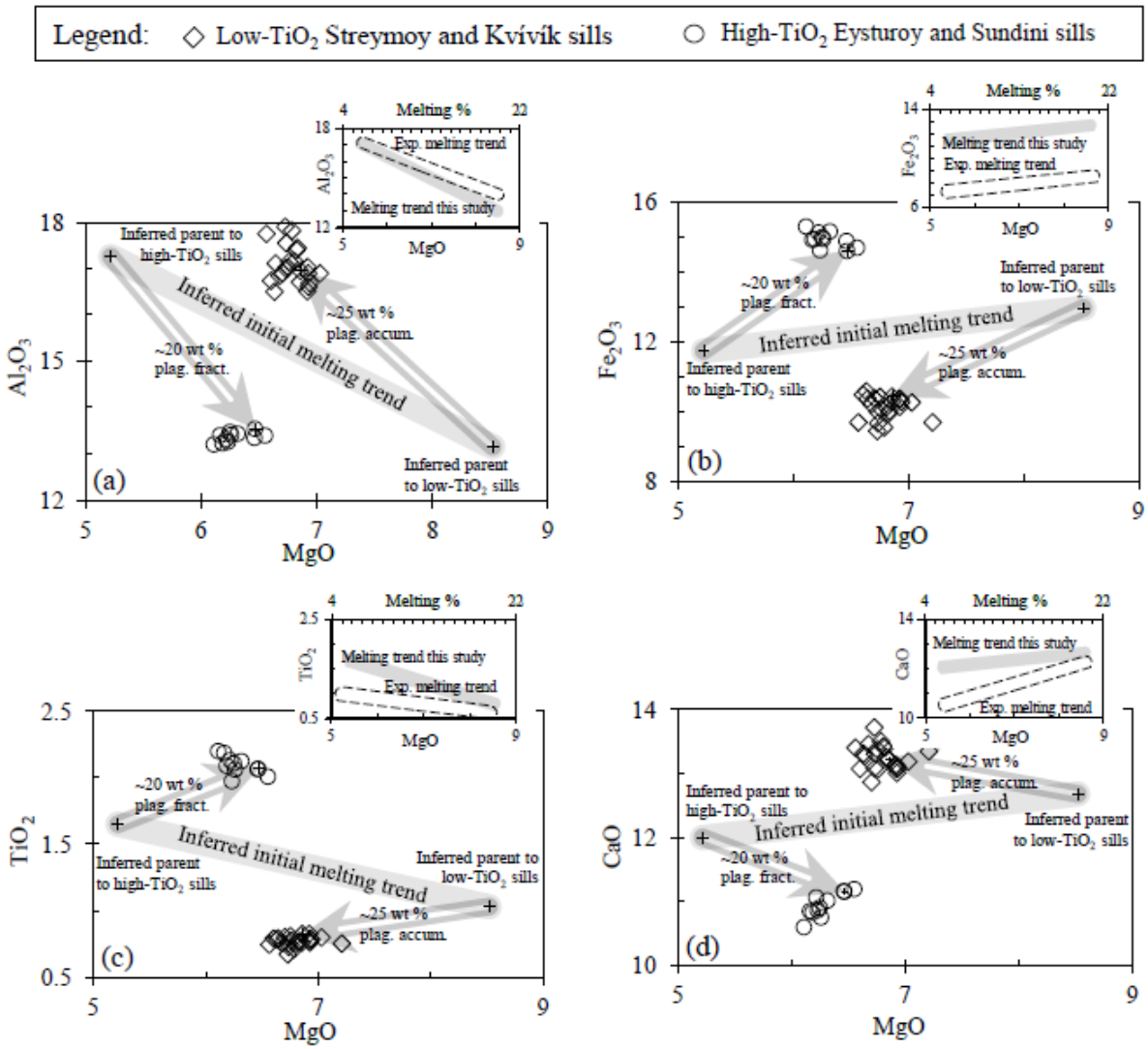

Fig. 9. Calculated plagioclase fractionation (roughly 20 wt %) and accumulation (roughly 25 wt %) during the evolvement of precursor melts to Faroese sills (from Table 4). It is presumed that parental melts to Faroese high-TiO_2 and low-TiO_2 sills experienced roughly equal amounts of olivine fractionation from their primary melts on previous occasions. a) Relative plots representing calculated parents to high-TiO_2 versus low-TiO_2 sills define a conspicuous negative trend/slope in a MgO versus Al_2O_3 diagram. b) Relative plots showing calculated parents to high-TiO_2 versus low-TiO_2 sills define a clear positive trend/slope in a MgO versus Fe_2O_3 diagram. c) Relative plots showing calculated parents to high-TiO_2 versus low-TiO_2 sills define a clear negative trend/slope in a MgO versus TiO_2 diagram. d) Relative plots representing calculated parents to high-TiO_2 versus low-TiO_2 sills define a clear positive trend/slope in a MgO versus CaO diagram. The inset diagrams show calculated melting trends from the main diagrams versus trends from an experimental melting project (Hirose and Kawamoto, 1995), with melt percentages spanning from ~5 to ~20 %. It is assumed that olivine fractionation shifted/extrapolated MgO contents in both calculated and experimental primary melts roughly horizontally to lower MgO values, as displayed in this figure. See main text and Table 4 for more details.

5.4. Partial melting

5.4.1. Constraints on depths of formation by partial melting

Since the Faroese archipelago rests on top of an Archaean continental crust, the melts that gave rise to their olivine tholeiites must have formed beneath an ancient microcontinent (Bott et al., 1974; Richardson et al., 1998). Such olivine tholeiitic basaltic magmas may form by partial melting of a range of mantle compositions under various T and P (Hirose and Kushiro, 1993; Kushiro, 1996, 2001; Kogiso et al., 1998), but the lack of HREE depletion in Faroese low-TiO_2 and most high-TiO_2 sill samples points to formation of their precursor melts by partial melting outside the garnet stability field, i.e. at $P \leq \sim 2.8$ GPa corresponding to depths of $\leq \sim 85$ km (Robinson and Wood, 1998; Presnall et al., 2002). Moreover, as melting of plagioclase-bearing mantle material would produce quartz tholeiitic basalts (Kushiro, 1996, 2001), the olivine tholeiitic sills of the Faroe Islands probably formed at depths outside the plagioclase stability field too, i.e. at $P \geq \sim 0.9$ GPa corresponding to depths of $\geq \sim 30$ km (Borghini et al., 2010; Presnall et al., 2002), thus leaving mantle sources within the spinel stability field as their most likely origin.

5.4.2. Batch melting calculations

Batch melting calculations (partition coefficients and the equation used are shown in Supplement 5 below) were carried out in this work, in order to estimate melting percentages of suitable mantle sources, which gave rise to the different types of melts that ultimately evolved to the Faroese sills. In these calculations, only realistic existing figures for mantle compositions are used, which have been reported for various sites worldwide previously. In addition, shallow mantle sources of late melts are considered, as hypothesized in earlier studies (e.g. Peate, 1997).

Calculations in this study suggest that partial melting of slightly LREE enriched mantle sources have the potential to reproduce the REE trends characterising Faroese low-TiO_2 and high-TiO_2 sills, while LREE and MREE depleted mantle sources are required in order to recreate the REE trend(s) of the intermediate-TiO_2 Morskranes Sill. Residual mineral assemblages utilised in these calculations are dominated by olivine (~80 to ~84 %) and orthopyroxene (~8 to ~16 %) that may be associated with minor amounts of clinopyroxene (0 to ~7 %) and spinel (0 to ~1 %), i.e in accordance with the mineralogy of many naturally occurring peridotites worldwide (e.g. Obata and Morten, 1987; Ionov et al., 2002; Downes et al., 2004; Choi and Kwon, 2005).

Trial partial melting calculations, performed in order to recreate measured REE trends of low-TiO_2 and most high TiO_2 sills, were carried out on a large number of mantle compositions from localities worldwide and from estimated average mantle values and include published material reported by e.g. McDonough (1994); McDonough and Sun (1995); Ionov et al. (2002); Downes et al. (2004); Ntaflos et al. (2008) and Lesnov et al. (2009). Melting percentages ranging from 15 to 20 % of fertile mantle material from Ntaflos et al. (2008) and ranging from 8 to 10.5 % of likewise fertile mantle material from Lesnov et al. (2009) best reproduce the ranges in REE compositions of low-TiO_2 and high TiO_2 sills respectively (Fig. 10a; Fig. 10c). It is clear that the measured REE trend representing the Langaregn Sill doesn't quite fit in with those of the rest of the high-TiO_2 sills (Fig. 4e; Fig. 10c). Its actual REE trend can be recreated by ~7 % partial melting of a fertile source (not shown), but it is likely that some garnet was a residual phase and that its source displayed slight depletion with respect to LREE when compared to sources to other local high-TiO_2 sills. Regarding measured REE in intermediate-TiO_2 sill samples, trial calculations included published material reported by e.g. Rampone et al. (2004); Workman and Hart (2005) and Villaseca et al. (2010), where 7 to 8 % of average depleted mantle from Workman and Hart (2005) best recreate the REE compositions of these samples (Fig. 10b).

When the effects on REE compositions representing Faroese sills from supposed fractionation of olivine and plagioclase and accumulation of plagioclase (previous Sect.) are taken into account, partial melting percentages to produce melts that gave rise to the Faroese sills should be corrected slightly. With respect to the low-TiO_2 sills, olivine fractionation and plagioclase accumulation would shift the range of partial melting percentages in their source(s) by +1 % from 15-20 % to 16-21. With respect to the high-TiO_2 sills, olivine and plagioclase fractionation would shift the range of partial melting percentages in their source(s) by –3 % from 8-10.5 % to 5-7.5 %, while the calculated melting for the Langaregn Sill should be shifted from ~7 to ~4 %. With respect to the intermediate-TiO_2 sill, olivine fractionation would shift the range of partial melting percentages in its source by –1% from 7-8 % to 6-7 %.

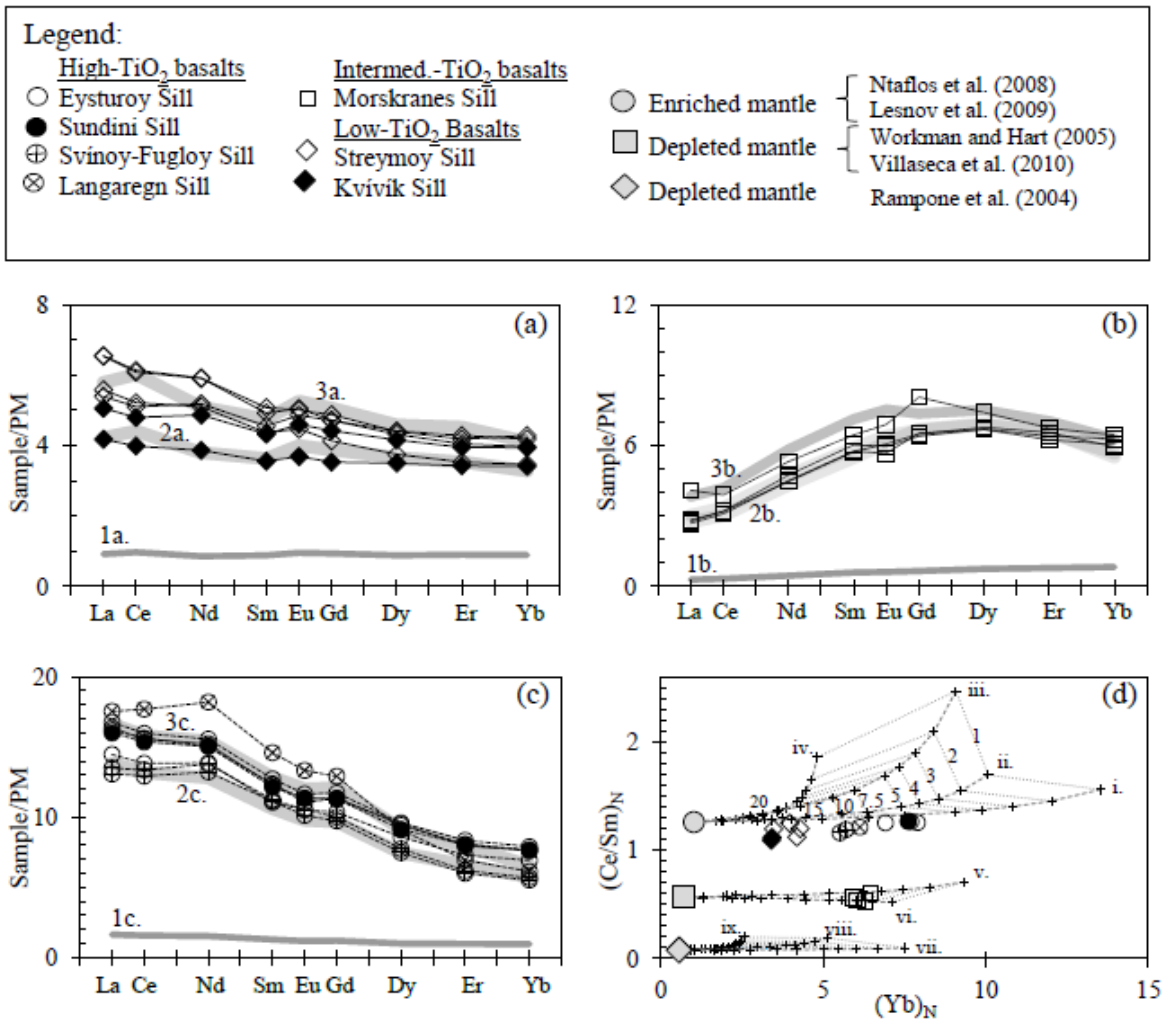

Fig. 10. Partial melting calculations involving various mantle lithologies. The grey shaded trends in the mantle normalised REE diagrams a), b) and c) indicate mantle sources (labelled 1.) and range in calculated melting percentages (labelled 2. and 3.). a) Low-TiO_2 sills: 1a.= Spinel lherzolite sample VL 5-12 (Ntaflos et al., 2008); 2a.= around 20 % melt of 1a. with 84 % Ol + 8.5 % Opx + 7 % Cpx + 0.5 % Spl residue; 3a.= around 15 % melt of 1a. with 84 % Ol + 8.5 % Opx + 7 % Cpx + 0.5 % Spl residue. b) Intermediate-TiO_2 sills: 1b.= average DMM (Workman and Hart, 2005); 2b.= around 8 % melt of 1b. with 84 % Ol + 15 to 15.5 % Opx + 0.5 to 1 % Spl residue. 3b.= around 7 % melt of 1b. with 84 % Ol + 16 % Opx residue. c) High-TiO_2 sills: 1c.= average spinel lherzolite sample (Lesnov et al., 2009); 2c.= around 10.5 % melt of 1c. with 84 % Ol + 15.75 % Opx + 0.25 % Spl residue; 3c.= around 8 % melt of 1c. with 84 % Ol + 15.5 % Opx + 0.5 % Spl residue. d) The labelled curves in the $(Yb)_N$ versus $(Ce/Sm)_N$ diagram indicate partial melting trends calculated from three mantle sources (enriched, moderately depleted and strongly depleted). Numbers along curves ii. and iii. refer to melting percentages that also apply for all the other curves in the actual diagram. Normalising primitive mantle values in all four diagrams are from McDonough and Sun (1995). Mineral abbreviations are from Kretz (1983). See Supplement 5 below for partition coefficients and equation used in calculations and Supplement 6 below for details on mineral residues from calculations shown

in d), as well as similar calculations on the same sill samples using a Zr versus Y/TiO_2 diagram. Datasets on calculated melting trends are shown in: Hansen et al. (2019).

Batch melting calculations based on selected REE, which are plotted in a binary $(Yb)_N$ versus $(Ce/Sm)_N$ diagram, are perhaps better suited to illustrate the effects of various residual mineralogies and general differences in source compositions on modelled melts. With respect to LREE-enriched mantle sources (Ntaflos et al., 2008; Lesnov et al., 2009), the results shown in the binary REE plots support the inferences above regarding formation of the low-TiO_2 and high-TiO_2 sills by different degrees of partial melting of enriched sources that left residual mineralogies composed mainly of olivine and orthopyroxene (curves i-iv in Fig. 10d). Similarly, partial melting of moderately LREE-depleted sources (Workman and Hart, 2005; Villaseca et al., 2010) with residual mineral assemblages dominated by olivine and orthopyroxene most realistically reproduces the REE composition of the intermediate-TiO_2 Morskranes Sill (curves v and vi in Fig. 10d). In addition, strongly LREE depleted mantle sources (e.g. Rampone et al., 2004) do not have the potential to reproduce REE compositions matching those of the Morskranes Sill, when exposed to partial melting, irrespective of which residual mineral assemblages are chosen (curves vii-ix in Fig. 10d). More details on Fig. 10d as well as additional modelling are shown in Supplement 6 below.

5.4.3. General considerations

Given that the mantle sources used in the partial melting calculations in this study were primarily selected because they best reproduce the REE trends representing the actual sills, the actual mantle sources to these sills could, in theory, have been less or more fertile relative to the chosen compositions; if so, then the outcome would require slightly lesser or greater degrees of partial melting relative to the calculated values. In cases where precursor melts to the actual sills experienced small-scale assimilation of felsic crustal materials upon ascent, it could have increased their LREE concentrations very slightly (e.g. Hansen, 2011). However, contamination with ≤ 1 % crustal material would not have had noticeable effects on the modelling carried out in this work. Altogether, the partial modelling and trace element characteristics of actual sill samples combined (Fig. 3; Fig. 10) point to distinct mantle sources for intermediate-TiO_2 versus high-TiO_2 and low-TiO_2 sill samples. In turn, some heterogeneities probably exist between sources to high-TiO_2 and low-TiO_2 sill samples and probably also to some degree within sources to the high-TiO_2 sills themselves. Here the Eysturoy and Sundini sills, the Langaregn Sill and the Svínoy-Fugloy Sill respectively

probably originated from three slightly different mantle sub-sources. These findings are in accordance with the isotopic characteristics recorded for the actual sills (Fig. 5). Interestingly, four slightly different mantle sub-sources were inferred for high-TiO_2 lavas of the Faroese Enni and Malinstindur formations in a recent study (Millet et al., 2017).

Processes involving partial melting of sources, comparable to those reported for SCLM, to produce Faroese sills, as is suggested by our modelling above, are at odds with previous theories on formation of their host-rocks (e.g. Holm et al., 2001; Søager and Holm, 2009, 2011).

5.5. Primary melts

Previous estimates on the MgO percentages present in primary magmas that evolved to basaltic rocks of the N Atlantic have come to various conclusions: 10.0-13.0 wt % and 17.0-18.5 wt % respectively for W Greenland (Yaxley, 2000; Larsen and Pedersen, 2009); 12.0-13.6 wt % and 16.6 wt % for E Greenland (Korenaga and Kelemen, 2000; Momme et al., 2006); 13.0-15.0 wt % for NW Britain (Scarrow and Cox, 1995); 13.5-17.7 wt % for Iceland and adjacent mid-ocean ridges (Korenaga and Kelemen, 2000) and 16.0-19 wt % MgO for the Faroe Islands (Holm et al., 2001: Søager and Holm, 2011). MgO contents of 10-15 wt % have been calculated for primary magmas that gave rise to average global Ocean Ridge Basalts (Klein and Langmuir, 1987).

Based on the results from the partial melting modelling and presumed subsequent fractional crystallisation of olivine and plagioclase, as well as inferred plagioclase accumulation, melting percentages of ~16 to 21 and ~4 to 7.5 % to produce primary melts that developed to Faroese low-TiO_2 and high-TiO_2 sills respectively appear to be reasonable estimates, if the following criteria are fulfilled: 1) fractionation of clinopyroxene did not play a major role during the early stages of their magmatic evolutions; 2) around 10 to 15 wt % olivine and minor amounts of magnetite and ilmenite fractionated from their primary melts, which contained ~15 wt % MgO and 3) ~15 to 20 wt % plagioclase fractionated from melts that gave rise to high-TiO_2 sills while about 15 to 25 wt % plagioclase accumulated in melts that evolved to the low-TiO_2 sills. The 16 to 21 % partial melting range to produce precursor melts to the Faroese low-TiO_2 sills correspond roughly to earlier estimates on melting percentages for primary melts that developed to low-TiO_2 basaltic rocks of W Greenland (Larsen and Pedersen, 2009), E Greenland (Momme et al., 2006), the Faroe Islands (Holm et al., 2001), southern Brazil (Fodor, 1987) and global ocean ridge basalts (Klein and Langmuir,

1987). The 4 to 7.5 % partial melting range proposed for production of Faroese high-TiO_2 sills correspond roughly to melting percentages estimated for primary melts, which evolved to high-TiO_2 basaltic rocks of southern Brazil (Fodor, 1987) and E Greenland (Momme et al., 2006), but reach slightly higher values than those estimated for primary melts that gave rise to other high-TiO_2 basalts of the Faroe Islands (Holm et al., 2001) and are slightly lower than those inferred for global ocean ridge basalts (Klein and Langmuir, 1987). However, as most sills of this study, being termed high-TiO_2 basaltic rocks, display TiO_2 compositions of only 2.0 to 2.5 wt % compared to 2.5 to 3.7 wt % for other high-TiO_2 basalts of e.g. the Faroe Islands (Holm et al., 2001; Søager and Holm, 2011), the proposed range in melting percentages for high-TiO_2 primary magmas in this study appear to be rather similar to other high-TiO_2 rocks within the N Atlantic area after all.

The 6-7 % melting range calculated/estimated for the LREE depleted primary melts giving rise to the Morskranes Sill contrast somewhat with the higher degrees of melting thought to have generated comparable LREE depleted Central Mull Tholeiites from the British Tertiary Igneous Province (BTIP) and with the melting percentages measured for experimentally produced MORB-like rocks (Kerr, 1995; Kushiro, 2001). It should be noted however, that the basalts reported by these authors presumably formed at relatively low pressures, e.g. 1.5 GPa for the experimental rocks (Kushiro, 2001). If the melts that evolved to the Morskranes Sill also experienced 10-15 wt % plagioclase fractionation, as could perhaps be suggested by its Eu/Eu* ratio (Fig. 8b), then slightly higher range in melting percentages of 7-9 % could be a more correct approximation. All the above estimated melting percentages rely on the assumption that crustal contamination did not significantly affect the overall trace element compositions used in the modelling.

5.6. Mantle sources

5.6.1. Geochemical implications from the literature

Depleted mantle materials probably represent residue(s) following earlier phases partial melting of primordial mantle reservoirs to produce basaltic melts (Wood, 1979; Rampone et al., 2004; Hofmann, 2003; Workman and Hart, 2005). By contrast, fertile mantle materials could result from metasomatic processes, where primordial mantle materials were contaminated with ascending low-degree basaltic magmas or with fluids expelled from these

(Wood, 1979; Dupuy et al., 1991; Grégoire et al., 2003; Lesnov et al., 2009), or they could originate from assimilation of recycled oceanic crust (Kogiso et al., 1998; Korenaga and Kelemen, 2000; Yaxley, 2000; Kogiso et al., 2004; Meyer et al., 2007). Total normative Fe-oxide values of ≥ 13 wt % in basaltic rocks are at times interpreted in terms of derivation from mantle sources contaminated with recycled oceanic crustal components (Kogiso et al., 1998). The Faroese high-TiO_2 sills display average measured Fe_2O_3 values of ~14.7 wt %, but their calculated parental melts contain less than 12 wt % of this oxide, compared to average measured Fe_2O_3 values of ~10 wt % for the Faroese low-TiO_2 sills and ~12.8 wt % for their calculated parental melts (Table 4; Fig. 9b). The iron contents of the actual sills also plot well within ranges displayed by common mid-ocean ridge and ocean island tholeiites (e.g. Blatt and Tracy, 1995).

Previous studies have attributed the trace element characteristics displayed by Faroese basaltic lavas and dykes to an origin from a heterogeneous mantle plume comprising distinct geochemical zones (Holm et al., 2001; Søager and Holm, 2011), while asthenospheric and/or SCLM sources have been inferred for Faroese lavas by other authors (Gariépy et al., 1983). Based chiefly on Zr, Nb and Y concentrations, Hanan et al. (2000) indicated an enriched plume component, a depleted astenospheric component and minor contributions from an additional EM 1- like component, entrained within the asthenosphere, as the main sources to Icelandic basalts. Fitton et al. (2003) demonstrated that an additional local depleted Iceland plume (DIP) component was required in order to adequately account for the Zr, Nb and Y characteristics of the Icelandic basalts combined. In theory, mantle sources broadly similar to those suggested by Hanan et al. (2000) and Fitton et al. (2003) for the Icelandic basalts could have been involved during formation of basaltic rocks of the Faroe Islands, as samples representing Faroese sills, lavas and dykes share many of the geochemical characteristics defined by the Icelandic basalts (Fig. 11a).

Importantly, it is evident from the inset to Fig. 11a that all Faroese low-TiO_2 and most high-TiO_2 sill samples combined define a “missing link” between fields outlining the bulk of Faroese low-TiO_2 and high-TiO_2 host-rocks, whilst the intermediate-TiO_2 Morskraness Sill and the high-TiO_2 Langaregn Sill plot within the fields for low-TiO_2 and high-TiO_2 host-rocks respectively. Overall, the bulk of Faroese basaltic rocks, including the local sills, define a trend quite similar to average values reported for Iceland previously (i.e. the bold curve in Fig. 11a, adopted from Hanan et al., 2000), but which is rotated by around 10° clockwise.

5.6.2. Geochemical implications on metasomatised mantle sources

Negative Nb and Ta anomalies in basaltic rocks have commonly been associated with mantle sources that were metasomatised previously with hydrous fluids, C-bearing fluids or low-degree basaltic melts, while positive Nb and Ta anomalies are commonly associated with residual dryer mantle materials from which the above-mentioned metasomatic agents were extracted previously (Thompson et al., 1983; Zhang et al., 2012). Negative Nb and Ta anomalies in suites of low-TiO_2 flood basalts from the Siberian Traps, and from Central Nicaragua, being virtually identical to low-TiO_2 sills from this study; were previously attributed to an origin from metasomatised upper mantle sources in subduction-zone environments (Walker et al., 1990; Ivanov et al., 2008), while negative Nb and Ta anomalies in low-TiO_2 basaltic rocks from the Emeishan Igneous Province, SW China, are thought to reflect partial melting of enriched SCLM materials (Xiao et al., 2004). Basaltic rocks of the Emeishan Igneous Province with higher TiO_2 contents that display positive Nb and Ta anomalies are interpreted in terms of partial melting of mantle sources being significantly affected by plume-derived components (Xiao et al., 2004), while relatively high-TiO_2 basaltic rocks from Central Nicaragua possessing positive Nb anomalies are thought to have developed from a mantle wedge comparable in composition to an enriched sub-oceanic mantle and unaffected by subduction zone processes (Walker et al., 1990).

Therefore, if the moderately negative Nb and Ta anomalies displayed by the Faroese low-TiO_2 sills resulted from melting of mantle sources affected by metasomatism, the moderately positive Nb and Ta anomalies of the high-TiO_2 sills (Fig. 3) could indicate magma tapping from dryer Nb and Ta enriched residual mantle sources, from which metasomatic agents were already extracted. The discussion above, suggesting formation of the Faroese low-TiO_2 sills by higher degrees of partial melting relative to the melting percentages required to produce their high-TiO_2 counterparts, would be in accordance with more metasomatised materials in sources to the former sills, as the presence of metasomatic agents supposedly enhance mantle melting (e.g. Hirose and Kawamoto, 1995; Peate, 1997; Green and Falloon, 2005). However, as all the investigated Faroese high-TiO_2 sills, except for the Langaregn Sill, are LREE enriched (Fig. 4), the formation of these sills by low-degree melting of a relatively dry Nb and Ta enriched source, which had already experienced a partial melting event, may appear to be problematic, if no other processes were involved, as the LREE within their source rocks would have been strongly partitioned into the first melts, leaving a relatively LREE depleted residue. Refertilisation of relatively dry mantle sources to the high-TiO_2 Faroese sills by other highly LREE enriched metasomatic agents could be a plausible explanation and would be in

accordance with geochemical modification of upper mantle sources by multiple metasomatic events, as reported for other igneous regions previously (e.g. Peccerillo, 1999). Based on the gentle REE slopes of most high-TiO_2 and low-TiO_2 sill samples and the modelling above, in addition to their Nb and Ta characteristics, we propose that these sills originated from melting of variously metasomatised mantle materials with compositions comparable to those reported for SCLM materials previously. Formation of basaltic rocks by melting of such materials would fit tentative suggestions by Gariépy et al. (1983) regarding petrogenesis of some of the Faroese lavas and would also fit inferences by Larsen et al. (2003) regarding origin of alkaline lavas from W Greenland, but would be at odds with earlier theories favouring magma supplies to Faroese lavas/dykes from a deep-rooted mantle plume (Holm et al., 2001; Søager and Holm., 2011).

5.6.3. Geochemical implications on heterogeneous mantle sources

While differences between some major elements of the low-TiO_2 Faroese sills in particular and local lavas/dykes (insets in Fig. 2) could reflect post-melting processes where plagioclase was accumulated in precursor melts to the actual sills, some of the observed differences in trace element characteristics between data for Faroese lavas/dykes and those of the investigated sills (insets in Fig. 3; Fig. 4; Fig. 11) most likely point to differences between their respective mantle sources.

The higher concentrations of LREE in high-TiO_2 sills and higher concentrations of LREE and MREE in low-TiO_2 sills relative to those of older local basaltic dykes and irregular intrusions with exactly similar TiO_2 contents (insets in Fig. 4) could indicate a temporal enrichment of these elements in the local upper mantle in Early Cenozoic times, if all these intrusions originated at broadly similar mantle depths. Alternatively, the Faroese sills formed at relatively shallower depths from distinct mantle sources that may or may not have been geochemically affected/metasomatised by the earlier melting to produce melts parental to local dykes and irregular intrusions at deeper mantle levels. The scenario where the enrichment of LREE in high-TiO_2 sills and enrichment of LREE and MREE in low-TiO_2 sills relative to REEs in their host-rock counterparts with similar TiO_2 contents (i.e. Fig. 4) could result from small-scale crustal contamination is not realistic, as this would require the contribution from at least a few percent of crustal materials (e.g. Hansen, 2011). The steeper HREE slopes in Faroese high-TiO_2 dykes and irregular intrusions relative to those of most high-TiO_2 sills could indicate some residual garnet or garnet fractionation during their

formation, suggesting that they may indeed have developed at mantle levels deeper than those of the sill sources.

Evolution of the Faroese high-TiO_2 sills by RTF processes from local low-TiO_2 magmas, as suggested for Early Cenozoic basalts of e.g. W Greenland (Larsen and Pedersen, 2009), could explain many of the differences in trace element concentrations between these two basalt groups. However, as Nb and Ta are not noticeably fractionated relative to e.g. La and Ce during common rock-forming processes, it is not likely that the moderately negative Nb and Ta anomalies in the Faroese low-TiO_2 sills developed to the moderately positive Nb and Ta anomalies, characterising many of the Faroese high-TiO_2 sill samples, by RTF processes. All things considered, it is tentatively suggested that the compositional characteristics of Faroese low-TiO_2 and high-TiO_2 sills developed in response to tapping of fertile SCLM-like sources affected by metasomatism in various ways, which resulted in slight geochemical differences between the sources to these two categories and also to some degree internally within the high-TiO_2 category. There is abundant evidence that metasomatised lithosphere domains exist in other regions of the NAIP such as W Greenland too (Larsen et al., 2003). If some of the inferred metasomatic agents to low-TiO_2 and high-TiO_2 Faroese sill sources were not supplied from local Early Cenozoic mantle melting, geological activities associated with the complex geological history within this part of the North Atlantic area could be an alternative explanation. A potential alternative to metasomatic source enrichment would be magma mixing at deeper mantle levels involving recycled crustal materials. The origin of basaltic rocks within a fertile and metasomatised SCLM source during waning stages of regional magmatism, as we tentatively suggest for melts parental to Faroese lowTiO_2 and high-TiO_2 saucer-shaped sills, would be in accordance with inferences regarding late stage magmatism in other LIPs too (e.g. Peate, 1997 and references therein). Peate (1997) pointed out that a thermal anomaly from some sort of a mantle plume at the base of the lithosphere in the Paraná-Etendeka province once provided the heat necessary for basaltic melt production

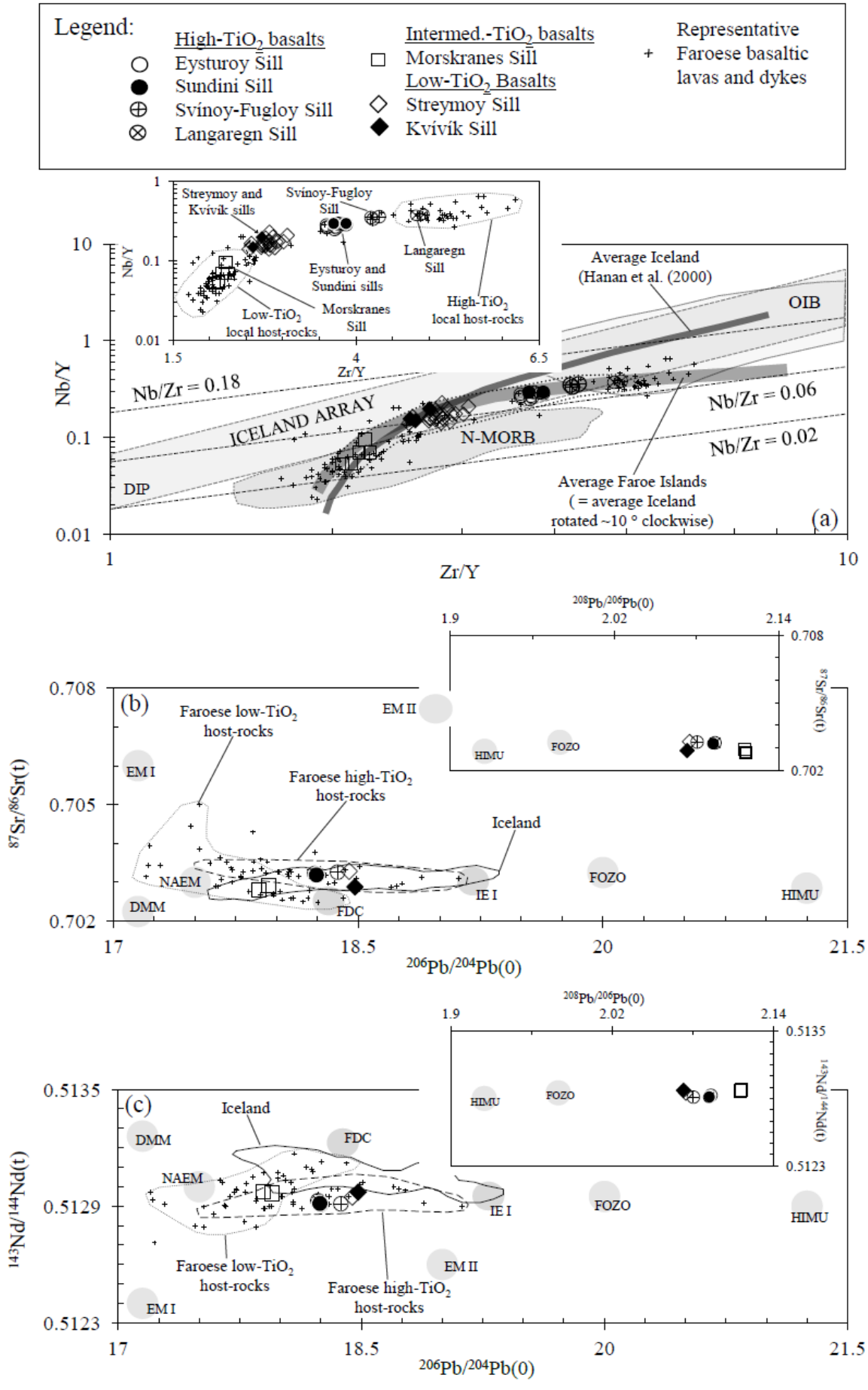

Fig. 11. Geochemical and isotopic data of Faroese sills are compared with data of local basaltic lavas/dykes, Icelandic basaltic rocks and with data from various mantle reservoirs reported for the northern hemisphere. a) Most Faroese low-TiO_2 and intermediate-TiO_2 basaltic samples, including sill samples of this study, plot slightly below the lower limit of the "Iceland Array" in a Zr/Y versus Nb/Y ratio diagram, while high-TiO_2 lavas/dykes/sills with relatively higher Zr/Y ratios straddle this same lower limit. Literature data in a): "Iceland Array" field, OIB, DIP (Depleted Iceland Plume) and N-MORB are from Fitton et al. (2003); Bold curve representing average Iceland is from Hanan et al. (2000). b) and c) Samples representing the Faroese sills exhibit relatively well defined trends between end-member mantle reservoirs NAEM and FOZO (and IE 1) in both $^{206}Pb/^{204}Pb(0)$ versus $^{87}Sr/^{86}Sr(t)$ and $^{206}Pb/^{204}Pb(0)$ versus $^{143}Nd/^{144}Nd(t)$ ratio diagrams, but the low-TiO_2 and high-TiO_2 sill samples are skewed slightly towards the EM reservoirs. The same good correlation is maintained in $^{208}Pb/^{206}Pb$ versus $^{87}Sr/^{86}Sr(t)$ and $^{208}Pb/^{206}Pb$ versus $^{143}Nd/^{144}Nd(t)$ ratio plots (insets). It is noteworthy that Faroese low-TiO_2 sill samples together with Faroese high-TiO_2 sill samples all plot in the field for local high-TiO_2 host-rocks in b) and c). Literature data: Iceland, EM I and EM II (Stracke et al., 2003); HIMU and FOZO (Stracke et al., 2005 and refs. therein); DMM (Zindler and Hart, 1986); IE 1 (Thirlwall et al., 2004); NAEM (Ellam and Stuart, 2000; Søager and Holm, 2011); FDC (Søager and Holm, 2011). (t) and (0) refer to age corrected and measured isotope ratios respectively. See text for more details.

within the overlying fertile metasomatised lithospheric mantle. He inferred melting at successively shallower lithospheric levels with time from the arrival of the presumed mantle plume, provided that overall lithospheric thicknesses exceeded 100 km. Larsen et al. (2003) inferred a slightly different scenario, where production of basaltic magmas within an enriched metasomatised W Greenland lithospheric mantle was triggered by hot asthenosphere-derived tholeiitic magmas traversing the lithosphere.

The complex geological history within this part of the North Atlantic area could be an alternative explanation. A potential alternative to metasomatic source enrichment would be magma mixing at deeper mantle levels involving recycled crustal materials. The origin of basaltic rocks within a fertile and metasomatised SCLM source during waning stages of regional magmatism, as we tentatively suggest for melts parental to Faroese lowTiO_2 and high-TiO_2 saucer-shaped sills, would be in accordance with inferences regarding late stage magmatism in other LIPs too (e.g. Peate, 1997 and references therein). Peate (1997) pointed out that a thermal anomaly from some sort of a mantle plume at the base of the lithosphere in the Paraná-Etendeka province once provided the heat necessary for basaltic melt production within the overlying fertile metasomatised lithospheric mantle. He inferred melting at successively shallower lithospheric levels with time from the arrival of the presumed mantle plume, provided that overall lithospheric thicknesses exceeded 100 km. Larsen et al. (2003) inferred a slightly different scenario, where production of basaltic magmas within an enriched

metasomatised W Greenland lithospheric mantle was triggered by hot asthenosphere-derived tholeiitic magmas traversing the lithosphere.

The intermediate-TiO_2 Morskranes Sill most probably developed in response to melting of a distinct and geochemically depleted source and the similarity between its REE trend and those representing the local low-TiO_2 and intermediate-TiO_2 dykes and irregular intrusions analysed in this study (Fig. 4) could indicate broadly similar geochemical compositions of their respective mantle sources.

5.6.4. NW Atlantic isotopic mantle reservoirs from the literature

Isotopic and geochemical similarities between Faroese low-TiO_2 lavas and MORB led Gariépy et al. (1983) to infer a depleted asthenospheric source for these lavas, while they attributed $^{87}Sr/^{86}Sr$ ratios of 0.7032 in local high-TiO_2 lavas to an origin from mantle materials comparable to sources inferred for ocean island basalts (OIB) within the sub-continental lithospheric mantle or from partial melting of deep mantle "blobs". The source to LREE depleted Faroese low-TiO_2 picritic dykes displaying very low ε_{Sr} and high ε_{Nd} has previously been interpreted to represent a true depleted end-member composition that may originate from deeper mantle levels when compared to sources to depleted recent basalts of the Reykjanes Ridge and Neogene-recent lavas from Iceland (Holm et al., 2001). The Pb isotopic compositions of Faroese high-TiO_2 magnesian dykes are thought to reflect mixing between this depleted source and a high $^{208}Pb/^{204}Pb$ end-member source comparable to the one that gave rise to Icelandic samples with the most radiogenic Pb (Holm et al., 2001). These authors ascribed the higher $^{208}Pb/^{204}Pb$ ratios at low $^{207}Pb/^{204}Pb$ ratios in most of the other Faroese high-TiO_2 dykes relative to those of e.g. comparable basaltic rocks from Iceland, to a main plume component possessing Pb isotopic characteristics that were particular for the Faroese mantle. According to a more recent study, Faroese low-TiO_2 basaltic lavas owe their isotopic variations to mixing between a primitive end-member component ($^{206}Pb/^{204}Pb$ = 17.5; $^{87}Sr/^{86}Sr$ = 0.703; $^{143}Nd/^{144}Nd$ = 0.5131), a Faroese depleted component (FDC, $^{206}Pb/^{204}Pb$ = 18.2; $^{87}Sr/^{86}Sr$ = 0.7025; $^{143}Nd/^{144}Nd$ = 0.5132) and an enriched EM-type component (Søager and Holm, 2011). These authors further stated that enriched Faroese high-TiO_2 lavas developed from two enriched mantle reservoirs similar to the IE1 and IE2 end-member mantle components proposed as sources to some Icelandic basaltic rocks (i.e. Thirlwall et al., 2004).

Thirlwall et al. (2004) suggested five end-member mantle components that could explain the entire isotopic range displayed by the basaltic rocks of Iceland, while Hanan and Schilling (1997) invoked a model based on three end-member mantle components/reservoirs *d*, *p* and *e* in order to explain the isotopic range of Icelandic volcanic rocks. Stracke et al. (2003) attributed the impressive correlation in radiogenic Pb isotope ratios of Icelandic basalts to contributions from HIMU-like components to a main primitive end-member source possessing Pb isotopic compositions comparable to Theistareykir picrites, probably with slight involvement of an additional EM I-like component too, i.e. a mechanism that resembles the model proposed earlier by Ellam and Stuart (2000) and Søager and Holm (2011) for the BTIB and Faroese lavas respectively. A more recent study suggested that involvement of isotopically enriched HIMU mantle components in NAIP mantle sources could be problematic, as these represent extreme isotopic compositions reported only in the southern hemisphere, whereas less enriched FOZO components are thought to occur widely in the mantle on both hemispheres (e.g. Stracke et al., 2005 and refs. therein). The isotopic NAEM component ($^{206}Pb/^{204}Pb$ = ~17.5, $^{207}Pb/^{204}Pb$ = ~15.4 and $^{208}Pb/^{204}Pb$ = ~37.4), invoked as a common primitive end-member reservoir throughout the NAIP (Ellam and Stuart, 2000), possesses isotopic composition broadly similar to a depleted end-member NAIP mantle component proposed by Søager and Holm (2011).

5.6.5. Faroese sill samples relative to NW Atlantic isotopic mantle reservoirs

Altogether, the Faroese sill samples define a rough trend between the isotopic mantle reservoirs NAEM and FOZO, but low-TiO_2 and high-TiO_2 sills are also skewed slightly towards EM-like mantle reservoirs, when plotted in $^{206}Pb/^{204}Pb$ versus $^{87}Sr/^{86}Sr$ and $^{143}Nd/^{144}Nd$ diagrams (Fig. 11b; Fig. 11c). The differences in Nd isotopic compositions between samples representing high-TiO_2, intermediate-TiO_2 and low-TiO_2 Faroese sill samples relative to those that outline Icelandic basalts (Fig. 11c) suggest that some of their end-member mantle sources differed with respect to their Nd isotopes in particular. The lead isotope signatures displayed by the LREE enriched samples of Faroese low-TiO_2 and high-TiO_2 sills differ noticeable from those of LREE depleted NAEM-like Faroese low-TiO_2 lavas/dykes and Icelandic low-TiO_2 lavas from the Theistareykir area, whilst samples of the LREE depleted Morskranes Sill plot closer to the NAEM (Fig. 11b; Fig. 11c). As the Faroese sill samples do not display any clear association with DMM and FDC isotopic end-member reservoirs (apart from a sample of the Kvívík Sill in Fig. 11b), inferred to have influenced the isotopic compositions in Icelandic and Faroese low-TiO_2 lavas (Fig. 11b; Fig. 11c), these are

unlikely to have contributed noticeable to the general isotopic characteristics displayed by the actual sill samples. Samples of the Faroese low-TiO_2 and high-TiO_2 sills in general could originate from mantle sources that displayed moderate isotopic enrichment towards IE 1 or FOZO-like reservoirs (Fig. 11b; Fig. 11c), a scenario that would be in accordance with the moderately fertile sources we infer to have resulted in their gentle negative REE slopes. The relatively low $^{87}Sr/^{86}Sr(t)$, $^{206}Pb/^{204}Pb$ and (to a lesser degree) $^{207}Pb/^{204}Pb$ ratios in samples representing the small Morskranes Sill relative to samples representing the other local sills point to (a) more depleted mantle source(s) for this small sill relative to those inferred for the other sills, perhaps related to the NAEM isotope reservoir (Fig. 5; Fig. 11).

On the one hand, samples representing low-TiO_2 and high-TiO_2 sills combined, as well as all samples representing the intermediate-TiO_2 Morskranes Sill, define two almost perfect linear trends when plotted in a $^{206}Pb/^{204}Pb$ versus $^{208}Pb/^{204}Pb$ ratios diagram (Fig. 5c). On the other hand, at least three samples representing the Morskranes Sill and two samples representing the Eysturoy and Sundini sills (and perhaps also two samples representing the Streymoy and Kvívík sills) are shifted towards higher $^{207}Pb/^{204}Pb$ ratios relative to other local sill samples in diagrams, where these lead isotope ratios are plotted against $^{208}Pb/^{204}Pb$ and $^{206}Pb/^{204}Pb$ ratios (Fig. 5b; Fig.5d). The lead isotope particularities of these Faroese sills could stem either from tapping from mantle reservoirs displaying isotopic heterogeneities (at short length scales in the case of the Morskranes Sill), or they could implicate crustal contamination (i.e. discussion in sub-Sect. 5.2 above).

Prytulak and Elliot (2007) suggest a link between increasing TiO_2 contents in OIBs worldwide and relative enrichments of their Sr and Nd isotopes, due to decreasing degrees of partial mantle melting of eclogite-bearing peridotites (~1 to ~10 % eclogite) with increasing mantle depths, in accordance with the lid effect (e.g. Fodor, 1987; Prytulak and Elliot, 2007; Niu et al., 2011). The lid effect has also been considered important in parts of the NAIP (e.g. Tegner et al., 1998, Momme et al., 2006; Søager and Holm, 2011; Waight and Baker, 2012; Millet et al., 2017). The distinct TiO_2 compositions, displayed by samples representing the various Faroese sills, could in theory have evolved in response to similar mantle processes, but no clear systematic Sr and Nd isotopic enrichments exist for Faroese high-TiO_2 versus low-TiO_2 sills (although the low TiO_2 sills display slightly elevated $^{143}Nd/^{144}Nd$ ratios relative to all high-TiO_2 sills). Also, the limited Sr and Nd isotopic data available for these sills (Fig. 5a) render it difficult to assess with any certainty whether they developed in accordance with the lid effect. If these sills indeed formed broadly contemporaneously according to the lid effect, it would imply a very steep or discontinuous local lithospheric

base, as lateral distances between most low-TiO_2 and high-TiO_2 Faroese sills only range from 10 to 15 km (Fig. 1). A discontinuous local lithospheric base in the Faroese area could have developed in response to previous regional or provincial tectonic activity. Alternatively, some of the magmas may have experienced noticeable lateral transport, like it has been suggested in recent studies for other low-TiO_2 Faroese lavas and during recent volcanic eruptions in Bali, Indonesia (Millet et al., 2017; Albino et al., 2019).

6. Summary and concluding remarks

The basaltic sills of the Faroe Islands can be grouped into three main categories according to their TiO_2 contents. The Streymoy and Kvívík sills define a low-TiO_2 category, the Eysturoy, Sundini, Langaregn and Svínoy-Fugloy sills define a high-TiO_2 category, while samples of the Morskranes Sill are intermediate-TiO_2 between these two. It is likely that the high-TiO_2 sills developed from three slightly dissimilar mantle sub-sources, i.e. the Eysturoy and Sundini sills, the Langaregn Sill and the Svínoy-Fugloy Sill respectively tapped mantle reservoirs of slightly different geochemical compositions Calculations suggest that differences in Al_2O_3, Fe_2O_3, TiO_2, CaO, MgO, Sr, Eu compositions in particular within the actual intrusions can be explained by various degrees of partial melting, olivine fractionation, as well as plagioclase fractionation and accumulation. Moderately positive and negative Nb and Ta anomalies in some of the sills seem to suggest that their mantle sources were affected by the addition or extraction of metasomatic agents at some point. The inferred petrogenetic sequences for the actual sills can briefly be summarised as follows:

- The Streymoy and Kvívík sills evolved by fractional crystallisation of mainly olivine (~15 wt %) and net accumulation of plagioclase (15 to 25 wt %) upon ascent. Their REE compositions can be explained by 16 to 21 % melting of a moderately fertile mantle at depths of $\leq$ 85 km and (e.g. Fig. 12a).
- The Eysturoy, Sundini, Svínoy-Fugloy and Langaregn sills evolved by fractional crystallisation of mainly olivine (~15 wt %) and plagioclase (15 to 20 wt %), while en-route to the upper crust. The REE compositions of the first three sills can be accounted for by 5 to 7.5 % melting of a moderately fertile mantle at depths of $\leq$ 85 km, while ~4 % melting of a slightly different mantle composition(s) at deeper levels is required for the Langaregn Sill (Fig. 12b; Fig. 12c).

- The primary magmas, which eventually evolved to the Morskranes Sill by fractional crystallisation of mainly olivine (~15 wt %) and perhaps some plagioclase (≤ 10 wt %) during ascent, most likely formed by 6 to 7 % melting of a moderately depleted mantle at depths of ≤ 85 km (Fig. 12d). Isotopic constraints suggest that parts of the Morskranes Sill have experienced slight crustal contamination, or their mantle source(s) displayed slight isotopic heterogeneities a short length scales. Such a contaminant would be of similar composition to that reported earlier for the Rockall Plateau basement and/or E Greenland basement (please see captions Fig. 7 for references).
- The entire Pb isotope range of local contaminated silicic lavas can be explained in terms of assimilation of materials comparable to those reported for E Greenland, while part of this isotope range could be explained by contamination with materials comparable in isotope compositions to those reported for NW Britain basement. Hence, E Greenland-type basement is apparently ubiquitous beneath the Faroe Islands (please see captions Fig. 7 for references).

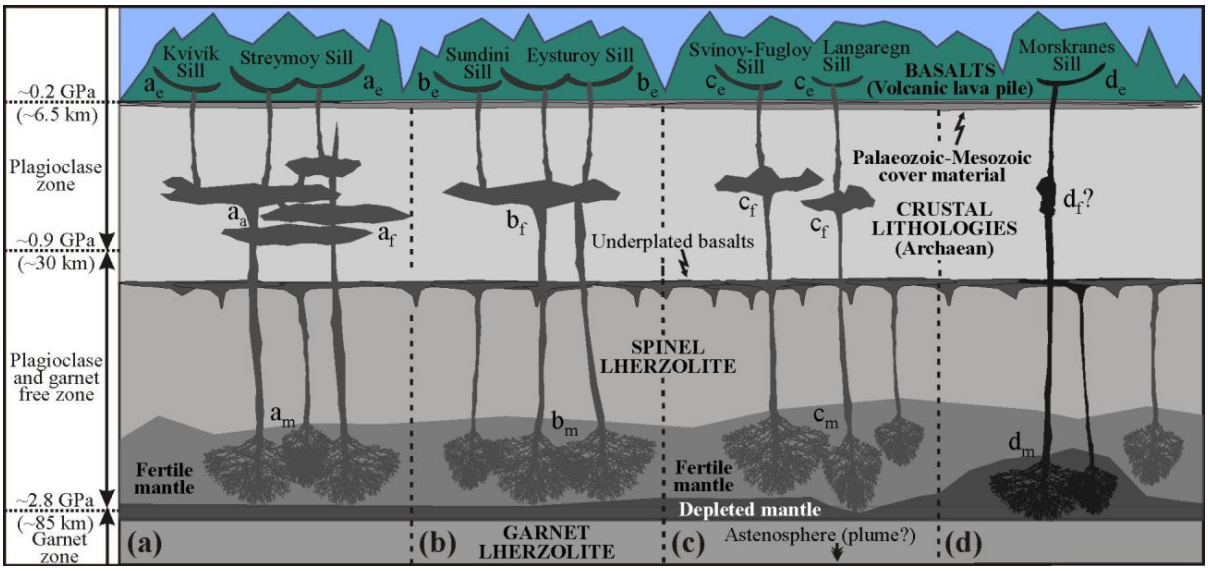

Fig. 12. The simplified profile summarises the inferred petrogenetic processes in action during formation of the Faroese sills. Vertical distances are drawn at arbitrary scales. a) The Streymoy and Kvívík sills. b) The Eysturoy and Sundini sills. c) The Svínoy-Fugloy and Langaregn sills. d) The Morskranes Sill. The garnet stability field is from Robinson and Wood (1998) and Presnall et al. (2002). The plagioclase stability field is from Borghini et al. (2010) and Presnall et al. (2002). Abbreviations where x represents the letters a-d are: x_m = partial melting; x_a = plagioclase accumulation; x_f = mineral fractionation; x_e = sill emplacement. See main text for a more detailed explanation.

Based on the limited data of this work, isotopic compositions of most Faroese sill samples can probably be explained in terms of the two well-known isotopic mantle reservoirs NAEM and FOZO, where low-TiO_2 and high-TiO_2 sills probably also contain slight amounts of materials originating from an EM-like mantle component. Hence, it is likely that at least three main end-member isotopic mantle reservoirs contributed to the isotopic characteristics displayed by the Faroese sills. It is proposed that melt generation to produce the Faroese sills occurred at relatively shallow mantle levels during the waning stages of basaltic magmatism in the NAIP, much similar to what has been envisaged previously for some Early Cretaceous Paraná-Etendeka flood basalts (Peate et al., 1997).

Data availability. All information on international and/or in-house standard geological samples, used in association with analyses related to this research (i.e. as mentioned in Supplement 2 below), are available at the actual laboratories: at the Open University, Milton Keynes, UK, and at NGU, Trondheim, NO, for XRF analyses; at Durham University, Durham, UK, and at GEUS, Copenhagen, DK, for the ICP-MS analyses; at Durham University, Durham, UK, and at the Copenhagen University (KU), Copenhagen, DK, for the MC-ICP-MS analyses.
Data on results from calculations/modelling performed in this study can be accessed via the link: DOI: 10.17632/47fzntf2b3.1

Author contributions. The actual manuscript is based upon a relatively recent Ph.D. thesis in geology, defended at Durham University in 2012 by the first author. The actual research and writing/preparation was performed by the first author Jógvan Hansen. All listed co-authors have acted as supervisors at various stages of thesis and paper preparation. In addition, Dougal Jerram initiated the actual research project at Durham University, while Mike Widdowson and Christopher Ottley ran XRF and ICP-MS laboratories at the Open University and at Durham University respectively, where the actual analyses were performed.

Competing interests. The authors declare that they have no conflict of interest.

Disclaimer. The authors declare that they have nothing to disclaim.

Acknowledgements. This manuscript is to a large degree based on data from a previous research project at Durham University, funded by BP, Chevron and Geysir Petroleum, via

Jarðfeingi (Faroese Geological Survey). In addition, key data and fieldwork, funded privately by the first author, are of utmost importance for the current version of this paper. AV Faroe Islands is appreciated for provision of basic living costs for the first author during production of parts of this work. Isotope analyses carried out at the Arthur Holmes Isotope Laboratory, Department of Earth Sciences, Durham University by Dr. Geoff M. Nowell are greatly appreciated. Dougal Jerram acknowledges the support from the Research Council of Norway through its Centres of Excellence funding scheme, project 22372 (CEED - Centre for Eath Evolution and Dynamics). Earlier versions of this paper benefited from comments by Tod Waight and an anonymous reviewer. The authors of this manuscript are indebted to fellow author Jon Davidson, Durham University, who sadly passed away in 2016, for his thorough work on earlier versions of this paper.

References

Albino, F., Briggs, J., Syahbana, D.K., 2019. Dyke intrusion between neighbouring arc volcanoes responsible for 2017 pre-eruptive seismic swarm at Agung, Nature Com. 10, 748, https://doi.org/10.1038/s41467-019-08564-9.

Babechuk, M.G., Widdowson, M., Kamber, B.S., 2014. Quantifying chemical weathering intensity and trace element release from two contrasting basalt profiles, Deccan Traps, India, Chem. Geol. 363, 56-75.

Bernstein, S., 1994. High-pressure fractionation in rift-related basaltic magmatism: Faeroe plateau basalts, Geology 22, 815-818.

Blatt, H., Tracy, R.J., 1995. Petrology, Igneous, Sedimentary, and Metamorphic, Second edition. W. H. Freeman and Company, New York pp. 529.

Blichert-Toft, J., Lesher, C.E., Rosing, M.T., 1992. Selectively contaminatcd magmas of the Tertiary East Greenland macrodyke complex, Contrib. Mineral. Petrol. 110, 154-172.

Borghini, G., Fumagalli, P., Rampone, E., 2010. The stability of plagioclase in the upper mantle: Subsolidus experiments on fertile and depleted lherzolite. J. Petrol. 51(1-2), 229-254.

Bott, M.H.P., Sunderland, J., Smith, P. J., Casten, U., Saxov, S., 1974. Evidence for continental crust beneath the Faeroe Islands. Nature 248, 202-204.

Bryce, J.G., DePaolo, D.J., 2004. Pb isotopic heterogeneity in basaltic phenocrysts. Geochim. Cosmochim. Acta 68(21), 4453-4468.

Charlier, B.L.A., Ginibre, C., Morgan, D., Nowell, G.M., Pearson, D.G., Davidson, J.P., Ottley, C.J., 2006. Methods for the microsampling and high precision analysis of strontium and rubidium isotopes at single crystal scale for petrological and geochronological applications, Chem. Geol. 232, 114-133.

Choi, S.H., Kwon, S-T., 2005. Mineral chemistry of spinel peridotite xenoliths from Baengnyeong Island, South Korea, and its implications for the paleogeotherm of the uppermost mantle, The Island Arc 14, 236-253.

Dasgupta, R., Hirschmann, M.M., Smith, N.D., 2007. Partial melting experiments of peridotite + CO_2 at 3 GPa and genesis of alkalic ocean island basalts., J. Petrol. 48(11), 2093-2124.

Day, J.M.D., Pearson, D.G., Macpherson, C.G., Lowry, D., Carracedo, J.C., 2010. Evidence for distinct proportions of subducted oceanic crust and lithosphere in HIMU-type mantle beneath El Hierro and La Palma, Canary Islands., Geochim. Cosmochim. Acta 74, 6565-6589.

Deer, W.A., Howie, R.A., Zussman, J., 1992. An introduction to the rock forming minerals. Second edition., Longman pp. 696.

Dickin, A.P., 1981. Isotope geochemistry of Tertiary igneous rocks from the Isle of Skye., J. Petrol. 22, 155-189.

Downes, H., MacDonald, R., Upton, B.G.J., Cox, K.G., Bodinier, J-L., Mason, P.R.D., James, D., Hill, P.G., Hearn, B.C., 2004. Ultramafic xenoliths from the Bearpow Mountains, Montana, USA: Evidence for multiple metasomatic events in the lithospheric mantle beneath the Wyoming Craton, J. Petrol. 45(8), 1631-1662.

Dowall, D.P., Nowell, G.M., Pearson, D.G., 2003. Chemical pre-concentration procedures for high-precision analysis of Hf-Nd-Sr isotopes in geological materials by plasma ionisation multi-collector mass spectrometry (PIMMS) techniques, In: Holland J.G. and Tanner S.D. Eds. Plasma Source Mass Spectrometry: Applications and Emerging Technologies, The R. Soc. Chem. Cambridge 321-337.

Dupuy, C., Mével, C., Bodinier, J-L., Savoyant, L., 1991. Zabargad peridotite: Evidence for multistage metasomatism during Red Sea rifting, Geology 19, 722-725.

Ellam, R.M., Stuart, F.M., 2000. The sub-lithospheric source of north Atlantic basalts: evidence for, and significance of, a common end-member, J. Petrol. 41(7), 919-932.

Ellis, D., Bell, B.R., Jolley, D.W., O'Callaghan, M., 2002. The Stratigraphy, environment of eruption and age of ther Faroes Lava Group, NE Atlantic Ocean, Geol. Soc. London, Spec. Publ. 197, 253-269.

Falloon, T.J., Green, D.H., Danyushevskyi, L.V., Faul, U.H., 1999. Peridotite Melting at 1·0 and 1·5 GPa: an Experimental Evaluation of Techniques using Diamond Aggregates and Mineral Mixes for Determination of Near-solidus Melts, J. Petrol. 40(9), 1343-1375.

Faure, G., 1986. Principles of isotope geology. Second edition. John Wiley & sons pp. 589.

Faure, G., 2001. Origin of igneous rocks: the isotopic evidence, Springer Verlag. Berlin, Heidelberg, New York pp. 495.

Fitton, J.G., Saunders, A.D., Kempton, P.D., Hardarson, B.S., 2003. Does depleted mantle form an intrinsic part of the Iceland plume?, Geochem. Geophys. Geosyst. 4(3), pp. 14.

Fodor, R.V., 1987. Low- and high-TiO_2 flood basalts of southern Brazil: origin from picritic parentage and a common mantle source, Earth Plan. Sci. Lett. 84, 423-430.

Font, L., Davidson, J.P., Pearson, D.G., Nowell, G.M., Jerram, D.A., Ottley, C.J., 2008. Sr and Pb IsotopeMicro-analysis of Plagioclase Crystals from Skye Lavas: an Insight into Open-systemProcesses in a Flood Basalt Province, J. Petrol. 49(8), 1449-1471.

Fram, M.S., Lesher, C.E., 1997. Generation and polybaric differentiation of East Greenland Early Tertiary flood basalts, J. Petrol. 38(2), 231-275.

Frei, R., Villa, I.M., Nägler, Th.F., Kramers, J.D., Pryzbylowicz, W.J., Prozesky, V.M., Hofmann, B.A., Kamber, B.S., 1997. Single mineral dating by Pb–Pb step-leaching method; assessing the mechanisms, Geochim. Cosmochim. Acta 61, 393–414.

Gariépy, C., Ludden, J., Brooks, C., 1983. Isotopic and trace element constraints on the genesis of the Faeroe Lava pile, Earth Plan. Sci. Lett. 63, 257-272.

Geldmacher, J., Haase, K.M., Devey, C.W., Garbe-Schönberg, C.D., 1998. The petrogenesis of Tertiary cone-sheets in Ardnamurchan, NW Scotland: petrological and geochemical constraints on crustal contamination and partial melting, Contrib Mineral Petrol. 131, 196-209.

Gibson, S.A., Thompson, R.N., Dickin, A.P., Leonardos, O.H., 1995. High-Ti and low-Ti mafic potassic magmas: Key to plume-lithosphere interactions and continental flood-basalt genesis, Earth Plan. Sci. Lett. 136, 149-165.

Green, D.H., Falloon, T.J., 2005. Primary magmas at mid-ocean ridges, ”hotspots,” and other intraplate settings: Constraints on mantle potential temperature, in Foulger GR, Natland JH, Presnall DC, Anderson DL, eds., Plates, plumes, and paradigms: Geol. Soc. of Am. Spec. Paper 388, 217-247.

Grégoire, M., Bell, D.R., Le Roex, A.P., 2003. Garnet lherzolites from the Kaapvaal Craton (South Africa): trace element evidence for a metasomatic history, J. Petrol. 44 (4), 629-657.

Hald, N., Waagstein, R., 1983. Silicic basalts from the Faeroe Islannds: evidence of crustal contamination, In: Bott MHP, Saxov S, Talvani M, Thiede J (eds) Structure and development of the Greenland-Scotland Ridge. New methods and concepts. Plenum New York 343-349, 1983.

Hald, N., Waagstein, R., 1984. Lithology and chemistry of a 2-km sequence of Lower Tertiary tholeiitic lavas drilled on Suðuroy, Faeroe Islands (Lopra-1), In: Berthelsen O., Noe-Nygaard A. and Rasmussen J. (eds) The deep drilling project 1980-1981 in the Faeroe Islands. Annales Societatis Scientiarum Færoensis, Tórshavn, Supplementum IX 15-38.

Hald, N., Waagstein, R., 1991. The dykes and sills of the Early Tertiary Faeroe Island basalt plateau, Trans. Royal Soc. Edinburg: Earth Sci. 82, 373-388.

Hall, A., 1996. Igneous Petrology, © Longman Group Limited, England. Second Edition pp. 551.

Hanan, B.B., Blichert-Toft, J., Kingsley, R., Schilling, J-G., 2000. Depleted Iceland mantle plume geochemical signature: artifact of multicomponent mixing?, Geochem. Geophys. Geosyst. 1(1), pp. 19.

Hanan, B.B., Schilling, J-G., 1997. The dynamic evolution of the Iceland mantle plume: the lead isotope perspective, Earth Plan. Sci. Lett. 151, 43-60.

Hanghøj, K., Storey, M., Stecher, O., 2003. An isotope and trace element study of the East Greenland Tertiary dyke swarm: constraints on temporal and spatial evolution during continental rifting, J. Petrol. 44(11), 2081-2112.

Hansen, J., 2011. Petrogenetic Evolution, Geometries and Intrusive Styles of the Early Cenozoic Saucer-Shaped Sills of the Faroe Islands. Doctoral thesis, Durham University. Available at Durham E-Theses Online http://etheses.dur.ac.uk/3631/.

Hansen, J., Davidson, J.P., Jerram, D.A., Ottley, C.J., Widdowson, M., 2019. Data sets showing calculations/modelling on basaltic rocks of the Faroe Islands. Mendeley, 2019, DOI: 10.17632/47fzntf2b3.1.

Hansen, J., Jerram, D.A., McCaffrey, K.J.W., Passey, S.R., 2009. The onset of the North Atlantic Igneous Province in a rifting perspective, Geol. Mag. 146(3), 309-325.

Hansen, J., Jerram, D.A., McCaffrey, K.J.W., Passey, S.R., 2011. Early Cenozoic saucer-shaped sills of the Faroe Islands: an example of intrusive styles in basaltic lava piles, J. Geol. Soc. London 168(1), 159-178.

Hart, S. R., 1988. Heterogeneous mantle domains: signatures, genesis and mixing chronologies, Earth Plan. Sci. Lett. 90, 273-296.

Higgins, N.C., Solomon, M., Varne, R., 1985. The genesis of the Blue Tier Batholith, northeastern Tasmania, Lithos 18, 129-149.

Hirose, K., Kawamoto, T., 1995. Hydrous partial melting of lherzolite at 1 GPa: The effect of H_2O on the genesis of basaltic magmas, Earth Plan. Sci. Lett. 133, 463-473.

Hirose, K., Kushiro, I., 1993. Partial melting of dry peridotites at high pressures: Determination of compositions of melts segregated from peridotite using aggregates of diamond, Earth Plan. Sci. Lett. 114, 477-489.

Hofmann, A. W., 1997. Mantle geochemistry: the message from oceanic volcanism, Nature 385, 219-229.

Hofmann, A.W., 2003. Treatise on Geochemistry, Volume 2. Editor: Richard W. Carlson. Executive Editors: Heinrich D. Holland and Karl K. Turekian, pp. 568, ISBN 0-08-043751-6, Elsevier 61-101.

Holm, P.M., Hald, N., Waagstein, R., 2001. Geochemical and Pb-Sr-Nd isotopic evidence for separate hot depleted and Iceland plume mantle sources for the Paleogene basalts of the Faroe Islands, Chem. Geol. 178, 95-125.

Ionov, D.A., Bodinier, J-L., Mukasa, S.B., Zanetti, A., 2002. Mechanisms and sources of mantle metasomatism: major and trace element compositions of peridotite xenoliths from Spitsbergen in the context of numerical modelling, J. Petrol. 43(12), 2219-2259.

Ivanov, A.V., Demonterova, E.I., Rasskazov, S.V., Yasnygina, T.A., 2008. Low-Ti melts from the southeastern Siberian Traps Large Igneous Province: Evidence for a water-rich mantle source, J. Earth. Syst. Sci. 117(1), 1-21.

Jerram, D.A., Single, R.T., Hobbs, R.W., Nelson, C.E., 2009. Understanding the offshore flood basalt sequence using onshore volcanic facies analogues: an example from the Faroe–Shetland basin, Geol. Mag. 146(3), 353-367.

Jerram, D.A., Widdowson, M., 2005. The anatomy of Continental Flood Basalt Provinces: geological constraints on the processes and products of flood volcanism, Lithos 79, 385-405.

Jolley, D.W., Passey, S.R., Hole, M., Millett, J., 2012. Large-scale magmatic pulses drive plant ecosystem dynamics, J. Geol. Soc. 169(6), 03-711.

Kalsbeek, F., 1995. Geochemistry, tectonic setting, and poly-orogenic history of Palaeoproterozoic basement rocks from the Caledonian fold belt of North-East Greenland, Precamb. Res. 72, 301-315.

Kays, M.A., Goles, G.G., Grover, T.W., 1989. Precambrian sequence bordering the Skaergaard Intrusion, J. Petrol. 30(2), 321-361.

Kerr, A. C., 1995. The geochemistry of the Mull-Morvern Tertiary lava succession, NW Scotland: an assessment of mantle sources during plume-related volcanism, Chem. Geol. 122(1-4), 43-58.

Kerr, A.C., Kempton, P.D., Thompson, R.N., 1995. Crustal assimilation during turbulent magma ascent (ATA); new isotopic evidence from the Mull Tertiary lava succession, N. W. Scotland, Contrib. Mineral. Petrol. 119, 142-154.

Kitagawa, H., Kobayashi, K., Makishima, A., Nakamura, E., 2008. Multiple pulses of the Mantle Plume: Evidence from Tertiary Icelandic Lavas, J. Petrol. 49(7), 1365-1396.

Klein, E.M., Langmuir, C.H., 1987. Global correlations of ocean ridge basalt chemistry with axial depth and crustal thickness, J. Geophys. Res. 92(B8), 8089-8115.

Klemme, S., Prowatke, S., Hametner, K., Günther, D., 2005. Partitioning of trace elements between rutile and silicate melts: Implications for subduction zones, Geochim. Cosmochim. Acta 69(9), 2361–2371.

Kogiso, T., Hirose, K., Takahashi, E., 1998. Melting experiments on homogeneous mixtures of peridotite and basalt: application to the genesis of ocean island basalts, Earth Plan. Sci. Lett. 162, 45-61.

Kogiso, T., Hirschmann, M.M., Pertermann, M., 2004. High-pressure partial melting of mafic lithologies in the mantle, J. Petrol. 45(12), 2407-2422, 2004.

Kokfeldt, T.F., Hoernle, K., Hauff, F., Fiebig, J., Werner, R., Schônberg, D. G-S., 2006. Combined Trace Element and Pb-Nd–Sr-O Isotope Evidence for Recycled Oceanic Crust (Upper and Lower) in the Iceland Mantle Plume, J. Petrol. 47(9), 1705-1749, 2006.

Korenaga, J., Kelemen, P.B., 2000. Major element heterogeneity in the mantle source of the North Atlantic Igneous Province, Earth Plan. Sci. Lett. 184, 251-268.

Kretz, R., 1983. Symbols for rock-forming minerals, Am. Mineral. 68, 277-279.

Kushiro, I., 1996. Partial melting of a fertile mantle peridotite at high pressures: An experimental study using aggregates of diamond, Geophys.Monogr. 95, 109-122.

Kushiro, I., 2001. Partial melting experiments on peridotite and origin of mid-ocean ridge basalts, Ann. Rev. Earth Plan., Sci. 29, 71-107.

Lange, A.E., Nielsen, R.L., Tepley, III.F.J., Kent, A.J.R., 2013. The petrogenesis of plagioclase-phyric basalts at mid-ocean ridges, Geochem. Geophys. Geosyst. 14(8), 3282-3296.

Larsen, L.M., Pedersen, A.K., 2009. Petrology of the Paleocene Picrites and Flood Basalts on Disko and Nuussuaq,West Greenland, J. Petrol. 50(9), 1667-1711.

Larsen, L.M., Pedersen, A.K., Sundvoll, B., Frei, R., 2003. Alkali picrites formed by melting of old metasomatized lithospheric mantle: Manîtdlat Member, Vaigat Formation, Palaeocene of West Greenland, J. Petrol. 44(1), 3-38.

Larsen, L.M., Waagstein, R., Pedersen, A.K., Storey, M., 1999. Trans-Atlantic correlation of the Palaeocene volcanic successions in the Faeroe Islands and East Greenland, J. Geol. Soc. London 156, 1081-1095.

Lesnov, F.P., Koz'menko, O.A., Nikolaeva, I.V., Palesskii, S.V., 2009. Residence of incompatible trace elements in a large spinel lherzolite xenolith from alkali basalt of Shavaryn Tsaram-1 paleovolcano (western Mongolia), Russ. Geol. Geophys. 50, 1063–1072.

Lugmair, G.W., Marti, K., 1978. Lunar initial $^{143}Nd/^{144}Nd$: differential evolution of the lunar crust and mantle, Earth Plan. Sci. Lett. 39, 349-357.

MacDonald, G.A., 1968. Composition and origin of Hawaiian lavas. In: Coats R. R., Hay R. L. and Anderson C. A. (eds), Studies in Volcanology: a memoir in honour of Howel Williams, Geol. Soc. Am. Mem. 116, 477-522.

McDonough, W.F., 1994. Chemical and isotopic systematics of continental lithospheric mantle, In: H.O.A. Meyer and O.H. Leonardos (Editors), Proc. 5th Int. Kimberlite Conf., CPRM (Comp. Pesq. Recurs. Miner.), Brasilia pp. 478-485.

McDonough, W.F., Sun, S.-s., 1995. The composition of the Earth, Chem. Geol. 120, 223-253.

Meyer, R., Nicoll, G.R., Hertogen, J., Troll, V.R., Ellam, R.M., Emelius, C.H., 2009. Trace element and isotope constraints on crustal anatexis by upwelling mantle melts in the North Atlantic Igneous Province: an example from the Isle of Rum, NW Scotland, Geol. Mag. 146(3), 382-399.

Meyer, R., Van Wijk, J., Gernigon, L., 2007. The North Atlantic Igneous Province: A review of models for its formation, Geol. Soc. Am. Spec. Pap. 430, 525-552.

Millett, J.M., Hole, M.J., Jolley, D.W., Passey, S.R., 2017. Geochemical stratigraphy and correlation within Large Igneous Provinces: The final preserved stages of the Faroe Islands Basalt Group, Lithos 286–287 1-15.

Momme, P., Tegner, C., Brooks, C.K., Keays, R.R., 2006. Two melting regimes during Paleogene flood basalt generation in East Greenland: combined REE and PGE modelling, Contrib. Mineral. Petrol. 151, 88-100.

Morton, A.C., Taylor, P.N., 1991. Geochemical and isotopic constraints on the nature and age of basement rocks from Rockall Bank, NE Atlantic, J. Geol. Soc. London 148, 631-634.

Niu, Y., Wilson, M., Humphreys, E.R., O'Hara, M.J., 2011. The origin of intra-plate ocean island basalts (OIB): the Lid Effect and its geodynamic implications, J. Petrol. 52(7&8), 1443-1468.

Noe-Nygaard, A., Rasmussen, J., 1968. Petrology of a 3,000 metre sequence of basaltic lavas in the Faeroe Islands, Lithos 1, 286-304.

Ntaflos, T., Tschegg, C., Coltorti, M., Akinin, V.V., Kosler, J., 2008. Asthenospheric signature in fertile spinel lherzolites from the Viliga Volcanic Field in NE Russia, From: Coltorti M. and Gregoire M. (eds) Metasomatism in Oceanic and Continental Lithospheric Mantle. Geol. Soc., London, Spec. Publ. 293, 57–81.

Obata, M., Morten, L., 1987. Transformation of Spinel Lherzolite to Garnet Lherzolite in Ultramafic Lenses of the Austridic Crystalline Complex, Northern Italy, J. Petrol. 28(3), 599-623.

O'Hara, M.J., Mathews, R.E., 1981. Geochemical evolution in an advancing, periodically replenished, periodically tapped, continuously fractionated magma chamber, J. Geol. Soc. London 138, 237-277.

Ottley, C.J., Pearson, D.G., Irvine, G.J., 2003. A routine method for the dissolution of geological samples for the analysis of REE and trace elements via ICP –MS, In: Plasma Source Mass Spectrometry, Applications and Emerging Technologies, (J.G. Holland, S.D. Taner, Eds.). Royal Soc. Chem. 221–230.

Passey, S.R., Bell, B. R., 2007. Morphologies and emplacement mechanisms of the lava flows of the Faroe Islands Basalt Group, Faroe Islands, NE Atlantic Ocean, Bull. Volc. 70, 139-156.

Passey, S.R., Jolley, D.W., 2009. A revised lithostratigraphic nomenclature for the Palaeogene Faroe Islands Basalt group, NE Atlantic Ocean, Earth and Environmental Science Transactions of the Royal Society of Edinburg 99, 127-158.

Peate, D.W., 1997. The Parana-Etendeka Province. Large Igneous Provinces: Continental, Oceanic, and Planetary Flood Volcanism, Geophys. Monogr. 100, 217-245.

Peate, D.W., Stecher, O., 2003. Pb isotope evidence for contributions from different Iceland mantle components to Palaeogene East Greenland flood basalts, Lithos 67, 39-52.

Peate, D.W., Hawkesworth, C.J., 1996. Lithospheric to asthenospheric transition in Low-Ti flood basalts from southern Paraná, Brazil, Chem. Geol. 127, l-24.

Peccerillo, A., 1999. Multiple mantle metasomatism in central-southern Italy: geochemical effects, timing and geodynamic implications, Geology 27(4), 315-318.

Prytulak, J., Elliott, T., 2007. TiO_2 enrichment in ocean island basalts, Earth Plan. Sci. Lett. 263, 388-403.

Rampone, E., Romairone, A., Hofmann, A.W., 2004. Contrasting bulk and mineral chemistry in depleted mantle peridotites: evidence for reactive porous flow, Earth Plan. Sci. Lett. 218, 491-506.

Rasmussen, J., Noe-Nygaard, A., 1969. Beskrivelse til geologisk kort over Færøerne i målestok 1:50000, Geol. Surv. Denm. 1. Series No. 24.

Rasmussen, J., Noe-Nygaard, A., 1970. Geology of the Faeroe Islands, Geol. Surv.Denm. I. Series No. 25, 1-142.

Raum, T., Mjelde, R., Berge, A.M., Paulsen, J.T., Digranes, P., Shimamura, H., Shiobara, H., Kodaira, S., Larsen, V.B., Fredsted, R., Harrison, D.J., 2005. Sub-basalt structures east of the Faroe Islands revealed from wide-angle seismic and gravity data, Petrol. Geosci. 11(4), 291-308.

Richardson, K.R., Smallwood, J.R., White, R.S., Snyder, D.B., Maguire, P.K.H., 1998. Crustal structure beneath the Faroe Islands and the Faroe-Iceland Ridge, Tectonophys. 300, 159-180.

Rickwood, P.C., 1989. Boundary lines within petrologic diagrams which use oxides of major and minor elements, Lithos 22, 247-263.

Robinson, J.A.C., Wood, B.J., 1998. The depth of the spinel to garnet transition at the peridotite solidus, Earth Plan. Sci. Lett. 164, 277-284.

Rollinson, H., 1998. Using geochemical data: evaluation, presentation, interpretation, Longman, pp. 352.

Saal, A.E., Hart, S.R., Shimizu, N., Hauri, E.H., Layne, G.D., 1998. Pb isotopic variability in melt inclusions from oceanic island basalts, Polynesia, Science 282, 1481-1484.

Sammarco, C., Cornwell, D.G., Rawlinson, N., 2017. Ambient noise tomography reveals basalt and sub-basalt velocity structure beneath the Faroe Islands, North Atlantic, Tectonophys. 721, 1-11.

Saunders, A.D., Norry, M.J., Tarney, J., 1988. Origin of MORB and chemically depleted mantle reservoirs: trace element constraints, J. Petrol. Spec. Lithosph, Issue 415-445.

Saunders, A.D., Fitton, J.G., Kerr, A.C., Norry, M.J., Kent, R.W., 1997. The North Atlantic Igneous Province, Geophys. Monogr. 100, 45-93.

Schaller, M., Steiner, O., Suder, I., Frei, R., Kramers, J. D., 1997. Pb stepwise leaching (PbSL) dating of garnet—addressing the inclusion problem. Schweiz, Min. Pet. Mitt. 77, 113–121.

Scarrow, J.H., Cox, K.G., 1995. Basalts generated by decompressive adiabatic melting of a mantle plume: A case study from the Isle of Skye, NW Scotland, J. Petrol. 36, 3-22.

Spulber, S.D., Rutherford, M. J., 1983. The Origin of Rhyolite and Plagiogranite in Oceanic Crust: An Experimental Study, J. Petrol. 24(1), 1-25.

Steiger, R.H., Jäger, E., 1977. Subcommission on geochronology: convention of the use of decay constants in geo- and cosmochronology, Earth Plan. Sci. Lett. 36, 359-362.

Storey, M., Duncan, R.A., Tegner, C., 2007. Timing and duration of volcanism in the North Atlantic Igneous Province: implications for geodynamics and links to the Iceland hotspot, Chem. Geol. 241, 264-281.

Stracke, A., Hofmann, A.W., Hart, S.T., 2005. FOZO, HIMU, and the rest of the mantle zoo, Geochem. Geophys. Geosyst. 6(5), pp. 20.

Stracke, A., Zindler, A., Salters, V.J.M., McKenzie, D., Blichert-Toft, J., Albaréde, F., Grønvold, K., 2003. Theistareykir revisited, Geochem. Geophys. Geosyst. 4(2), pp. 49.

Svensen, H.H., Jerram, D.A., Polozov, A.G., Planke, P., Neal, C.R., Augland, L.E., Emeleus, H.C., 2018. Thinking about LIPs: a brief history of ideas of large igneous province research, Tectonophysics (In press) DOI: https://doi.org/10.1016/j.tecto.2018.12.008

Søager, N., Holm, P.M., 2009. Extended correlation of the Paleogene Faroe Islands and East Greenland plateau basalts, Lithos 107, 205-215.

Søager, N., Holm, P.M., 2011. Changing compositions of the Icfeland plume; Isotopic and elemental constraints from the Paleogene Faroe flood basalts, Chem. Geol. 280, 297-313.

Taylor, P.N., Kalsbeek, F., Bridgwater, D., 1992. Discrepancies between neodymium, lead and strontium model ages from the Precambrian of southern East Greenland: Evidence for a Proterozoic granulite-facies event affecting Archaean gneisses, Chem. Geol. 94, 281-291.

Tegner, C., Lesher, C.E., Larsen, L.M., Watt, W.S., 1998. Evidence from the rare-earth-element recordof mantle melting for cooling of theTertiary Iceland Plume, Nature 395, 591-594.

Thompson, R.N., Morrison, M.A., Dickin, A.P., Gibson, I.L., Harmon, R.S., 1986. Two contrasting styles of interaction between basic magmas and continental crust in the British Tertiary Igneous Province, J. Geophys. Res. 91(B6), 5985-5997.

Thompson, R.N., Morrison, M.A., Dickin, A.P., Hendry, G.L., 1983. Continental flood basalts . . . Arachnids Rule OK?, In: Hawkesworth C. J., Norry M. J. (eds) Continental flood basalts and mantle xenoliths, Shiva, Nantwick, UK 158-185.

Thompson, R.N., Ottley, C.J., Smith, P.M., Pearson, D.G., Dickin, A.P., Morrison, M.A., Leat, P.T., Gibson, S.A., 2005. Source of the Quaternary alkalic basalts, picrites and basanites of the Potrillo Volcanic Field, New Mexico, USA – lithosphere or convecting mantle?, J. Petrol. 46, 1603-1643.

Thrane, K., 2002. Relationships between Archaean and Palaeoproterozoic crystalline basement complexes in the southern part of the East Greenland Caledonides: an ion microprobe study, Precamb. Res. 113, 19-42.

Thirlwall, M.F., Gee, M.A.M., Taylor, R.N., Murton, B.J., 2004. Mantle components in Iceland and adjecent ridges investigated using douple-spike Pb isotope ratios, Geochim. Cosmochim. Acta 68(2), 361-386.

Todt, W., Cliff, R.A., Hanser, A., Hofmann, A.W., 1993. Re-calibration of NBS lead standards using ^{202}Pb + ^{205}Pb double spike, Terra Abstract 5, 396.

Troll, V.R., Donaldson, C.H., Emeleus, C.H., 2004. Pre-eruptive magma mixing in ash-flow deposits of the Tertiary Rum Igneous Centre, Scotland, Contrib Mineral Petrol. 147, 722-739.

Turner, S.R., Platt, J.P., George, R.M.M., Kelley, S.P., Pearson, D.G., Nowell, G.M., 1999. Magmatism associated with orogenic collapse of the Betic–Alboran domain, SE Spain, J. Petrol. 40, 1011–1036.

Upton, B.G.J., 1988. History of Tertiary igneous activity in the N Atlantic borderlands, Geol. Soc. London, Spec. Publ. 39, 429-453.

Villaseca, C., Ancochea, E., Orejana, D. and Jeffries, T.E., 2010. Composition and evolution of the lithospheric mantle in central Spain: inferences from peridotite xenoliths from the Cenozoic Calatrava volcanic field, From: Coltorti, M., Downes, H., Gregoire, M. & O'Reilly, S. Y. (eds) Petrological Evolution of the European Lithospheric Mantle, Geol. Soc. London, Spec. Publ. 337, 125–151.

Waagstein, R., 1988. Structure, composition and age of the Faeroe basalt plateau, Geol. Soc. London, Spec. Publ. 39, 225-238.

Waagstein, R., Guise, P., Rex, D., 2002. K/Ar and ^{39}Ar/^{40}Ar whole-rock dating of zeolite facies metamorphosed flood basalts: the upper Paleocene basalts of the Faroe Islands, NE Atlantic, Geol. Soc. London, Spec. Publ. 197, 219-252.

Waight, T.E., Baker, J.A., 2012. Depleted basaltic lavas from the Proto-Iceland Plume, Central East Greenland, Journal of Petrology 53(8), 1569-1596.

Walker, J.A., Carr, M.J., Feigenson, M.D., Kalamarides, R.I., 1990. The petrogenetic significance of interstratified high- and low-Ti basalts in central Nicaragua, J. Petrol. 31(5), 1141-1164.

Weaver, B.L., Tarney, J., 1980. Rare earth geochemistry of Lewisian granulite-facies gneisses, northwest Scotland: implications for the petrogenesis of the Archaean lower continental crust, Earth Plan. Sci., Lett. 51, 279-296.

Wood, D.A., 1979. A variably veined suboceanic upper mantle – Genetic significance for mid-ocean ridge basalts from geochemical evidence, Geology 7, 499-503.

Wood, D.A., Gibson, I.L., Thompson, R.N., 1976. Elemental mobility during zeolite facies metamorphism of the Tertiary basalts of eastern Iceland, Contrib. Mineral. Petrol. 55, 241-254.

Workman, R.K., Hart, S.R.H., 2005. Major and trace element composition of the depleted MORB mantle (DMM), Earth Plan. Sci. Lett. 231, 53-72.

Wright, K.A., Davies, R.J., Jerram, D.A., Morris, J., Fletcher, R., 2012. Application of seismic and sequence stratigraphic concepts to a lava-fed delta system in the Faroe-Shetland Basin, UK and Faroes. Basin Research 24(1), 91-106.

Xiao, L., Xu, Y.G., Mei, H.J., Zheng, Y.F., He, B., Pirajno, F., 2004. Distinct mantle sources of low-Ti and high-Ti basalts from the western Emeishan large igneous province, SW China: implications for plume-lithosphere interaction. Earth Plan. Sci. Lett. 228, 525-546.

Yaxley, G.M., 2000. Experimental study of the phase and melting relations of homogeneous basalt + peridotite mixtures and implications for the petrogenesis of flood basalts, Contrib. Mineral. Petrol. 139, 326-338.

Zhang, P-F., Tang, Y-J., Hu, Y., Zhang, H-F., Su, B-X., Xiao, Y., Santosh, M., 2012. Review of melting experiments on carbonated eclogite and peridotite: insights into mantle metasomatism, Int. Geol. Rev. 54(12), 1443-1455.

Zindler, A., Hart, S., 1986. Chemical geodynamics, Ann. Rev. Earth Plan. Sci. 14, 493-571.

Supplement 1

Petrography of seven saucer-shaped sills of the Faroe Islands.

S1.1.

The Streymoy and Kvívík sills (Fig. S1.1)

Intergranular plagioclase constitutes ~35 % in most samples, occurring as 0.07-0.75 mm randomly oriented subhedral laths or as 0.75-1 mm equant anhedral grains. Additional 1.5 to 3 mm subhedral chemically zoned plagioclase phenocrysts count for 15-20 %. Intergranular anhedral equant 0.07-0.75 mm grains of clinopyroxene count for ~40 % of these rocks. Randomly strewn <0.25 mm anhedral equant olivine grains, partly altered to phyllosilicates, make up 2-6 % of rock volume joined by <3 % oxide grains of roughly

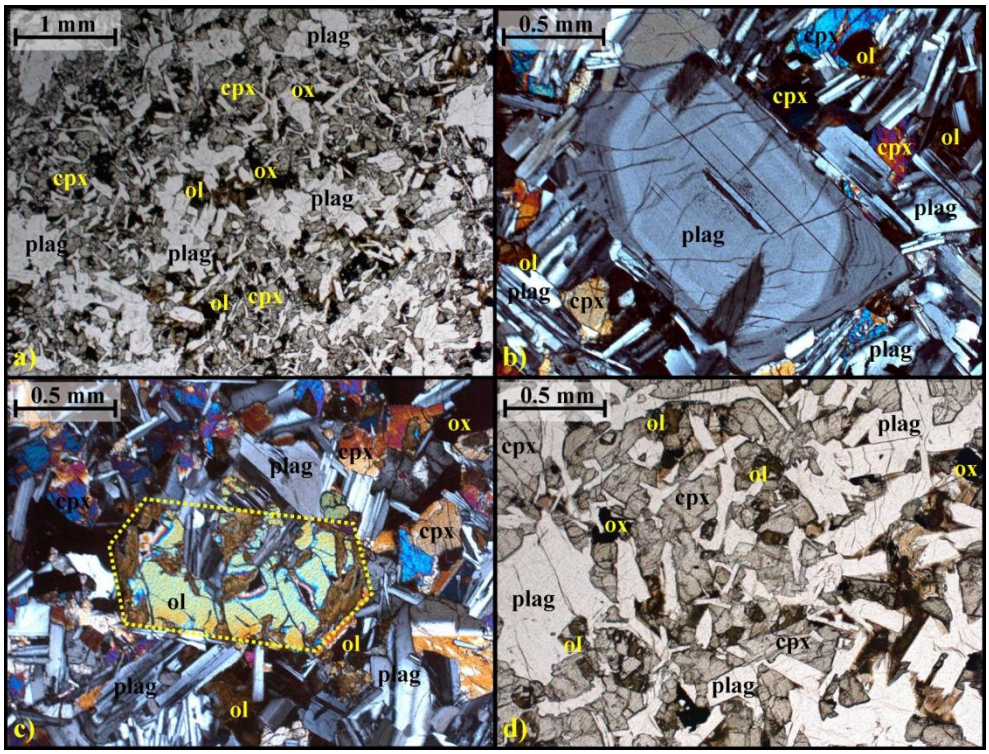

Fig. S1.1. Photomicrographs of the Streymoy and Kvívík sills. a) General distribution of most common minerals under planed polars. b) Chemically zoned plagioclase phenocryst under crossed polars. c) Partially resorbed olivine phenocryst under crossed polars (yellow dotted line). d) Closer view of a) showing distribution of tiny partially resorbed olivines under plane polars. plag = plagioclase; cpx = clinopyroxene; ol = olivine; ox = oxide. similar sizes. A few larger 0.5 – 1 mm partially resorbed olivine grains constitute <1 % of these intrusions.

S1.2.

The Eysturoy and Sundini sills (Fig. S1.2)

Randomly oriented subhedral lath-shaped 0.07-1 mm subhedral plagioclase grains make up 35-40 % of these sills. Anhedral to subhedral 0.1-0.75 mm equant clinopyroxene grains constitute 45-50 %. Clinopyroxene and plagioclase grains may be intergranular or pyroxene grains may partly enclose smaller plagioclase laths. Eentirely pseudomorphed <0.25 mm olivine grains constitute 4-6 % of these sills. Anhedral to subhedral oxides (0.05-0.5 mm) count for 4-6 % of the total volume.

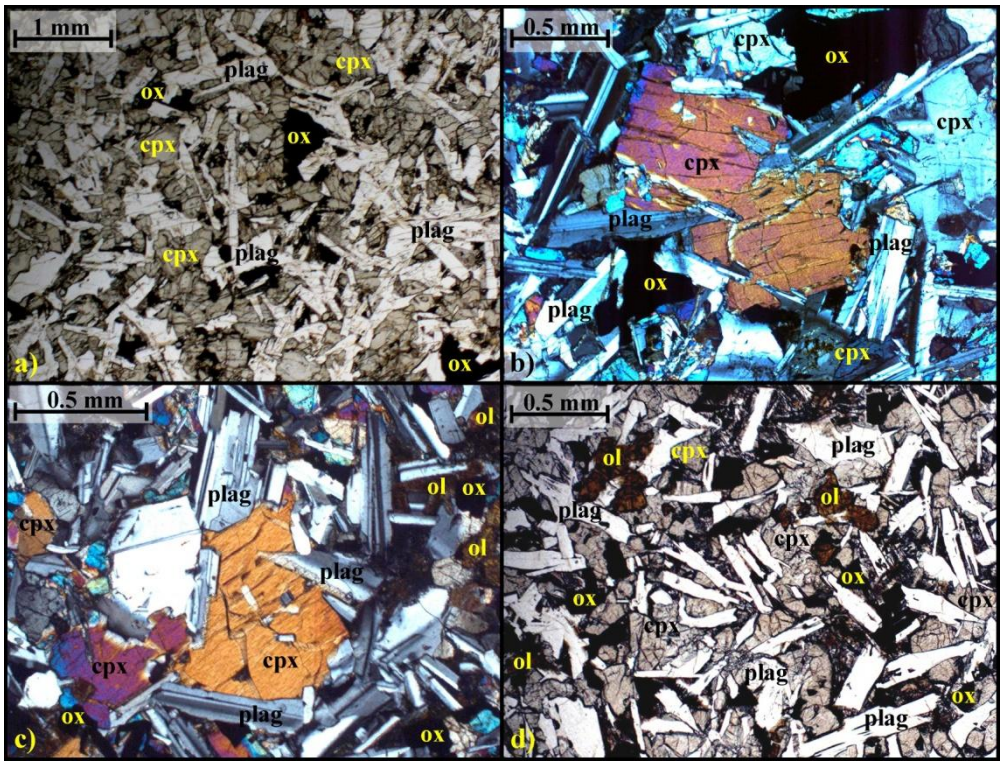

Fig. S1.2. Photomicrographs of the Eysturoy and Sundini sills. a) General distribution of three of the most common minerals under plane polars. b) Subophitic texture under crossed polars. c) Broadly similar to b), but also showing small pseudomorphed olivine grains under crossed polars. d) Most common minerals including pseudomorphed olivines under plane polars. Abbreviations are as in Fig. S1.1.

S1.3.

The Svínoy-Fugloy Sill (Fig. S1.3)

Laths of subhedral 0.05-0.75 mm plagioclase grains, amounting to 35-40 % of this sill, are poikilitically enclosed by larger ophitic to subophitic 0.35-2 mm anhedral equant clinopyroxene grains that make up 45-50 % the intrusion. Partly or entirely pseudomorphed anhedral 0.05-0.35 mm olivine grains, and oxides of similar grain sizes, constitute 5-10 % of this sill each.

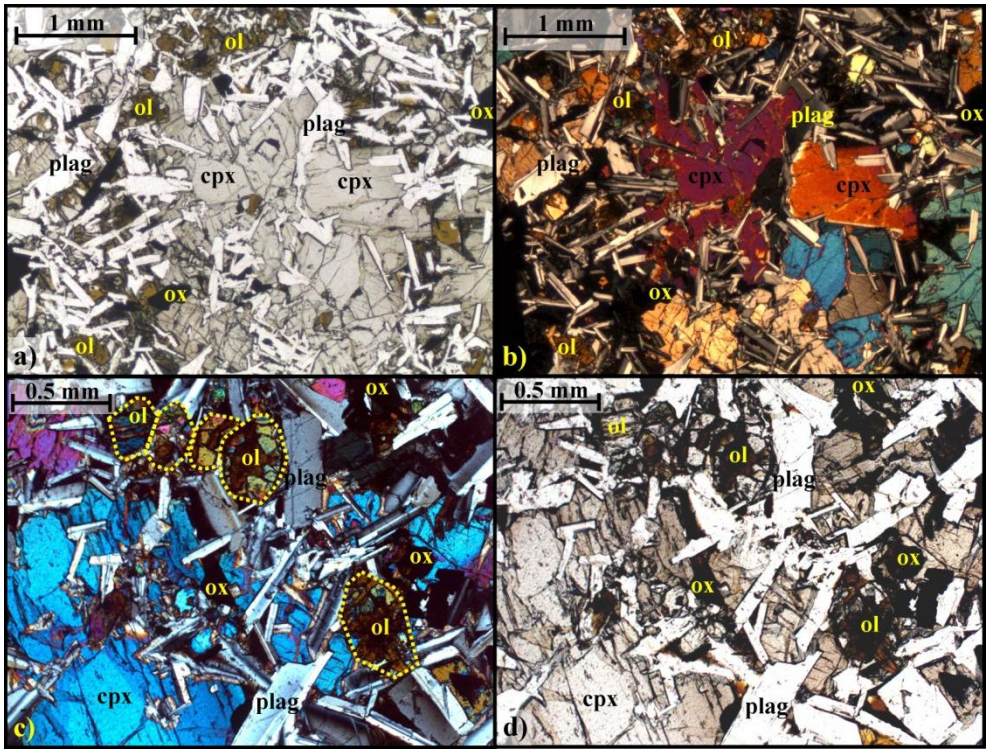

Fig. S1.3. Photomicrographs of the Svínoy-Fugloy Sill. a) Ophitic to subophitic texture and general distribution of the most common minerals under plane polars. b) Same as a), but under crossed polars. c) Partly resorbed olivines (yellow outlines). d) Same as c), but under plane polars. Abbreviations are as in Fig. S1.1.

S1.4.

The Morskranes Sill (Fig. S1.4)

The petrography of this sill resembles that of the Svínoy-Fugloy Sill, only with slightly larger amounts of olivines and oxides. Parts of the Morskranes Sill contain ~5 % by volume of secondary mineral phases occurring as <0.7 mm sub-spherical grains or as <1 mm irregular oikocrysts that partially enclose laths of plagioclase and the odd clinopyroxene.

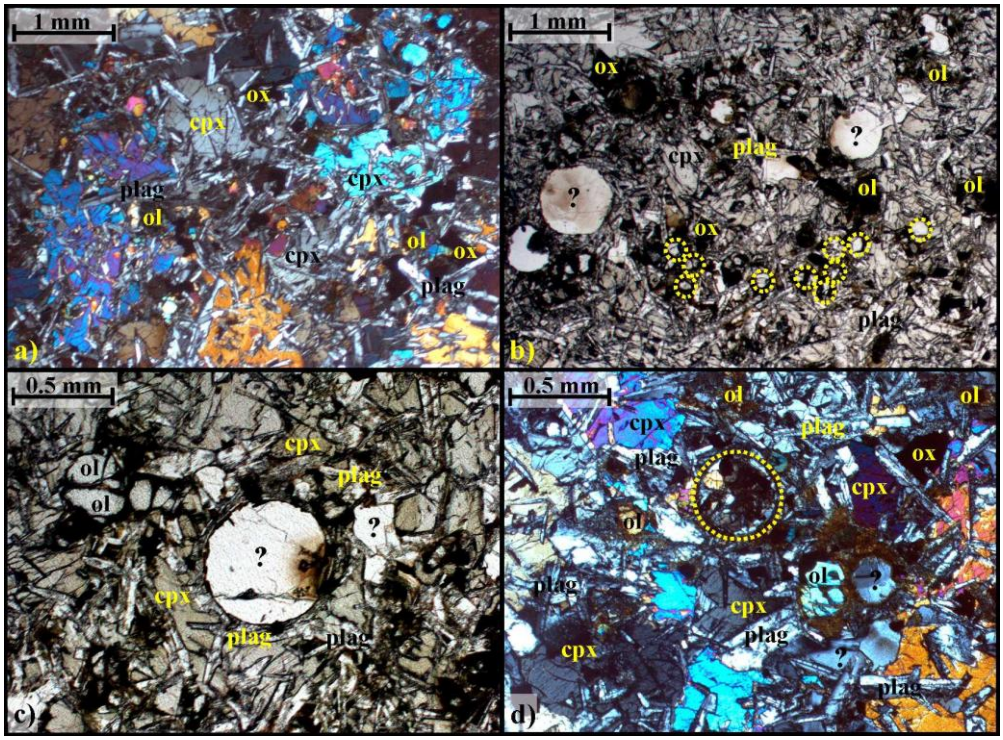

Fig. S1.4. Photomicrographs of the Morskranes Sill. a) Ophitic texture under crossed polars. b) Sub-spherical minerals (secondary) and olivines in ophitic sill material under plane polars. c) Closer view from b) under plane polars. d) Partly resorbed olivines and remnants of secondary mineral (yellow circle) set in ophitic material under crossed polars. Abbreviations are as in Fig. S1.1.

S1.5.

The Langaregn Sill (Fig. S1.5)

Subhedral <5 mm plagioclase phenocrysts make up <10 % of this sill. <0.5 % of total volume of partly resorbed olivine microphenocrysts (0.15-0.7mm) are commonly embedded within plagioclase phenocrysts. Matrix is made up of intergranular (0.02-0.35 mm) subhedral randomly oriented plagioclase laths counting for 35-40 % of total volume joined by 45-50 % anhedral equant clinopyroxenes (0.02-0.35 mm). Scattered (<0.12 mm) grains of partly altered olivines count for <5 % and oxides (<0.2 mm) count for 3-6 % of total volume.

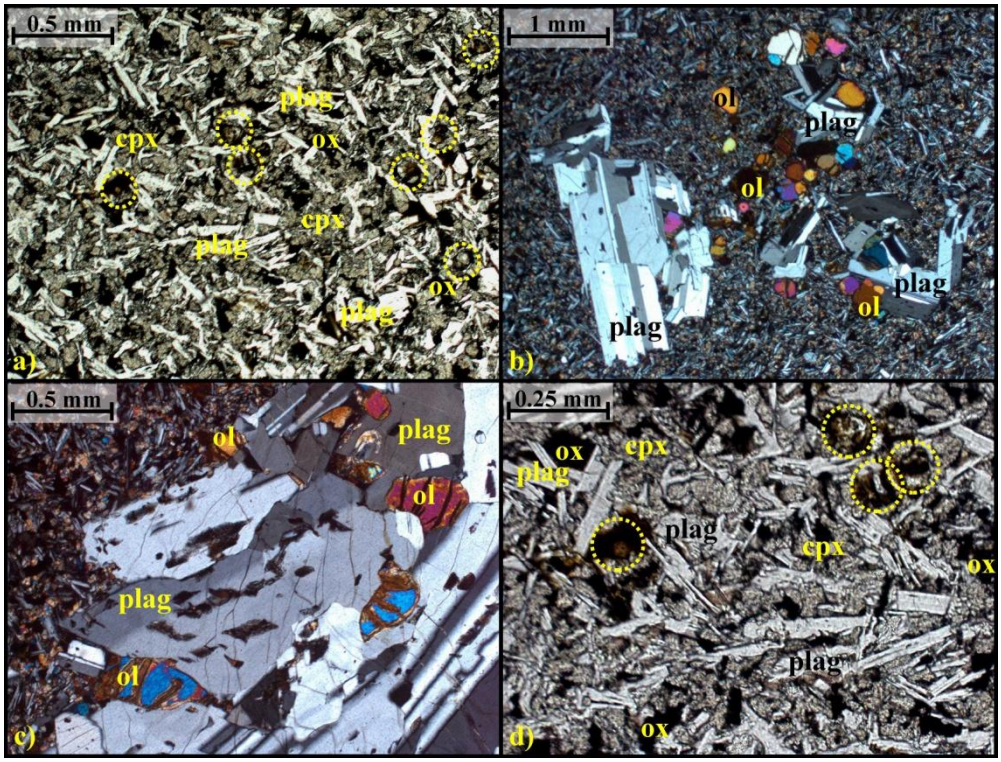

Fig. S1.5. Photomicrographs of the Langaregn Sill. a) General distribution of the most common matrix minerals under plane polars (olivines in yellow circles). b) Sub-spherical brightly coloured olivine microphenocrysts aand resorbed plagioclase phenocrysts matrix of plagioclase, clinopyroxene, olivine and oxide under crossed polars. c) Same as in b), but with olivine microphenocrysts included in plagioclase phenocrysts under crossed polars. d) Closer view of matrix minerals as in a) under plane polars. Abbreviations are as in Fig. S1.1.

S1.6.

Feeder dykes to the Streymoy Sill (Fig. S1.6)

Feeders to the Streymoy Sill contain around 15-20 % plagioclase (micro) phenocrysts. These phenocrysts and the odd clinopyroxene grains occur in basaltic glasses immediately at feeder to host-rock contacts, but the glasses gradually give way to minute plagioclase and clinopyroxene grains at distances greater than 1-2 cm from these contacts. Plagioclase phenocrysts in the glassy matrix are euhedral to subhedral and completely fresh, while those occurring in a matrix of glass, plagioclase and clinopyroxene are subhedral to anhedral and partly resorbed.

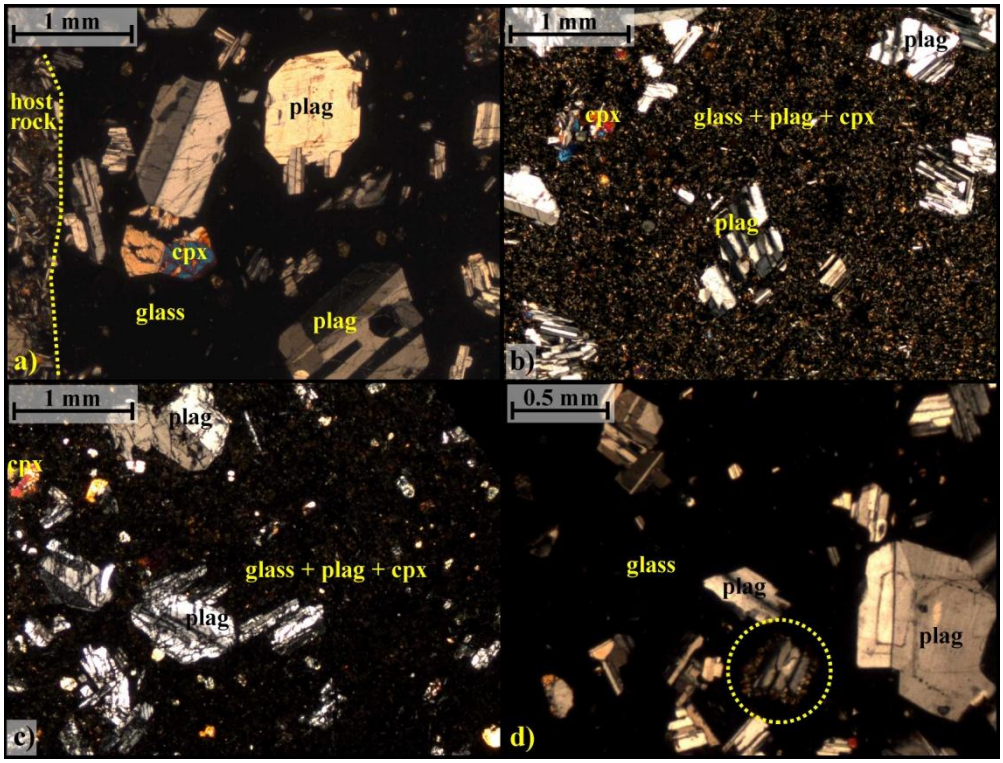

Fig. S1.6. Photomicrographs under crossed polars of feeder dykes to the Streymoy Sill. a) Euhedral completely fresh plagioclase grains and the odd clinopyroxene set in basaltic glass immediately at dyke contact (yellow dotted line). b) Slightly resorbed plagioclase grains set in a fine grained matrix of glass, plagioclase and clinopyroxene □□2 cm from the dyke contact. c) Broadly similar to b, but with the larger plagioclase grains being slightly more altered/resorbed. d) Similar scenario as in a, but also showing an individual plagioclase grain acting as a nucleus for the growth of tiny clinopyroxene crystals (enclosed by yellow dotted circle). Abbreviations as in Fig. S1.1.

Supplement 2

Techniques employed during XRF, ICP-MS and MC-ICP-MS analyses of mafic rock samples representing seven saucer-shaped sills and other selected intrusives of the Faroe Islands.

S2.1.

XRF analyses

Following careful selection, 56 rock samples representing 7 Faroese sills and a number of local dykes and irregular intrusions were crushed to fine gravel/sand using a steel jaw crusher and a steel hammer and subsequently ground to fine rock powder using agate ball mills at the Department of Earth Sciences, Durham University, UK. A few additional samples were processed in a similar manner at the Geological Survey of Norway (NGU), Trondheim. During preparation of samples for analyses of major elements at the Department of Earth Sciences, Open University, Milton Keynes, United Kingdom, finely ground rock powder from each sample and a flux of metaborate/tetraborate were dried overnight in an oven at ~110°C. Exactly 0.7 g of each dry sample and 3.5 g of the flux were weighed out and mixed in Pt crucibles. Each mixed sample was fused at 1100°C for 15-20 minutes and the melted samples were subsequently poured into pre-heated brass moulds and pressed to glass discs ready for analyses. In-house standards WS-E and G94 were produced parallel to rock samples from this study and analysed simultaneously with these. The reproducibility of these standards was usually better than 1 %. During preparation of samples for analyses of selected trace elements, ~9 g of finely ground powder from each sample was mixed with ~0.9 ml of polyvinylpyrollidone (P.V.P.) binder. The mixed samples were subsequently pressed to powder pellets in a mould at ~5 ton for a few moments and subsequently dried overnight at ~110°C. Powder pellets for the four United States Geological Survey standards BHVO-1; QLO-1; DNC-1 and W-2 were produced parallel to rock samples from this study and analysed parallel to these. The reproducibility of the standards was usually better than 4 % apart from Y that was usually better than 5 to 10 %.

During preparation of samples for analyses of major elements at the Norwegian Geological Survey (NGU), Trondheim, Norway, finely ground rock powder from each of the samples were pre-heated at 1000 °C in an oven for a suitable amount of time. The major elements were then determined on glass discs prepared by fusion of 0.6 g powder from each of the rock samples with 4.2 g of powdered litiumtetraborate ($Li_2B_4O_7$). The analysed data were subsequently calculated back to the state of powdered samples prior to pre-heating. Precision of analytical results from XRF analyses at NGU are outlined in the table just below:

Table S2.1. Lower detection limits (LLQ) and analyse uncertainties for major elements (given in percentages) for XRF analyses at NGU, Trondheim, Norway

Elements	SiO_2	Al_2O_3	Fe_2O_3	TiO_2	MgO	CaO	Na_2O	K_2O	MnO	P_2O_5
LLQ:	0.5	0.02	0.01	0.01	0.04	0.01	0.1	0.01	0.01	0.01
Concentration %	± %	± %	± %	± %	± %	± %	± %	± %	± %	± %
0.01	--------	--------	0.005	0.005	--------	0.005	--------	0.005	0.005	0.005
0.1	--------	0.01	0.027	0.009	0.036	0.027	0.02	0.031	0.004	0.009
0.5	0.05	0.031	0.046	0.015	0.062	0.046	0.03	0.054	0.008	0.015
1	0.09	0.042	0.063	0.021	0.084	0.063	0.04	0.073	0.01	0.021
5	0.2	0.09	0.135	0.05	0.181	0.135	0.09	0.158	0.05	0.05
10	0.29	0.127	0.191	0.1	0.254	0.191	0.13	0.222	0.1	0.1
25	0.45	0.25	0.301	--------	0.401	0.301	0.25	0.351	0.25	--------
50	0.64	0.5	0.5	--------	0.566	0.5	--------	--------	--------	--------
75	0.78	0.75	0.75	--------	0.75	0.75	--------	--------	--------	--------
100	1.0	--------	--------	--------	--------	--------	--------	--------	--------	--------

The listed uncertainties represent a covering factor 1 (68 % confidence interval). 95 % confidence interval can be attained by multiplication with 2. Loss on Ignition (LOI) is reported for a lower limit of 0.05 % and an uncertainty of 2.5 % rel. (2σ).

In-house control samples/standards are analysed routinely/frequently at NGU, Norway, parallel to analyses of other rock samples. If required, the results from analyses of standards can be obtained by requests on: lab@ngu.no

S2.2.

ICP-MS analyses

During preparation of solutions representing rock samples for the ICP-MS analyses at the Department of Earth Sciences, Durham University, United Kingdom, 0.100 ± 0.001 g of finely ground powder from the actual samples were dissolved in a mixture of 1 ml HNO_3 (69 %) + 4 ml HF (40 %) in sealed Savillex 22 ml PFA vials and left on hotplates at ~150°C for ~48 hours reflux. The sample vials were unsealed and subsequently allowed to evaporate to near dryness. 1 ml HNO_3 was applied to each sample, which was again allowed to evaporate

to near dryness; this procedure was repeated once. 2.5 ml HNO_3 + 10 ml 18MΩ H_2O was subsequently applied to each sample, which was left on a hotplate at ~100°C overnight in the sealed vials. Prior to final dilution, 1ml of 1ppm Re and Rh internal standard was applied to each of the cooled samples to yield 20 ppb in solution followed by the addition of 18MΩ H_2O until each sample was diluted to exactly 50 ml in order to yield a solution of approximately 3.5 % HNO_3. Prior to analyses each sample was diluted 10 fold by the addition of 3 % HNO_3. One international standard (NBS 688) and three blanks were prepared parallel with the rock samples. More details on dissolution methods are presented in Ottley et al. (2003) and Thompson et al. (2005). Calibration of the ICP-MS was achieved by means of in-house standards and international reference materials (W-2, BHVO-1, AGV1, BE-N and NBS 688), together with procedural blanks. In order to ascertain the magnitude of calibration drift, three blanks and the five standards were run at the start and at the end of the performed analyses and one blank and standard were analysed several times interspersed between the samples during the analytical sequence. The reproducibility of trace elements from in-house standards analysed on this apparatus is usually better than 5 % and frequently 3 % (we can look at the actual data and give precise values if required, the values used here 5 and 3 % are typical values cited in Ottley et al., 2003). RSD % values for the international standard NBS 688 at n = 7 during analyses parallel to those of actual rock samples are as follow: Rb = 2.11, Sr = 1.35, Y = 1.05, Zr = 1.16, Nb = 0.88, Ba = 3.43, La = 2.96, Ce = 2.67, Pr = 3.35, Nd = 3.54, Sm = 2.95, Eu = 2.25, Gd = 1.53, Tb = 2.43, Dy = 2.55, Ho = 2.62, Er = 1.99, Yb = 1.21, Lu = 1.40, Hf = 0.74, Ta = 1.67, Pb = 0.78, Th = 1.15, U = 1.55.

Dissolution of 3 additional sill samples at GEUS, Denmark, (Table 2) were carried out using a modified version of the procedure used by Turner et al. (1999) and Ottley et al. (2003). Calibration was done using two certified REE solutions and three international reference standards including BHVO-2, GH, BIR-1, MRG-1 (reference values from Govindaraju, 1994; Jochum and Nehring, 2006). Results for reference samples processed and run simultaneously with the unknowns are normally within 5 % of the reference values for most elements with concentrations >0.1ppm.

The table just below illustrates accuracies during ICP-MS analyses of three rock standards (Disko-1, BHVO-2 and BCR-2 with n = 2), which were run contemporaneously with the analyses of three sill samples from the Faroe Islands at GEUS, Denmark.

Table S2.2. Analyses of three standards at GEUS, Denmark, performed by Olga Nielsen.

Elements	**DISKO-1 (expected)**	DISKO-1 (measur.)	DISKO-1 (measur.)	**BHVO-2 (expected)**	BHVO-2 (measur.)	BHVO-2 (measur.)	**BCR-2 (expected)**	BCR-2 (measur.)	BCR-2 (measur.)
Rb	**3.22**	3.24	3.27	**9.11**	9.15	9.10	**46.90**	46.41	46.23
Sr	**206.94**	212.58	212.64	**396.00**	391.54	390.72	**340.00**	334.93	335.55
Y	**33.04**	32.69	32.90	**26.00**	26.66	26.22	**37.00**	36.49	36.85
Zr	**117.07**	116.92	116.31	**172.00**	170.68	170.30	**184.00**	185.67	187.09
Nb	**4.48**	4.26	4.27	**18.10**	18.91	18.80	**12.60**	12.69	12.75
Ba	**47.45**	45.78	46.33	**131.00**	133.59	131.77	**677.00**	688.81	689.59
La	**6.49**	6.45	6.56	**15.20**	15.29	15.04	**24.90**	24.94	24.90
Ce	**17.21**	17.40	17.50	**37.50**	37.67	37.15	**52.90**	52.10	52.50
Pr	**2.90**	2.80	2.81	**5.35**	5.39	5.33	**6.70**	6.92	6.95
Nd	**14.93**	14.59	14.49	**24.50**	24.71	24.44	**28.70**	29.13	29.65
Sm	**4.59**	4.56	4.52	**6.07**	6.08	6.10	**6.58**	6.61	6.65
Eu	**1.58**	1.59	1.67	**2.07**	1.97	2.01	**1.96**	2.05	1.92
Gd	**5.87**	5.59	5.75	**6.24**	6.36	6.22	**6.75**	6.96	6.91
Tb	**0.99**	0.94	0.96	**0.92**	0.94	0.94	**1.07**	1.10	1.08
Dy	**5.90**	5.95	6.04	**5.31**	5.21	5.21	**6.41**	6.48	6.39
Ho	**1.20**	1.20	1.19	**0.98**	0.97	0.97	**1.28**	1.30	1.31
Er	**3.13**	3.23	3.27	**2.54**	2.45	2.48	**3.66**	3.68	3.59
Yb	**2.83**	2.88	2.89	**2.00**	1.96	1.96	**3.38**	3.39	3.37
Lu	**0.45**	0.42	0.44	**0.27**	0.29	0.28	**0.50**	0.51	0.50
Hf	**3.14**	3.16	3.17	**4.36**	4.39	4.27	**4.90**	4.83	4.96
Ta	**0.30**	0.29	0.29	**1.14**	1.13	1.16	**0.74**	0.77	0.76
Pb	**1.18**	1.25	1.25	**1.60**	1.69	1.63	**11.00**	9.93	10.25
Th	**0.60**	0.58	0.59	**1.22**	1.23	1.19	**5.70**	5.88	5.92
U	**0.14**	0.14	0.14	**0.40**	0.41	0.41	**1.69**	1.66	1.65

Concentrations are given in parts per million (ppm).

S2.3.

MC-ICP-MS analyses

The basic analytical method used for each element on the Neptune, during analyses at the Arthur Holmes Isotope Geology Laboratory (AHIGL) Durham University, Durham, United Kingdom, comprises a static multi-collection routine of 1 block of 50 cycles with an integration time of 4 sec per cycle; total analysis time 3.5 mins. Isotopic ratios were determined on the standards NBS 987, J&M and NBS 981 simultaneous to analyses of actual rock samples in order to evaluate accuracy of Sr, Nd and Pb analyses.

For the Sr and Nd chemistry, samples were dissolved in Teflon beakers with 1ml l6N HNO_3 and 3mls 29N HF at 120°C for 48 hrs. After dissolution Sr and Nd were separated using a combination of cation and anion exchange columns (Dowall et al., 2003). After chemistry, Sr samples were taken up in 1ml of 3 % HNO_3 and introduced into the Neptune using an ESI PFA50 nebuliser and a dual cyclonic–Scott Double Pass spraychamber. With this sample introduction set up, and the normal H skimmer cone, the sensitivity for Sr on the Neptune is typically ~60V total Sr ppm^{-1} at an uptake rate of 90 µl min^{-1}. Prior to analysis a small aliquot

was first tested to establish the Sr concentration of each sample by monitoring the size of the ^{84}Sr beam (^{88}Sr was too high in non-diluted aliquot to measure directly), from which a dilution factor was calculated to yield a beam of approximately 20V ^{88}Sr. Instrumental mass bias was corrected for using a $^{88}Sr/^{86}Sr$ ratio of 8.375209 (the reciprocal of the $^{86}Sr/^{88}Sr$ ratio of 0.1194) and an exponential law. The rock samples from the Faroe Islands were analysed in a single session during which the average $^{87}Sr/^{86}Sr$ value for the NBS 987 standard was 0.710270 ± 0.000016 (2SD = 21.8 ppm; n = 9). Following chemistry the REE cuts containing the Nd fraction were taken up in 1ml of 3 % HNO_3 and introduced into the Neptune using an ESI PFA50 nebuliser and a dual cyclonic–Scott Double Pass spraychamber. With this sample introduction set up, and the normal H skimmer cone, the sensitivity for Nd on the Neptune is 60-80V total Nd ppm^{-1} at an uptake rate of 90 µl min^{-1}. Instrumental mass bias was corrected using a $^{146}Nd/^{145}Nd$ ratio of 2.079143 (equivalent to the more commonly used $^{146}Nd/^{144}Nd$ ratio of 0.7219) and an exponential law. The $^{146}Nd/^{145}Nd$ ratio is used for correcting mass bias since at Durham Nd isotopes are measured on a total REE-cut from the 1st stage cation columns and this is the only Ce and Sm-free stable Nd isotope ratio. This approach requires a correction for isobaric interferences from Sm on ^{144}Nd, ^{148}Nd and ^{150}Nd. The correction used is based on the method of Nowell and Parrish (2001). The accuracy of the Sm correction method during analysis of a total REE fraction is demonstrated by repeat analyses of BHVO-1, which gave an average $^{143}Nd/^{144}Nd$ ratio of 0.512982 ± 0.000007 (13.5 ppm 2SD; n = 13) after Sm correction; identical to the TIMS ratio of 0.512986 ± 0.000009 (17.5 ppm 2SD; n = 19) obtained by Weis et al. (2005). During analysis of the rock samples from the Faroe Islands the pure and Sm-doped J&M standards gave an average $^{143}Nd/^{144}Nd$ ratio of 0.511115 ± 0.000014 (26.7 ppm 2SD; n = 9).

Pb from rock samples was separated using small Sr Spec resin columns (Charlier et al., 2006). After chemistry, Lead samples were taken up in 1ml of 3 % HNO_3. Prior to analysis each sample was tested on the Neptune to determine its Pb concentration and thereby calculate the appropriate amount of tantalum spike to add in order to obtain a Pb/Tl ratio of ~12. After spiking with Tl each sample was introduced into the Neptune using an ESI PFA50 nebuliser and a dual cyclonic-Scott Double Pass spraychamber. With this set-up, and the normal H skimmer cone, the sensitivity for Pb on the Neptune is typically ~100V total Pb ppm^{-1} at an uptake rate of 90 µl min^{-1}. Pb mass bias was corrected for externally using the $^{205}Tl/^{203}Tl$ ratio of the admixed Tl spike and an exponential law. The $^{205}Tl/^{203}Tl$ ratio used for correcting the Pb ratios is determined for each analytical session by minimising the difference

in offset between the session average Pb ratios (all ratios) and the Galer and Abouchami (1998) values, i.e. it is the ratio that gives the best fit for all the Pb ratios to the values of Galer and Abouchami (1998) simultaneously that is used. Samples were analysed in a single analytical session during which the $^{205}Tl/^{203}Tl$ ratio used for mass bias correction was 2.38835 and the average $^{206}Pb/^{204}Pb$, $^{207}Pb/^{204}Pb$ and $^{208}Pb/^{204}Pb$ ratios for the NBS 981 Pb std were 16.9402 ± 0.0020, 15.4972 ± 0.0024 and 36.7176 ± 0.0060 respectively (119.46, 151.76 and 164.19 ppm 2SD respectively; n = 9).

Whole-rock Pb isotope analyses were carried out at the Geological Institute, University of Copenhagen, Denmark. Dissolution of the powder samples was achieved in two successive, but identical steps, which consisted of a strong 8 N HBr attack that has been shown to effectively dissolve accessory phosphates (Frei et al., 1997; Schaller et al., 1997), followed by a concentrated HF-14 N HNO_3 mixture, and finally by strong 9 N HCl. Chemical separation of Pb from whole rocks was performed over conventional glass stem and subsequently miniature glass-stem anion exchange columns containing, respectively 1 ml and 200 µl 100-200 mesh Bio-Rad AG 1×8 resin. Lead was analyzed in a static multi-collection-mode where fractionation was controlled by repeated analysis of the NBS 981 standard using values of Todt et al. (1993). The average fractionation amounted to 0.105±0.008 % (2σ, n = 5) per atomic mass unit during these analyses. Over the last ten years, analyses in the actual laboratory have produced the 206Pb/204Pb ratio of the NBS 981 standard as 16.896 ± 0.007 (n = 300; 2σ). Total procedural blanks remained below 200 pg Pb, compared to ~100 ng Pb loads, insignificantly affecting Pb isotopic ratios of the samples.

Calculations of $^{87}Rb/^{86}Sr$ and $^{147}Sm/^{144}Nd$ ratios. As $^{87}Rb/^{86}Sr$ and $^{147}Sm/^{144}Nd$ ratios were not supplied together with the Sr and Nd isotope data, these values had to be calculated separately using the expressions (Faure, 1986, 2001):

$$^{87}Rb/^{86}Sr = (Rb/Sr) \times (Ab^{87}Rb \times WSr) / (Ab^{86}Sr \times WRb) \text{ and}$$

$$^{147}Sm/^{144}Nd = (Sm/Nd) \times (Ab^{147}Sm \times WNd) / (Ab^{144}Nd \times WSm)$$

where Ab refer to isotopic abundances and W refer to atomic weights. Isotopic abundances of ^{87}Rb and ^{147}Sm are 0.278346 and 0.150000 respectively (Faure, 1986). Calculations of unknown ^{86}Sr and ^{144}Nd isotopic abundances can be tabulated as (e.g. Faure, 2001):

Table S2.3.1.

	Ratio	Isotope	Abundance
$^{84}Sr/^{88}Sr$	[a]Calculated	$^{84}Sr \rightarrow$	$(^{84}Sr/^{88}Sr)/Sum$
$^{86}Sr/^{88}Sr$	[b] 0.119400	$^{86}Sr \rightarrow$	$(^{86}Sr/^{88}Sr)/Sum$
$^{87}Sr/^{88}Sr$	[c]Calculated	$^{87}Sr \rightarrow$	$(^{87}Sr/^{88}Sr)/Sum$
$^{88}Sr/^{88}Sr$	1.000000	$^{88}Sr \rightarrow$	$(^{88}Sr/^{88}Sr)/Sum$
	[d]Sum		

[a]$(^{84}Sr/^{86}Sr)/(^{86}Sr/^{88}Sr)$ where $^{84}Sr/^{86}Sr = 0.056584$ (Steiger and Jäger, 1977); [b]Steiger and Jäger (1977); [c]$(^{86}Sr/^{88}Sr)/(^{87}Sr/^{86}Sr)_{measured}$; [d]combined value of Sr isotopic ratios.

and

Table S2.3.2.

	Ratio	Isotope	Abundance
$^{145}Nd/^{146}Nd$	[a]Calculated	$^{145}Nd \rightarrow$	$(^{145}Nd/^{146}Nd)/Sum$
$^{144}Nd/^{146}Nd$	[b] 1.389535	$^{144}Nd \rightarrow$	$(^{144}Nd/^{146}Nd)/Sum$
$^{143}Nd/^{146}Nd$	[c]Calculated	$^{143}Nd \rightarrow$	$(^{143}Nd/^{146}Nd)/Sum$
$^{146}Nd/^{146}Nd$	1.000000	$^{146}Nd \rightarrow$	$(^{146}Nd/^{146}Nd)/Sum$
	[d]Sum		

[a]$(^{145}Nd/^{144}Nd)/(^{144}Nd/^{146}Nd)$ where $^{145}Nd/^{144}Nd = 0.347280$ (Faure, 2001); [b]Faure (2001); [c]$(^{144}Nd/^{146}Nd)/(^{143}Nd/^{144}Nd)_{measured}$; [d]combined value of Nd isotopic ratios.

Equation used for age correction of $^{87}Sr/^{86}Sr$ ratios (Faure, 1986). $^{87}Rb/^{86}Sr$ ratios may be either measured or calculated (as shown above).

$$(^{87}Sr/^{86}Sr)^{54\ Ma} = (^{87}Sr/^{86}Sr)_{measured} - {}^{87}Rb/^{86}Sr * (EXP(\lambda_{Rb\rightarrow Sr}*54\ Ma) - 1)$$

Equation used for age correction of $^{143}Nd/^{144}Nd$ ratios (Faure, 1986). $^{147}Sm/^{144}Nd$ ratios may be either measured or calculated (as shown above).

$$(^{143}Nd/^{144}Nd)^{54\ Ma} = (^{143}Nd/^{144}Nd)_{measured} - {}^{147}Sm/^{144}Nd * (EXP(\lambda_{Sm\rightarrow Nd}*54\ Ma) - 1)$$

References

Charlier, B. L. A., Ginibre, C., Morgan, D., Nowell, G. M., Pearson, D. G., Davidson, J. P. and Ottley, C. J.: Methods for the microsampling and high precision analysis of strontium and rubidium isotopes at single crystal scale for petrological and geochronological applications, Chem. Geol., 232, 114-133, 2006.

Dowall, D. P., Nowell, G. M. and Pearson, D. G.: Chemical pre-concentration procedures for high-precision analysis of Hf-Nd-Sr isotopes in geological materials by plasma ionisation multi-collector mass spectrometry (PIMMS) techniques, In: Holland J.G. and Tanner S.D. Eds. Plasma Source Mass Spectrometry: Applications and Emerging Technologies, The R. Soc. Chem. Cambridge, 321-337, 2003.

Faure, G.: Principles of isotope geology. Second edition. John Wiley & sons pp. 589, 1986.

Faure, G.: Origin of igneous rocks: the isotopic evidence, Springer Verlag. Berlin, Heidelberg, New York, pp. 495, 2001.

Frei, R., Villa, I. M., Nägler, Th. F., Kramers, J. D., Pryzbylowicz, W. J., Prozesky, V. M., Hofmann, B. A. and Kamber, B. S.: Single mineral dating by Pb–Pb step-leaching method; assessing the mechanisms, Geochim. Cosmochim. Acta, 61, 393–414, 1997.

Galer, S. J. G. and Abouchami, W.: Practical application of lead triple spiking for correction of instrumental mass discrimination, Mineral. Mag. 62A, 491-492, 1998.

Govindaraju, K.: 1994 compilation of working values and sample description for 383 geostandards, Geostandards Newsletter, 18: 1–158, 1994.

Jochum, K. P. and Nehring F.: BCR-2G, BIR-1G, BHVO-2G: GeoReM preferred values (11/2006). GeoReM database (http://georem.mpch-mainz.gwdg.de), 2006.

Nowell, G. M., and Parrish, R. R.: Simultaneous acquisition of isotope compositions and parent/daughter ratios by non-isotope dilution solution-mode Plasma ionisation Multi-collector Mass Spectrometry (PIMMS), In: Holland, J. G. & Tanner, S.D., Eds. Plasma Source Mass Spectrometry The New Millenium, Royal Soc. Chem., 298-310, 2002.

Ottley, C. J., Pearson, D. G. and Irvine, G. J.: A routine method for the dissolution of geological samples for the analysis of REE and trace elements via ICP –MS, In: Plasma

Source Mass Spectrometry, Applications and Emerging Technologies, (J.G. Holland, S.D. Taner, Eds.). Royal Soc. Chem., 221–230, 2003.

Schaller, M., Steiner, O., Suder, I., Frei, R. and Kramers, J. D.: Pb stepwise leaching (PbSL) dating of garnet—addressing the inclusion problem. Schweiz, Min. Pet. Mitt., 77, 113–121, 1997.

Steiger, R. H. and Jäger, E.: Subcommission on geochronology: convention of the use of decay constants in geo- and cosmochronology, Earth Plan. Sci. Lett., 36, 359-362, 1977.

Thompson, R. N., Ottley, C. J., Smith, P. M., Pearson, D. G., Dickin, A. P., Morrison, M. A., Leat, P. T. and Gibson, S. A.: Source of the Quaternary alkalic basalts, picrites and basanites of the Potrillo Volcanic Field, New Mexico, USA – lithosphere or convecting mantle?, J. Petrol., 46, 1603-1643, 2005.

Todt, W., Cliff, R. A., Hanser, A. and Hofmann, A. W.: Re-calibration of NBS lead standards using $^{202}Pb + ^{205}Pb$ double spike, Terra Abstract, 5, 396, 1993.

Turner, S. R., Platt, J. P., George, R. M. M., Kelley, S. P., Pearson, D. G. and Nowell, G. M.: Magmatism associated with orogenic collapse of the Betic–Alboran domain, SE Spain, J. Petrol., 40, 1011–1036, 1999.

Weis D., Kieffer, B., Maerschalk, C., Pretorius, W. and Barling J.: High precision Pb-Sr-Nd-Hf isotopic characterisation of USGS BHVO-1 and BHVO-2 reference materials, Geochem. Geophys. Geosyst. 6. pp. 10, 2005.

Supplement 3:

Supplementary data on intrusive host-rocks of the Faroe Islands, utilised in figures 2, 3 and 4.

Table S3. Major and trace element data on selected dykes and irregular intrusions of the Faroe Islands.

Sample	08-JMS-15	08-JES-12	09-JES-07	07-JSS-54	09-JES-06	08-JES-02
	Dyke	Dyke	Dyke	Dyke	Dyke	Dyke
Wt %	Low-TiO_2	Low-TiO_2	Low-TiO_2	Intermed.-TiO_2	Intermed.-TiO_2	Intermed.-TiO_2
SiO_2	46.02	47.48	47.46	47.74	48.82	49.14
TiO_2	0.78	0.89	0.90	1.14	1.38	1.68
Al_2O_3	13.88	14.48	14.85	14.74	14.72	13.50
Fe_2O_3	10.96	11.26	11.33	11.84	12.44	15.76
MnO	0.17	0.18	0.18	0.18	0.20	0.24
MgO	12.30	11.07	11.03	9.23	7.50	6.13
CaO	11.19	12.48	12.24	12.71	12.69	11.38
Na_2O	1.50	1.69	1.77	1.89	2.14	2.31
K_2O	0.05	0.03	0.05	0.04	0.06	0.18
P_2O_5	0.06	0.07	0.07	0.09	0.10	0.14
LOI	1.68	0.17	0.07	0.43	-0.25	-0.10
Total	98.60	99.79	99.94	100.02	99.80	100.37
ppm						
Rb	0.868	0.597	--------	0.538	--------	--------
Sr	73.0	86.0	--------	113	--------	--------
Y	21.0	24.6	--------	26.0	--------	--------
Zr	39.0	47.6	--------	62.4	--------	--------
Nb	0.655	0.908	--------	1.78	--------	--------
Ba	8.4	8.2	--------	11.6	--------	--------
La	1.12	1.23	--------	2.16	--------	--------
Ce	3.52	3.87	--------	6.40	--------	--------
Pr	0.723	0.780	--------	1.24	--------	--------
Nd	4.28	4.77	--------	7.00	--------	--------
Sm	1.84	2.01	--------	2.64	--------	--------
Eu	0.731	0.775	--------	0.986	--------	--------
Gd	3.09	3.34	--------	4.05	--------	--------
Tb	0.555	0.590	--------	0.692	--------	--------
Dy	3.46	3.61	--------	4.25	--------	--------
Ho	0.757	0.789	--------	0.887	--------	--------
Er	2.11	2.23	--------	2.47	--------	--------
Tm	0.327	0.328	--------	0.368	--------	--------
Yb	2.01	2.13	--------	2.26	--------	--------
Lu	0.319	0.345	--------	0.366	--------	--------
Hf	1.18	1.30	--------	1.76	--------	--------
Ta	0.049	0.065	--------	0.108	--------	--------
Pb	0.259	0.293	--------	0.311	--------	--------
Th	0.112	0.126	--------	0.143	--------	--------
U	0.032	0.033	--------	0.047	--------	--------
Nb/Ta	13.37	16.21	--------	16.45	--------	--------
$(Ce/Sm)_N$	0.48	0.48	--------	0.60	--------	--------
$(Sm/Yb)_N$	0.98	0.99	--------	1.23	--------	--------

Continued

Sample	08-JVS-26	08-JVS-27	08-JSUS-28	08-JSS-25	07-JSS-14	08-JES-35
	Irreg. Intrus.	Irreg. Intrus.	Irreg. Intrus.	Dyke	Dyke	Dyke
Wt %	High-TiO_2	High-TiO_2	High-TiO_2	High-TiO_2	High-TiO_2	High-TiO_2
SiO_2	49.34	48.35	48.70	48.86	48.19	48.53
TiO_2	2.03	2.11	2.40	2.59	2.86	2.98
Al_2O_3	13.78	13.54	13.34	13.58	14.16	13.65
Fe_2O_3	11.53	12.59	12.67	15.11	14.50	14.17
MnO	0.56	0.19	0.19	0.21	0.20	0.19
MgO	7.06	7.86	9.00	6.45	6.63	7.00
CaO	12.49	12.13	11.62	10.77	10.69	10.49
Na_2O	2.04	2.16	2.12	2.39	2.31	2.26
K_2O	0.22	0.16	0.25	0.25	0.43	0.37
P_2O_5	0.17	0.18	0.22	0.24	0.26	0.23
LOI	0.60	0.71	0.08	-0.21	0.30	0.02
Total	99.83	99.99	100.58	100.24	100.52	99.87
ppm						
Rb	3.04	--------	3.27	4.16	9.78	5.27
Sr	288	--------	305	256	274	279
Y	26.3	--------	31.0	35.0	36.3	35.4
Zr	136	--------	161	173	200	187
Nb	9.04	--------	11.8	13.9	13.4	12.5
Ba	47.1	--------	55.5	69.5	71.7	67.0
La	7.21	--------	9.36	11.8	10.5	10.4
Ce	20.0	--------	25.1	30.6	28.2	27.7
Pr	3.38	--------	4.19	4.92	4.65	4.64
Nd	17.0	--------	20.5	23.8	22.9	22.8
Sm	4.84	--------	5.61	6.30	6.11	6.28
Eu	1.66	--------	1.90	2.04	2.03	2.06
Gd	5.54	--------	6.49	7.07	7.16	7.27
Tb	0.877	--------	0.999	1.13	1.13	1.12
Dy	4.72	--------	5.43	6.35	6.22	6.30
Ho	0.936	--------	1.04	1.23	1.17	1.23
Er	2.27	--------	2.61	3.23	2.96	3.11
Tm	0.332	--------	0.381	0.462	0.424	0.436
Yb	1.97	--------	2.24	2.87	2.56	2.65
Lu	0.299	--------	0.338	0.443	0.396	0.410
Hf	3.43	--------	3.98	4.37	4.60	4.59
Ta	0.704	--------	0.704	0.895	0.775	0.765
Pb	0.750	--------	0.750	1.13	1.11	1.06
Th	0.580	--------	0.580	0.894	0.786	0.751
U	0.194	--------	0.194	0.280	0.255	0.248
Nb/Ta	15.73	--------	16.80	15.51	17.27	16.36
$(Ce/Sm)_N$	1.02	--------	1.10	1.19	1.10	1.07
$(Sm/Yb)_N$	2.64	--------	2.68	2.42	2.65	2.62

Supplement 4

Comparison between measured and age-corrected Pb isotope ratios in Faroese sills

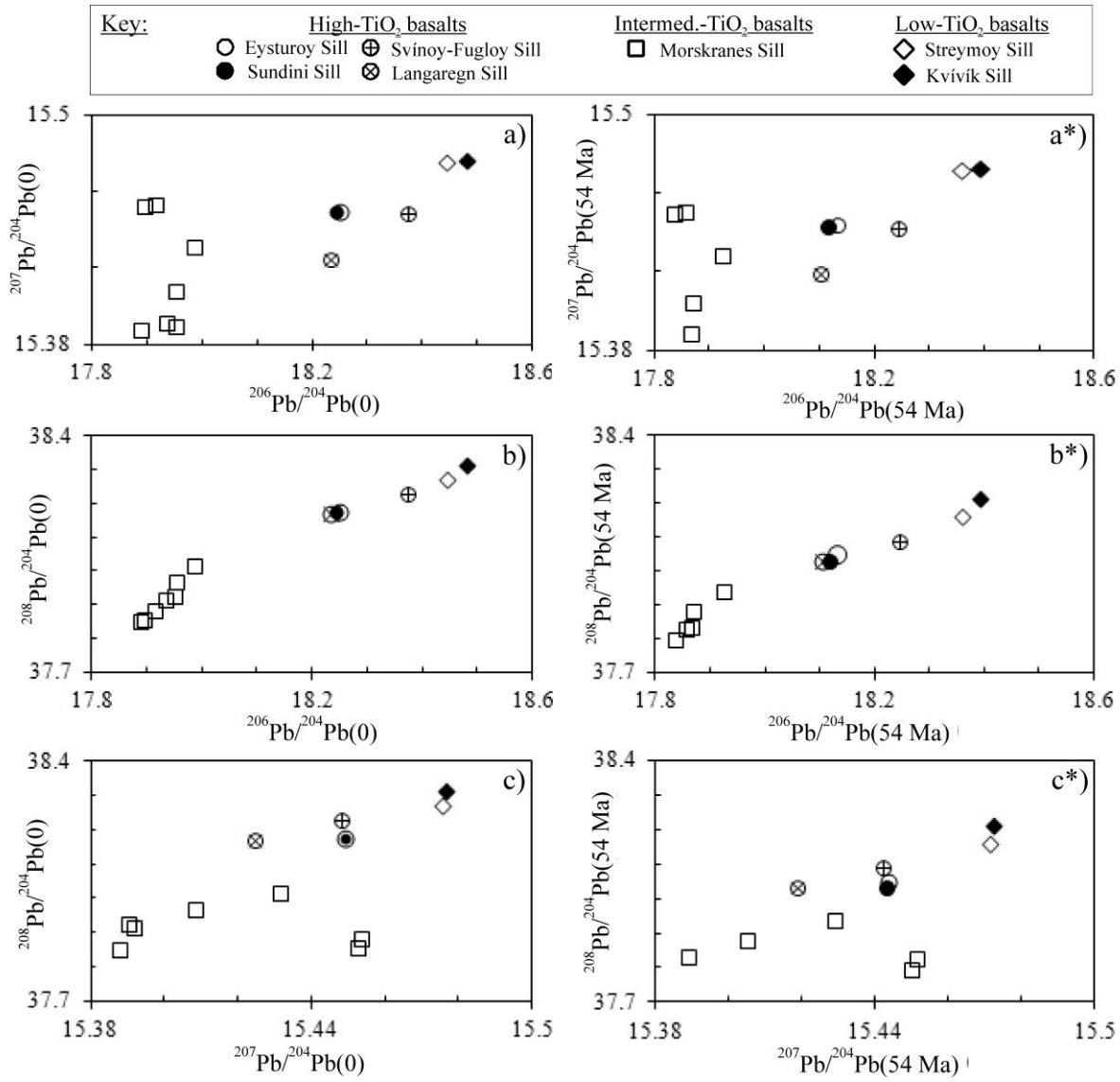

Figure S4. Measured isotope ratios in a), b) and c) representing Faroese sills are compared to age-corrected versions at 54 Ma of these same data, as shown in a*), b*) and c*) (see Table D below for data). Measured and age-corrected isotope ratios display broadly similar configurations, but high-TiO_2 and low-TiO_2 sills display a slightly larger decrease in age-corrected $^{208}Pb/^{204}Pb$ ratios relative to age-corrected samples of the intermediate-SiO_2 Morskranes Sill, when compared to measured ratios for these same sills.

Table S4. Measured versus age-corrected lead isotopes in Hansen et al. (2017). (Analysed by Geoff Nowell DU, UK and Robert Frey CU, DK)

Samples	$^{206/204}$Pb	$^{207/204}$Pb	$^{208/204}$Pb	U (ppm)	Th (ppm)	^{238}U/^{204}Pb	^{235}U/^{204}Pb	^{232}Th/^{204}Pb	$^{206/204}$Pb (t)	$^{207/204}$Pb (t)	$^{208/204}$Pb (t)
08-JES-01	18.2442	15.4493	38.1727	0.287	0.961	15.1993	0.1102	52.5894	18.1163	15.4432	38.032
08-JES-10	18.2501	15.4493	38.1765	0.285	0.949	14.0222	0.1017	48.2471	18.1321	15.4438	38.0474
08-JSVS-22	18.3736	15.4482	38.2266	0.208	0.661	15.4473	0.1120	50.7252	18.2437	15.4421	38.0909
07-JSS-49	18.4802	15.4765	38.3115	0.111	0.374	10.4119	0.0755	36.2505	18.3926	15.4724	38.2145
07-JSS-50	18.2326	15.4246	38.1692	0.262	0.854	15.2110	0.1103	51.2328	18.1046	15.4186	38.0321
07-JSS-52	18.4444	15.4756	38.2700	0.138	0.526	10.3049	0.0747	40.5868	18.3578	15.4715	38.1614
08-JMS-14	17.9131	15.4536	37.8876	0.050	0.150	7.0954	0.0515	21.9955	17.8534	15.4508	37.8288
16-JMS-14	17.8932	15.4524	37.8611	0.050	0.150	6.9720	0.0506	21.8239	17.8345	15.4497	37.8017
08-JMS-16	17.9314	15.3916	37.9184	0.045	0.167	7.9780	0.0579	30.3615	17.8643	15.3885	37.8372
08-JMS-17	17.9505	15.4086	37.9737	0.050	0.171	9.7974	0.0711	34.6236	17.8681	15.4048	37.8811
16-JMS-18	17.9825	15.4315	38.0194	0.041	0.163	7.1161	0.0516	28.9933	17.9226	15.4286	37.9418
16-JMS-19	17.9490	15.3901	37.9272	----------	----------	----------	----------	----------	----------	----------	----------
16-JMS-20	17.8862	15.3878	37.8542	----------	----------	----------	----------	----------	----------	----------	----------

Decay constants used in age-correction to 54 Ma, as shown in the three last columns, are as recommended by the IUGS and are: $238U \rightarrow 206Pb = 1.55125 \times 10^{-10}$ yr^{-1}; $235U \rightarrow 207Pb = 9.8485 \times 10^{-10}$ yr^{-1} and $232Th \rightarrow 208Pb = 4.9475 \times 10^{-11}$ yr^{-1} (Steiger and Jäger, 1977).

Equation used for age correction of $^{206}Pb/^{204}Pb$ ratios (Faure, 1986). $^{238}U/^{204}Pb$ ratios may be either measured or calculated.

$$(^{206}Pb/^{204}Pb)^{54\ Ma} = (^{206}Pb/^{204}Pb)_{measured} - {}^{238}U/^{204}Pb * (EXP(\lambda_{U\rightarrow Pb}*54\ Ma) - 1)$$

Equation used for age correction of $^{207}Pb/^{204}Pb$ ratios (Faure, 1986). $^{235}U/^{204}Pb$ ratios may be either measured or calculated.

$$(^{207}Pb/^{204}Pb)^{54\ Ma} = (^{207}Pb/^{204}Pb)_{measured} - {}^{235}U/^{204}Pb * (EXP(\lambda_{U\rightarrow Pb}*54\ Ma) - 1)$$

Equation used for age correction of $^{208}Pb/^{204}Pb$ ratios (Faure, 1986). $^{232}Th/^{204}Pb$ ratios may be either measured or calculated.

$$(^{208}Pb/^{204}Pb)^{54\ Ma} = (^{208}Pb/^{204}Pb)_{measured} - {}^{232}Th/^{204}Pb * (EXP(\lambda_{Th\rightarrow Pb}*54\ Ma) - 1)$$

References

Faure, G.: Principles of isotope geology. Second edition. John Wiley & sons pp. 589, 1986.

Steiger, R. H. and Jäger, E.: Subcommission on geochronology: convention of the use of decay constants in geo- and cosmochronology, Earth Plan. Sci. Lett., 36, 359-362, 1977.

Supplement 5

Partition coefficients and equations from the literature used in calculations/modelling

Table S5. Partition coefficients used in calculations of batch-melting and fractional crystallisation.

	ol	opx	cpx	plag	grt	spl
Sr	[a] 0.0050	[b] 0.0037	0.060	[c] 1.715	0.012	------
Nb	[a] 0.0005	[b] 0.0023	0.005	[c] 0.029	0.020	------
Th	[a] 0.0015	[b] 0.0010	0.030	[c] 0.173	[d] 0.010	------
Ta	[e] 0.0010	[b] 0.0070	0.013	[c] 0.042	0.060	------
K	0.0068	0.0140	0.038	0.170	0.015	------
Ti	0.0200	0.1000	0.400	0.040	0.300	------
Rb	0.0098	0.0220	0.031	0.071	0.042	------
Ba	0.0099	0.0130	0.026	0.230	0.023	------
Zr	0.0120	0.1800	0.100	0.048	0.650	------
Y	0.0100	0.1800	0.900	0.030	9.000	------
La	[f] 0.0074	[f] 0.0100	[f] 0.056	[f] 0.180	0.001	2.25
Ce	0.0069	0.0200	0.092	0.120	0.007	2.15
Nd	0.0066	0.0300	0.230	0.081	0.026	2.00
Sm	0.0066	0.0500	0.500	0.067	0.290	1.65
Eu	0.0068	0.0500	0.474	0.340	0.243	1.05
Gd	0.0077	0.0900	0.556	0.063	0.680	------
Dy	0.0096	0.1500	0.582	0.055	1.940	------
Er	0.0110	0.2300	0.583	0.063	4.700	------
Yb	0.0140	0.3400	0.620	0.067	11.500	1.35

Partition coefficients are for basaltic rocks from Table 4.1 in Rollinson (1998). [a]Bédard (2005). [b]Frei et al. (2009). [c]Aigner-Torres et al. (2007). [d]Berlo et al. (2004). [e]Interpolated values. [f]Extrapolated values. plag = plagioclase, other mineral abbreviations are from Kretz (1983).

Partial melting (batch melting) calculations were carried out using the following expression (from compilation in Rollinson, 1998 and references therein):

$$C_L / C_0 = 1 / (D_{RS} + F(1 - D_{RS})) \quad (1)$$

where C_L is the weight concentration of a trace element in the produced liquid, C_0 is the weight concentration of a trace element in the original unmelted solid, D_{RS} is the bulk distribution coefficient of the residual solids and F is the weight fraction of melt produced by partial melting.

Fractional crystallisation (Rayleigh fractionation) calculations were carried out using the following expression (from compilation in Rollinson, 1998 and references therein):

$$C_L / C_0 = F^{(D-1)} \quad (2)$$

where C_L is the weight fraction of a trace element in the residual liquid, C_0 is the weight fraction of a trace element in the parental liquid, D is the bulk distribution coefficient of the fractionating assemblage during crystal fractionation and F is the fraction of remaining melt.

References

Aigner-Torres, M., Blundy, J., Ulmer P. and Pettke T.: Laser Ablation ICPMS study of trace element partitioning between plagioclase and basaltic melts: an experimental approach, Contrib. Mineral. Petrol. 153, 647-667, 2007.

Bédard, J. H.: Partitioning coefficients between olivine and silicate melts, Lithos 83, 394-419, 2005.

Berlo, S., Turner, J. and Blundy, C. H.: (2004) The extent of U-series disequilibria produced during partial melting of the lower crust with implications for the formation of the Mount St. Helens dacites, Contrib. Mineral. Petrol. 148, 122-130, 2004.

Frei, D., Liebscher, A., Franz, G., Wunder, B., Klemme S. and Blundy J.: Trace element partitioning between orthopyroxene and anhydrous silicate melt on the lherzolite solidus from 1.1 to 3.2 GPa and 1,230 to 1,535° C in the model system Na_2O–CaO–MgO–Al_2O_3–SiO_2, Contrib. Mineral. Petrol. 157, 473-490, 2009.

Kretz, R.: Symbols for rock-forming minerals, Am. Mineral. 68, 277-279, 1983.

Rollinson, H.: Using geochemical data: evaluation, presentation, interpretation, Longman pp. 352, 1998.

Supplement 6

Mantle geochemistry and residual mineral compositions etc. used during partial melting calculations shown in Fig. 10 in main manuscript and in Fig. S6 below.

Partial melting calculations involving various mantle lithologies. The labelled curves in the $(Yb)_N$ versus $(Ce/Sm)_N$ diagram in Fig. 10d in the main manuscript text indicate partial melting trends calculated from three mantle sources (enriched: Yb = 0.45, Ce = 2.65, Sm = 0.51; moderately depleted: Yb = 0.31, Ce = 0.4, Sm = 0.17; strongly depleted: Yb = 0.25, Ce = 0.038, Sm = 0.118). Residual mineral assemblages are: curve i. = 84 % olivine + 16 % orthopyroxene; curve ii. = 76 % olivine + 24 % orthopyroxene; curve iii. = 76 % olivine + 20 % orthopyroxene + 4 % clinopyroxene; curve iv. = 76 % olivine + 23 % orthopyroxene + 1 % garnet; curve v. = 84 % olivine + 16 orthopyroxene; curve vi. = 83 % olivine + 15 % orthopyroxene + 2 % spinel; curve vii. = 84 % olivine + 16 % orthopyroxene; curve viii. = 80 % olivine + 12 % orthopyroxene + 8 % clinopyroxene; curve ix. = 80 % olivine + 11 % orthopyroxene + 8 % clinopyroxene + 1 % garnet. Numbers along curves ii. and iii. refer to melting percentages that also apply for all other curves in the actual diagram (and for curves in Fig. F below). Normalising primitive mantle values are from McDonough and Sun (1995). See Supplement 5 above for partition coefficients used in the calculations.

Additional partial melting calculations presented as binary Zr versus Y/TiO_2 plots in Fig. S6 below, with source data from the fertile mantle materials used in some of the REE calculations in Fig. 10 in the main manuscript (i.e. Lesnov et al., 2009), provide a slightly more varied picture with respect to potential source compositions and/or residual mineral assemblages when compared to Fig. 10 in the main manuscript. The curves in the Bivariate Zr versus Y/TiO_2 diagram in figure F below reflect partial melting of an enriched mantle source (Zr = 15 ppm, Y = 5.2 ppm and TiO_2 = 0.22 wt %). Residual mineral assemblages are: curve i. = 84 % olivine + 16 % orthopyroxene; curve ii. = 76 % olivine + 24 % orthopyroxene; curve iii. = 76 % olivine + 16 % orthopyroxene + 8 % clinopyroxene and curve iv. = 76 % olivine + 19 % orthopyroxene + 4 % clinopyroxene + 1 % garnet. Curve v. is similar to curve iii, but is based on a lower initial Y/TiO_2. Numbers along curves ii. and iii. refer to melting percentages that also apply for all the other curves. If residual mineral assemblages were dominated by olivine and orthopyroxene with only traces of clinopyroxene and spinel (curves i and ii in figure S6 below), three fertile mantle components with slightly

varying Y/TiO_2 ratios could explain the configuration displayed by the sill samples shown in this figure, while significant residual clinopyroxene (curves iii and v in figure S6 below) would indicate two slightly different fertile mantle components. Small amounts of residual garnet could in theory be responsible for the low Y/TiO_2 ratios of some of the high-TiO_2 sills (curve iv in figure S6 below), but REE calculations presented in the main manuscript argue against other than traces of this mineral in residues to sill sources (Fig. 10c and Fig. 10d in main manuscript).

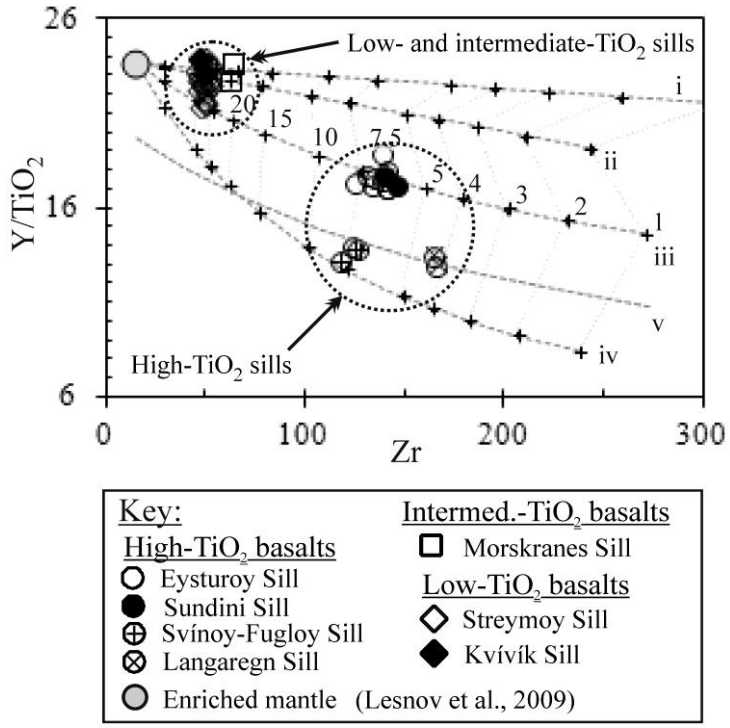

Fig. S6. Please see text above for details on this figure.

References

Lesnov, F. P., Koz'menko, O. A., Nikolaeva, I. V. and Palesskii, S. V.: Residence of incompatible trace elements in a large spinel lherzolite xenolith from alkali basalt of Shavaryn Tsaram-1 paleovolcano (western Mongolia), Russ. Geol. Geophys., 50, 1063–1072, 2009.

McDonough, W. F. and Sun, S.-s.: The composition of the Earth, Chem. Geol., 120, 223-253, 1995.